TOWARDS BETTER UNDERSTANDING OF FAILURE MODES IN LITHIUM-ION BATTERIES: DESIGN FOR SAFETY

by

Alex Francis

A Dissertation Submitted in

Partial Fulfillment of the

Requirements for the Degree of

Doctor of Philosophy

in Engineering

at

The University of Wisconsin-Milwaukee

August 2018

ABSTRACT

TOWARDS BETTER UNDERSTANDING OF FAILURE MODES IN LITHIUM-ION BATTERIES: DESIGN FOR SAFETY

by

Alex Francis

The University of Wisconsin-Milwaukee, 2018
Under the supervision of Professor Ilya Avdeev

In this digital age, energy storage technologies become more sophisticated and more widely used as we shift from traditional fossil fuel energy sources to renewable solutions. Specifically, consumer electronics devices and hybrid/electric vehicles demand better energy storage. Lithium-ion batteries have become a popular choice for meeting increased energy storage and power density needs. Like any energy solution, take for example the flammability of gasoline for automobiles, there are safety concerns surrounding the implications of failure. Although lithium-ion battery technology has existed for some time, the public interest in safety has become of higher concern with media stories reporting catastrophic cellular phone- and electric vehicle failures. Lithium-ion battery failure can be dangerously volatile. Because of this, battery electrochemical and thermal response is important to understand in order to improve safety when designing products that use lithium-ion chemistry. The implications of past and present understanding of multi-physics relationships inside a lithium-ion cell allow for the study of variables impacting cell response when designing new battery packs. Specifically, state-of-the-art design tools and models incorporate battery condition monitoring, charge balancing, safety checks, and thermal management by estimation of the state of charge, state of health, and internal electrochemical parameters. The parameters are well understood for healthy batteries and more

recently for aging batteries, but not for physically damaged cells. Combining multi-physics and multi-scale modeling, a framework for isolating individual parameters to understand the impact of physical damage is developed in this work. The individual parameter isolated is the porosity of the separator, a critical component of the cell. This provides a powerful design tool for researchers and OEM engineers alike. This work is a partnership between a battery OEM (Johnson Controls, Inc.), a Computer Aided Engineering tool maker (ANSYS, Inc.), and a university laboratory (Advanced Manufacturing and Design Lab, University of Wisconsin-Milwaukee). This work aims at bridging the gap between industry and academia by using a computer aided engineering (CAE) platform to focus battery design for safety.

Dedicated to the passion, motivation, and memory of John Francis.

TABLE OF CONTENTS

LIST OF FIGURES

LIST OF TABLES

LIST OF EQUATIONS

ACKNOWLEDGMENTS

I would like to express my immeasurable gratitude for my advisor, Dr. Ilya Avdeev, whose guidance has been essential to my growth as a student, researcher, professional, and as a person. I also would like to thank the industry partner of this project, Johnson Controls, Inc. and key personnel driving the research initiative, Steven Cash and Paul Frank. Also, my friends and colleagues at UWM, especially Dr. Joshua Harris, Caleb Abegglen, and Dr. Steven Hardcastle. Additional thanks to Dr. Junhong Chen, Dr. Ben Church, and Dr. Anoop Dhingra, Dr. Konstantin Sobolev and Dr. Deyang Qu for serving on my thesis committee and offering valuable feedback.

The support from members of the Advanced Manufacturing and Design Lab, Mehdi Gilaki, Mason Pingel, Douglas Wicker, Daniel Bautista, and Michael Powley, has also been of immense assistance which must not go unnoticed. Finally, I am grateful for the support of my parents, family, and friends through this journey inside and outside academics.

1. Introduction

We live in an era in which energy storage markets have been overtaken by lithium-ion batteries. Lithium-ion batteries are now not only widely used in consumer electronics market, but also in automotive industry (hybrid- and electric vehicles), and certain aerospace applications. As new applications and products adopt lithium-ion technology the need for increased power density becomes a significant R&D driver. However, with a continuous push for better battery performance, safety concerns become increasingly important. Recent catastrophic malfunctions of lithium-ion batteries ranging from thermal runaway fires in Samsung Note 7 mobile phones to hover boards – both banned due to their dangers to consumers – and vehicles, both consumer (Tesla [1], [2]) and commercial (Boeing, [3]–[5]) demonstrate an urgent need for improved battery safety. The key motivation of this research is ***focus on energy storage design for safety***.

1.1. Battery Failure

Although the statistics seem low for the likelihood of failure, the number of catastrophic event occurrences in cell phone and EV applications are interestingly the same, one in ten thousand [6], [7]; these numbers are significant. They have influenced responsive policy changing, testing standards, and design changes. Most important, it has influenced researchers to address the problem for better understanding failure mechanisms in effort to reduce the collateral impact of faulty lithium-ion cells.

Lithium-ion batteries can fail under various circumstances such as normal aging, accelerated testing or due to catastrophic events. Take for instance the 24-month average lifetime of a cellphone by consumers before it is replaced [8]. The average lithium-ion battery in a cell phone is designed to last about two years or between 500 and 750 charge cycles [9]. The phone replacement time may be influenced by purchasing decisions or based on the performance of the mobile technology itself. In an automotive market, average consumers are expected to use their vehicle for 15 years or 300,000 miles, but cars can last above 1,000,000 miles with proper maintenance [10]. Electric vehicles (EVs) pose new challenges to existing automotive cycle and lifetime routine maintenance. A consortium of American electric vehicle manufacturing companies (FreedomCAR) introduced EV industry goals and performs state-of-the-art research analysis hoping to reach a battery- pack lifetime of 10 years or 1,000 cycles [11]. Tesla Motors offers eight-year, infinite mile warranty for their 85 kWh batteries [12]. This data represents normal operating conditions for some lithium-ion battery applications. Over time the battery ages, causing the battery operation to be inconsistent and even dangerous. Normal aging can lead to battery failures. Other failure modes can occur suddenly in the form of catastrophic events.

1.1.1. Catastrophic Failures

Catastrophic failures of lithium-ion battery packs are highly publicized prompting a lot of debate and ramping-up concerns about their safety [1], [7], [13]–[15]. When a lithium-ion battery catastrophically fails, the results can be very dangerous because the flammable electrolyte solution inside can combust. The dangers of battery failure have influenced the FAA to ban certain types of consumer devices from being allowed on aircrafts. There have been five

lithium-ion related safety alerts issued by the FAA, Safety Alerts for Operators (SAFOs), since 2015 for lithium-ion battery procedures on aircrafts, one in particular that forbids safety-recalled lithium-ion batteries on aircrafts [16]–[20]. This ban applies not only to the Samsung Note 7 but, more broadly, to all hazardous lithium-ion batteries

The recall of the Samsung Note 7 is a result of catastrophic failure of the lithium-ion battery that powers the device. Preliminary investigations point at the failure caused by the phone being too thin as well as to battery manufacturing errors [6], [21]–[24]. The phone design flaw was twofold: 1) there was not enough space for battery swelling over time and 2) mechanical deformation of the phone and manufacturing errors may lead to separator failure inside battery jellyroll. Sadoway also speculates that when dendrites form they can puncture through the thin separator material [6]. Ultimately, the separator integrity is the primary concern whether from a structural point of view, manufacturing concern, or aging with the accumulative dendrite formation. When the separator inside the battery fails, a short circuit can occur between the cathode and the anode, generating enough heat to set the flammable electrolyte on fire.

The dangers of lithium-ion batteries in consumer products might are also present in electric vehicles. Electric vehicle lithium-ion battery packs have been reported to catch fire in various situations involving battery pack puncture, during and after a crash [7], [14]. Although all vehicles, not just electric vehicles, are at risk of fire in the event of a serious crash the media has focused on electric vehicle issues since the market for electric vehicles has started to emerge. Notable manufacturers publicized by EV failure events are Tesla and Chevrolet. In 2013, early Tesla vehicles reported battery fires due to puncturing the underside of the battery pack while

driving. Since the incidents Tesla has included a protective plate under the battery pack as a preventative measure [7]. For Chevrolet, in 2011 a Volt electric vehicle caught fire long after structural damage from the impact of a crash. The National Highway Traffic and Safety Administration (NHTSA) reported three weeks after side-impact crash testing, the stationary vehicle caught fire [15]. They reported that the battery pack encountered a thermal runaway situation that lead to the catastrophic event [25].

1.2. State-of-the-Art in Lithium-Ion Battery Modeling

Structural integrity of a lithium-ion battery is important for protection of the active electro-chemical process ongoing inside the cell. The safety of lithium-ion batteries stems to multiple variables in multiple physical domains and influenced by even small abnormalities. Understanding the impact of just one variable, the separator, and the effect of battery chemistry and mechanical damage at the component level on the safety of an entire electric vehicle can be accomplished with through a refined understanding of lithium-ion battery modeling and computer simulations accompanied by experimental validation.

1.2.1. Multi-Scale and Multi-Physics Motivation

Researchers have developed models to predict and understand each type of physical response in a lithium-ion battery. The majority of studies are compartmentalized to a specific discipline and do not address the multi-field effects and difficulties of coupling them. There are, however, studies that attempt to create comprehensive simulations of lithium-ion battery cell behavior.

Modeling lithium-ion batteries is becoming refined by researchers at the National Renewable Energy Lab (NREL) and at The Massachusetts Institute of Technology (MIT) [26], [27]. The latter study contributes to state-of-the-art by expanding upon the multi-scale and multi-physics efforts with a full vehicle numerical model and parametric failure analysis protocol indicating most influential design parameters. Through the utilization of homogenization methods, reduced order modeling, and high performance computing resources, the goal of this study is to contribute to the understanding of lithium-ion battery safety in electric vehicles from the full scale of a vehicle to the internal components of an individual battery cell. The framework to do so is presented and explored by isolating a critical variable of the separator, porosity.

1.3. Motivation

The motivation of this work is to ultimately improve crash safety of electric vehicles by contributing to better-informed lithium-ion battery design considerations. This study focuses specifically on the Johnson Controls, Inc. 6P spirally wound cylindrical cells, larger variants of the popular 18,650 cells. Each 6P cell is 3.6 V/6.8 Ah, coated with NCA/Graphite, with a length of 140 mm and diameter of 40 mm. We aim to unify understanding of cylindrical cell geometries by electrochemical verification with coin cells and thermal characterization with pouch cells. Chapter 2 provides a review of Li-Ion modeling and experiments that are foundational to this work; developing an approach for rebuilding deformed cell geometry after abuse and validation of structural simulation results using the method. Chapter 3 provides a comprehensive review of state-of-the-art work, alternative approaches, and the gaps in knowledge in Li-Ion battery modeling motivating this research. Chapter 4 describes the framework and methods to pursue the next generation li-ion battery modeling capabilities isolating cell design variables specific to

the influence of damage on cell performance and phenomena that govern the changes. Chapter 5 illustrates how to experimentally verify the framework and modeling capabilities. Chapter 6 is an in-depth review of the results, conclusions, and contributions to the field of li-ion battery modeling.

2. Review of State-of-the-Art in Lithium-Ion Battery Modeling

This study investigates the influence of the cell's structural parameters on how dependent the response is relative to each physical design variable with a critical focus on safety. Analysis of structural parameters such as optimal active layer thicknesses for maximum structural strength and electrical efficiency, temperature response and thermal runaway considerations as well as the impact of structural deformations and short circuits can all benefit from a multi-scale and multi-physics simulation. Additional capabilities of the computational battery model include the quantification of battery deformation and swelling during charge/discharge cycles, ideal pack temperature, or even understanding the safety implications of structural deformation.

On a micro-scale of lithium-ion storage systems, chemistry in the cell is dominated by energy and thermal producing Li diffusion and transport reactions. Electrical phenomena such as charge balancing, electrical potential and current distribution is analyzed in the micro-scale active layers and macro-scale module and pack level influence. At the cell level, heat generation due to electrochemical interactions as well as structural capabilities are included in the analysis. At the module and pack level, individual cell response effects surrounding cells, thus thermal management and control is important as well as the structural integrity. Catastrophic battery failure happens quickly and needs to be better understood for improved battery safety. The most newsworthy occurrences of battery design malfunction include those in consumer cellular electronics [6], [6], [21], [22], [24], battery failure on aircrafts [16]–[20] and, a focus of this study, electric vehicles [7], [25].

2.1. Overview of Prior Work

2.1.1. Experimental Work

Experimental testing of lithium-ion batteries mimicking the damage in real-world situations is essential to collecting data of actual battery response and for a refined understanding of the modes of failure. With a broad focus on multi-scale and multi-physics relationships, experimental data is critical for developing accurate numerical and computational models. Collectively, researchers have conducted experiments to understand multiple phenomena in the electrochemical, thermal, and structural domains using 2032 coin cells [28], [29], 18650 cylindrical cells [30]–[38] and various sizes of pouch cells [7], [27], [39]–[41]. Little research has been conducted on the state-of-the art 6P cylindrical battery geometry, those who have, studied the geometry using electrochemical impedance spectroscopy [42].

One way to address a complex multi-scale system is to simplify the analysis. In case of lithium-ion batteries with heterogeneous internal layered structures, the "jellyroll" can be modeled as a homogenized structure. This simplification must be verified through material modeling, characterization and experimentation for the most accurate simulation results. Homogenization of lithium-ion cells can be achieved using various approaches: through cell representation as a laminated composite structure [43], through a classical laminated shell theory [44], or by a multilinear interpolation of the stress-strain curve [45]. However, Avdeev and Gilaki [46] have established the groundwork for lithium-ion battery cell homogenization used in this study.

The lithium-ion cell contains an energy storing jellyroll, which is a repeated series of layers rolled into a cylindrical form. The layers consist of a graphite coated copper anode (~80 μm)

and LiNiCoAlO2 coated aluminum cathode (~75 μm), separated by a polymer separator (~20 μm); Figure 1 depicts the layers. Each layer is approximately 175 μm in thickness and there are 61 layers per cell. The micro-scale layer thicknesses compared to dimensions of the cell, measured in millimeters, makes full scale structural simulations computationally intensive requiring small elements discretizing the jellyroll layers relative to the size of the cell itself. At the full vehicle pack level containing hundreds of cells and even the module level containing twelve cells, representing all layers is extremely inefficient and unnecessary for most situations.

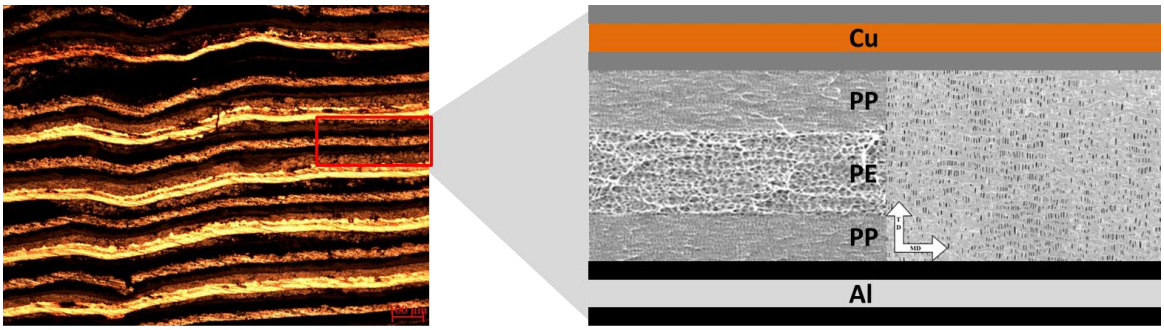

Figure 1. Jellyroll layers [46] (from top to bottom): copper anode (graphite coating), separator (tri-layer) [47], [48], aluminum cathode ($LiNiCoAlO_2$ coating).

Material characterization of jellyroll components guided the homogenization process. A representative material model that can be applied to a solid construction of the jellyroll was developed. Multiple homogenization procedures were conducted and compared by Avdeev/Gilaki [46] and Martinsen [48]. They compared homogenization procedures through analysis of structural response via compression and tensile testing of individual layers in the jellyroll separately, under various strain rates and environmental conditions as well as performing compression testing on representative samples of the combined jellyroll samples themselves.

Two methods of homogenization were studied: (1) indirect homogenization and (2) direct homogenization. An indirect homogenization method using the virtual work principal showed better accuracy for smaller cells. This method assumes the compressive load is mainly carried by the central area of the jellyroll for which the average stress and strain is calculated using the virtual work principal. Direct homogenization methods showed improved accuracy for the larger 6P cells associated with our study. This method used the stress-strain results obtained from experimental compression data of sections taken from the full cell.

Since this problem is an intensive multi-scale and multi-physics study, understanding the dynamics of each level is critical. The range is from micro-meters to meters, taking into consideration chemical and physical fields; Figure 2 depicts the multi-scale nature of the investigation. At the active layer level, much of the consideration is with respect to the chemistry of the battery. At the scale of a single battery cell and components, structural considerations and electrical characteristics dominate the analysis. Multiple single cells make up a battery pack module, shown in Figure 3. A full electric vehicle battery pack is a combination of all scales, the battery pack, the battery module, the battery cell, and the layers of each cell; see Figure 4. At this level, computational efficiency is important and can be obtained through parallel computing, homogenization and model order reduction. The high performance computing (HPC) resources at UWM are critical for achieving results at this multi-scale level.

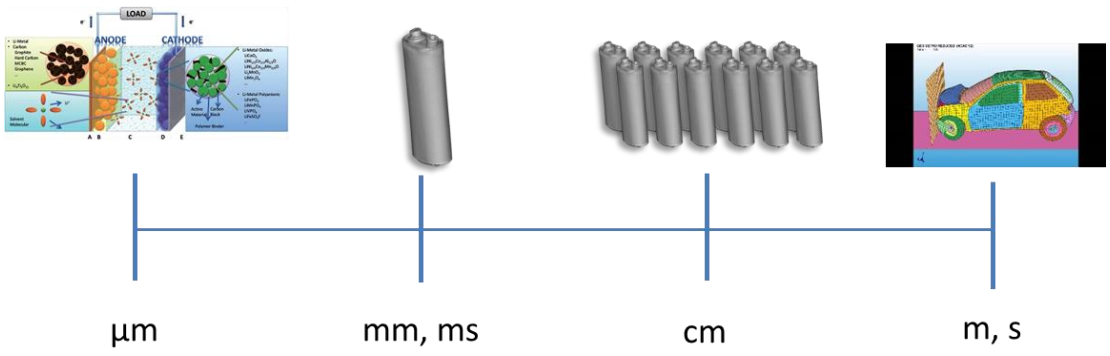

Figure 2. Electric Vehicle Lithium-Ion Battery Multi-scale Considerations

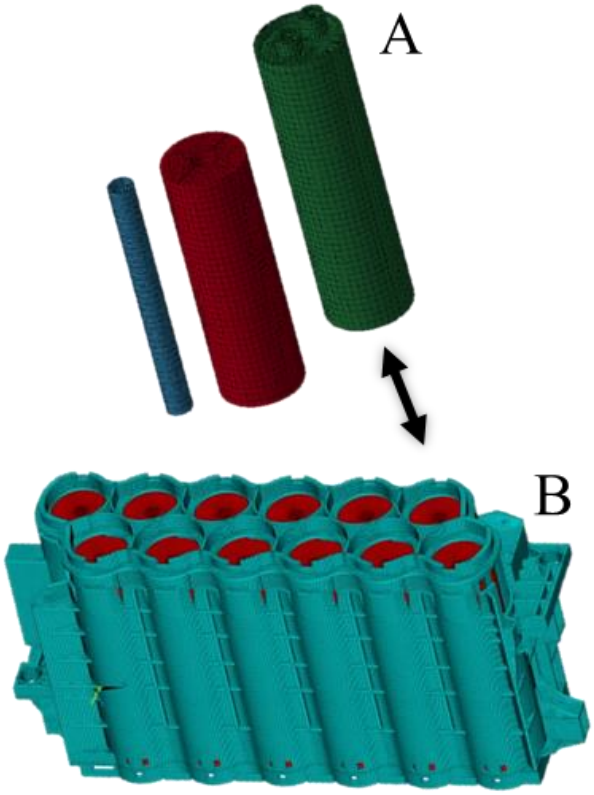

Figure 3. Exploded view of battery module: a) depiction of battery cell internal components b) battery back module

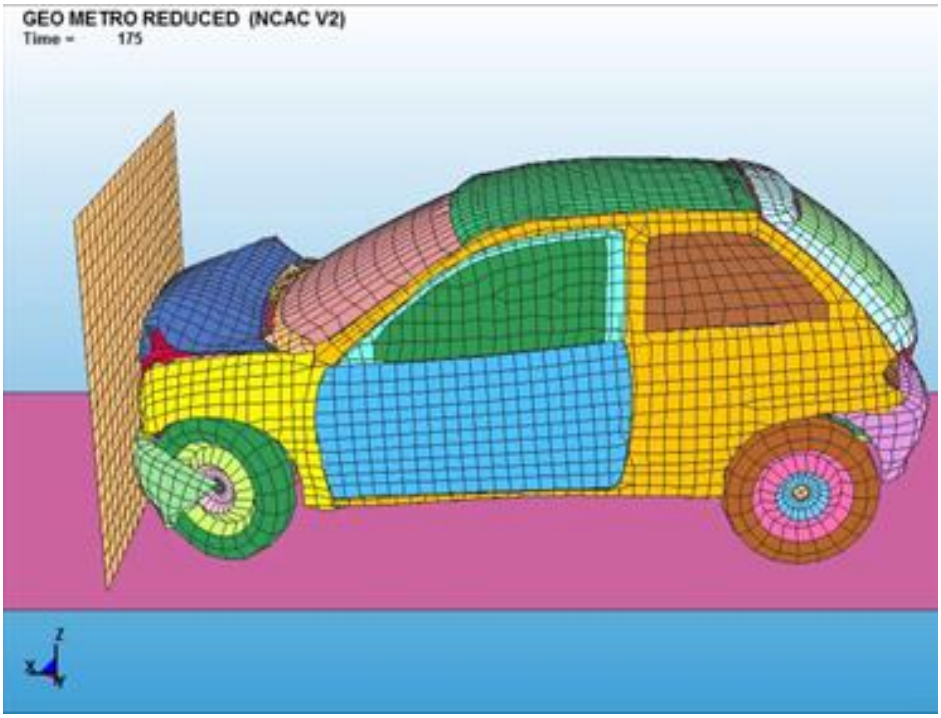

Figure 4. Vehicle battery pack scale simulation [49]

2.1.2. Modeling Work

Since lithium-ion battery failure is dangerous for testing live cells, modeling the battery can be a safer alternative for adjusting design parameters and studying the response. Representative models for lithium-ion phenomena have been developed in support of understanding of cell operation, design of improved battery packs, and control of the batteries during operation. Comprehensive analytical modeling of the governing physics has lead the way for the evolution of cell models into full battery pack modeling. Full pack modeling is valuable for the accurate characterization of current and future operation in Battery Management Systems (BMS). Industry requirements of battery control with BMSs have especially motivated the need for reduced order models (ROM) with a balance of capability, accuracy, and speed.

3. Multi-Physics Modeling

Multi-physics modeling allows us to study complex real-world systems. Multi-physics modeling is an all-encompassing term for multi-field, multi-domain and multi-scale analysis. Multi-field, or coupled field, analysis itself can represent various types of problems: single domain and single field, single domain and multi-field, multi-domain and multi-field, multi-domain and multi-field [50]. Fluid, structural, and interactions between the two are examples of domains and structural, thermal, and chemical responses are examples of physical fields. Multi-scale analysis spans discrete increments, for our case we consider length scales from micro-meters to meters. We will discuss how complex heterogeneous battery components can be simplified using homogeneous models in order to bridge the gap between multi-scale increments.

Coupled-field analysis has been observed by influential scientists like Seebeck, Peltier, Navier and Maxwell. Their investigation into the coupled nature of physics established the future for two- and three- field analysis such as the relationships fluid and structural domains, thermal and structural (thermo-elastic), electrical and chemical (electrochemical), thermal and electric (thermoelectric), as well as thermoelectro-elasticity.

The power of multi-field analysis has been utilized to study fluid-structural interactions in the aerospace, automotive and consumer product industries helping understand phenomena such as the aerodynamic structures like the efficiency of bicycle rider position [51], the electronics industry to develop microelectromechanical systems (MEMS) for applications in accelerometers

and printing components [52], as well as the harmonic electromagnetic-thermal effects of induction heating for material processing [53].

Battery specific multi-physics modeling has gained interests with the evolution of electric vehicles that use lithium-ion batteries as a primary power source. Modeling the processes of lithium-ion batteries is multi-scale, multi-field, and multi-purpose. Since Randles' [54] development of a lumped parameter model in 1947, researchers have built upon equivalent circuit methods, analytical, and empirical based models to capture the complex nature of lithium-ion battery operation.

Battery performance modeling can be divided into three categories: (1) analytical models (closed-form) models, (2) electrochemical reduced order models, and (3) equivalent circuit models. Variants and combinations of these modeling categories is possible in battery management systems and numerical simulations for design of cells, modules, and full battery packs. Models that are fast enough to provide critical information to battery management systems are generally called real-time models often originating from simplified electrochemical models or equivalent circuit models (ECM). The importance of using representative models in EV applications is to predict the age of the battery, thus remaining life, improve the safety of operation during charge/discharge, especially fast charging, as well as optimization of cell usage in a pack [55]

3.1. Analytical Modeling

When selecting a modeling approach, one must consider a balance of accuracy, calibration effort, and the ability to use the model for the intended purposes [56]. The most accurate type of modeling is electrochemical modeling using PDE's to describe the governing equations of the electrode solid concentration, electrode potential, electrolyte concentration, and electrolyte potential. Electrochemical modeling's accuracy can fit to experimental data with little error allowing it to be used for verification of other models and providing specific insight into internal states which are not observable [55]. Examples of commonly used multi-physics models are electrochemical impedance based models [38], [57]–[60], linear parameter varying models [56], pseudo 2D models [58], [58], [61]–[64].

Electrochemical models can be further segmented into general electrochemical models, single particle concentration models (SPM), and models incorporating thermal physics [55]. Pure electrochemical models include representation of internal battery components of the positive electrode, negative electrode, electrolyte, separator, and current collectors, building governing equations defined in the x-direction through layers [55]. SPM models define positive and negative particles with equations in spherical coordinates [55]. Models have evolved to include thermal capabilities powerful to represent cell types used by EVs. However, with additional multi-physics capabilities and multi-scale EV cell, module, and pack geometries, the order of the model increases dramatically. Thus, some researchers use computational methods such as CFD and FEA to represent the systems [55], [62], [65].

Several literature review papers have been published summarizing modeling approaches in the past three years [2], [55], [61], [66]–[68]. The different approaches to li-ion battery modeling, specifically equivalent circuit modeling, are summarized by the following diagram; Figure 5. The most recent improvements in battery modeling include SOH and age prediction capabilities using 1D ECM networks for representation of the electrodes (electron binders in current collectors and intercalated in the active material) and separator (li-ions in the bulk electrolyte). Since research of healthy undamaged batteries is understood, the approach to this research is to determine modeling and characterization of damaged li-ion chemistry cells with a focus on a critical component of the system and the model, the separator; also highlighted in Figure 1.

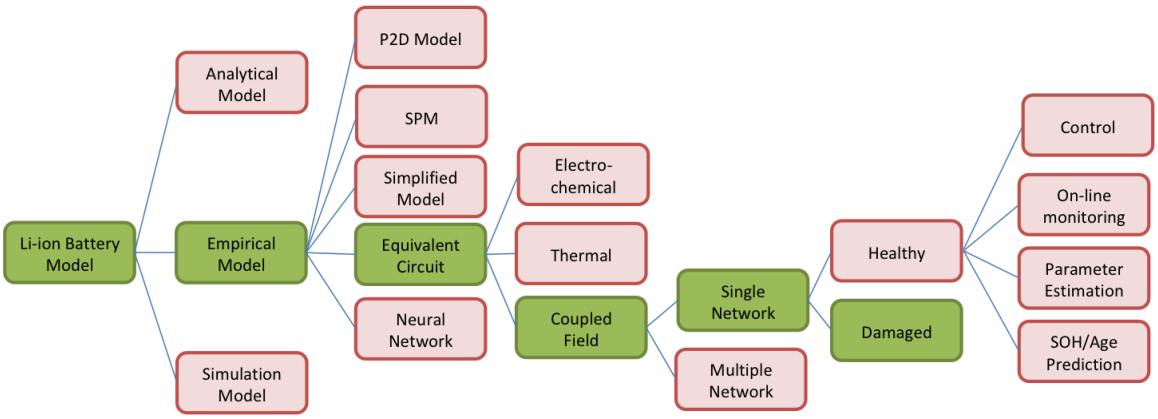

Figure 5. Classification of Li-ion battery models based on [Jokar 2016]

3.1.1. Thermal Domain

Thermal response of lithium-ion batteries is modeled as a combination of electrochemical reactions, phase changes, mixing effects, and joule heating [57]; a result of the homogeneous activity [44] that originates within the energy producing layers. Originally shared by Bernardi

et.al. [57], this model has been adapted and adjusted by many researchers to follow. Table 8. Thermal modeling research matrix. of the Appendix describes the landscape of li-ion thermal modeling research.

Lithium-ion battery thermal failure can become rapidly catastrophic and is influenced by prolonged abuse or immediate response to external stressors to internal components such as the separator. Actually, the separator component of the cell is designed to fail, melting at elevated temperatures and sealing the micro-pores, stopping energy production before thermal runaway occurs [69], [70]. Thermal runaway is an occurrence of an uncontrollable increase in battery temperature leading to failure [71], [72]. An understanding of thermal failure mechanisms can better inform design. Han et al, Pesaran et al, and Shah are some researchers who have developed experimentally validated thermal models, which are able to predict heat generation inside a lithium-ion cell [73]–[75].

Recent research efforts focused on better understanding of thermal behavior of lithium-ion batteries during normal operation and catastrophic events focused on three areas: (1) experimental battery abuse studies, (2) analytical heat generation models, and (3) finite element models. Bandhauer et al. conducted a comprehensive review of thermal issues with lithium-ion batteries referencing work that investigated scenarios leading to thermal runaway including critical operating temperatures, effects of temperature on jellyroll components, and sources of heat generation [76]. Through experiments, Zhang, Khasawneh, and Onda studied the heat generation response during charging and discharging lithium-ion batteries, showing that 1800 mAh cells operate between 25 and 50 degrees Celsius with heat generation rates up to 1 W; for

example, see Onada's results below in Figure 6 [34], [77], [78]. Research has shown a strong influence of cycling temperature on thermal stability [Borner, 2017].

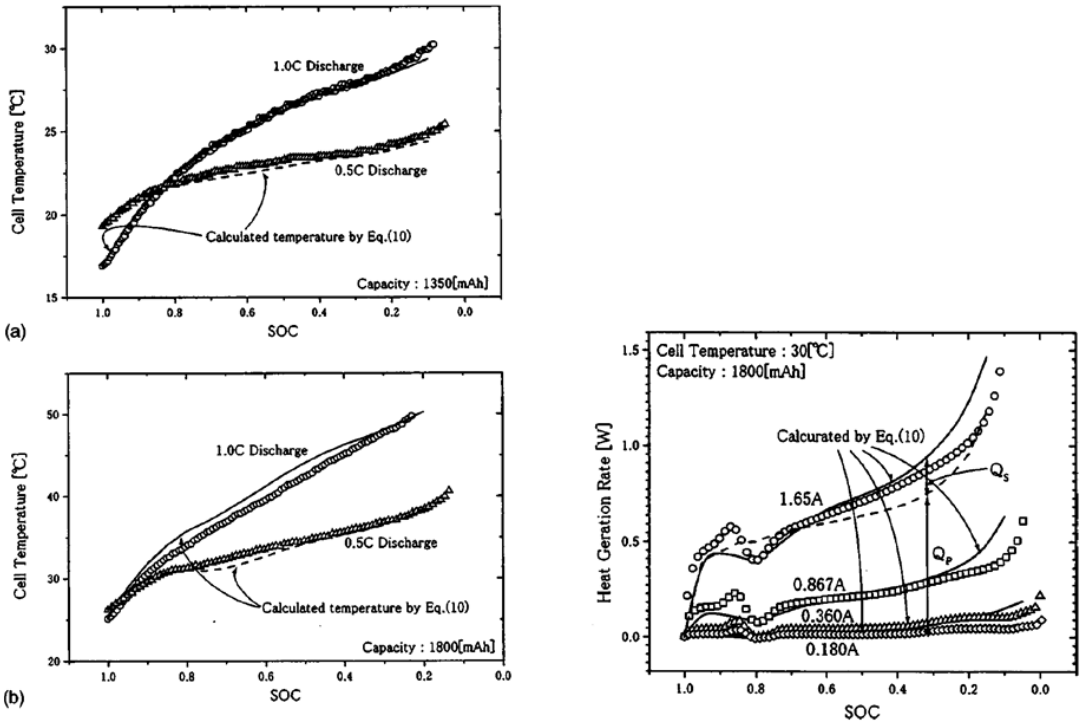

Figure 6. Temperature profile and heat generation values published by Onada [78].

Chen et al., Sievers et al., and Zhang. investigated analytical modeling of the thermal response of a battery [69], [79], [80]. The Bernardi [81] model is adapted by many. His contribution shows that heat generation within the battery is a combination of phenomena distributed evenly within the energy producing section of the battery; see Bernardi's thermal model in Equation (**3.1**) [81]

$$q - IV = \cdots$$

$$\sum_{i}\left[I_i T^2 \frac{d\frac{U_{i,avg}}{T}}{dT}\right] \ldots \quad \text{enthalpy-of-reaction}$$

$$-\sum_{j}\frac{d}{dt}\left[\int_{v_j}\sum_{1} c_{i,j} R T^2 \frac{\partial}{\partial T} ln\left(\frac{\gamma_{i,j}}{{\gamma_{i,j}}^{avg}}\right) dv_j\right] \ldots \quad \text{enthalpy-of-mixing}$$

$$-\sum_{j,j\neq m}\sum_{i}\left[\left(\Delta H_{\circ_{ij\rightarrow m}} - RT^2 \frac{d}{dT} ln\left(\frac{{\gamma_{i,m}}^{avg}}{{\gamma_{i,j}}^{avg}}\right)\right)\frac{dn_{i,j}}{dt}\right] \ldots \quad \text{phase-change}$$

$$+\frac{dT}{dt}\left[\sum_{j}\sum_{i} n_{i,j}^{0} {\bar{C}_{Pi,j}}^{avg} + \sum_{1}\frac{\int_0^t I_i dt}{n_1 \mathbf{F}}\Delta C_{pi}\right.$$

$$\left.+\sum_{j,j\neq m}\sum_{i}\left({\bar{C}_{Pi,j}}^{avg} - {\bar{C}_{Pi,m}}^{avg}\right)\left(n_{i,j} - n_{i,j}^{0}\right)\right] \quad \text{heat-capacity}$$

(3.1)

Notice how this equation evolved from the general heat transfer equation below; (3.2.

$$\rho C \frac{\partial T}{\partial t} + \nabla \cdot \mathbf{q} = \dot{q}$$

(3.2)

The thermal model of a lithium-ion battery contains sources of heat generation from more complex electro-chemical reactions and is carefully controlled by thermal management systems

regulating its environment through convection. Heat generation inside the battery is found by Baba et al. to be a collection of local heat generation across the entire electrode plane, caused by the electrochemical reaction that results from lithium-ion intercalation or deintercalation [82].

Somasundaram et al used a two-dimensional, transient mathematical model for cylindrical lithium-ion cells encompassing conservation of charges, species, and energy together with electroneutrality, constitutive relations and relevant initial and boundary conditions. This was accomplished with two-way coupling of heat generation and temperature-dependent physical property terms in electrochemical and thermal equations. The model was also solved numerically for passive thermal management with and without a phase change material (PCM) at various galvanostatic discharge rates. The study revealed characteristics of spirally wound cylindrical cells, such as edge effects from variations in heat generation in the functional layers [83]. Many battery chemistries and geometries have been studied experimentally, modeled, and simulated numerically. For example, cylindrical li-ion batteries consisting of electrode/electrolyte combinations of graphite and LiFP6 in a propylene carbonate/ethylene carbonate/dimethyl carbonate (PC/EC/DMC) solution electrolyte [80].

The model studied by Zhang, considers the electrolyte transport properties as a function of temperature and lithium-ion concentration. Specifically, heat in the cell is understood to be generated by three sources [80]. Ohmic heat, the heat generated by electrical current traveling through the components of a cell, contributing to approximately 54% of the heat generated [80]. Reaction heat, the exothermic or endothermic heat transfer generated by the thermal electrochemical reactions of the cell, contributing to approximately 30% of the heat generated by

the electrochemical reaction [80]. In the case of a cell discharge, the reaction is exothermic with the rise in temperature being dependent on the thickness of both separator and electrodes [27], [80]. Finally, active polarization heat, the heat generated by the diffusion of Lithium ions in the cell and remaining sources contribute the least to the state of temperature in the cell [47], [55], [84]. Conclusions indicate that Li ion concentration gradients in electrolyte are the major factors giving the effect on the heat generations of active polarization and electrolyte electric resistance [80]. Additionally, temperature increase during discharge is positive related with the thickness of both separator and electrodes [Zhang, 2010]. The study of li-ion heat generation extends into investigations of entropy, model based studies of reversible heat [85], and simulation based studies of reversible heat [86].

3.1.2. Coupled-Field Models

Research of specific physical phenomena is useful for deep understanding of battery behavior. An overlap of electrochemical and thermal physics is inherent in some models, but, ultimately, full multi-field modeling is necessary for a more comprehensive analysis. Lithium-ion battery multi-scale and multi-field analysis is of increased interest. For example, NREL is working on developing a Computer Aided Engineering for Electric Drive Batteries (CAEBAT) modeling tool in order to "couple structural models with electro-chemical-thermal models to simulate crash-induce crush and thermal runaway." [26]. Moreover, combinations exist of analytical electrochemical models [64], [87]–[89] and thermo-electrochemical models [55], [63], [72], [83], [90]–[96].

Thermal management and application to battery management systems (BMS) are relevant because thermal management improves charge-discharge efficiency and cycle life [92]. Low and high temperature operation effect the battery performance in different ways. Low temperature operation decreases the battery capacity while high temperatures age batteries faster [61].

Evolution of battery models is marked by the following milestones: energy balance [81], a single battery P2D model combined with heat generation [97], heat generation analysis of a battery stack [98], battery models with uniform temperature environmental conditions [99], [100], 2D and 3D models with harsh environmental condition [79], empirically based simulations focused on heat generation [101], [102][, empirically based simulations focused on battery parameters [32], [103]. Thermal and electrochemical models are the most common tools used to accurately predict battery performance, safety, and reliability. When thermal and electrochemical models are combined, the accuracy of prediction is improved. However, as the accuracy and robustness of the model increased along with the growing number of battery parameters, the computational price paid has increased as well,. Specific heat capacity, thermal diffusivity, and thermal conductivity are the parameters that are required for the thermal model [61]. When considering accuracy, discharge rate has been shown to be a critical factor of effecting electrolyte concentration and potential parameters above 1 C rates [104] while at lower discharge rates below 1 C the electrolyte properties can be assumed to be constant [61].

The accuracy of the Newman model is accepted as a reliable method of representing the electrochemical performance of a li-ion cell. Further research has expanded upon the Newman model to incorporate thermal [62], [91] [105] and mechanical capabilities [106], [107].

The electrochemical model used by Wu is a combination of the Newman's Model, porous electrode theory and concentrated solution theory [108], [109]. The porous electrode theory considers the porous electrode and electrolyte interfaces as one homogenized component. The concentrated solution theory has more to do with the mass transportation within the electrolyte. Both the solid and electrolyte phase are represented by the Butler-Volmer equation [110].
Ion transportation in the electrolyte phase consists of diffusion and migration described by the following governing equation.

$$\varepsilon_2 \frac{d_{c_2}}{dt} = \nabla \cdot \left(D_2^{eff} \nabla c_2\right) - \frac{1}{F} i_2 \cdot \nabla t_+ + \frac{S_a j_n}{F}(1 - t_+)$$

(3.3)

Where Fick's second law describes the mass transport phenomena in spherical coordinates; see equation #. It is believe that the surface of the electrode contains spherical particles. At this particle surface, the Li-ion flux and current density are related by the following equation.

$$\frac{\delta c_1}{\delta t} + \frac{1}{r^2}\frac{\delta}{\delta r}\left(-r^2 D_1 \frac{\delta c_1}{\delta r}\right) = 0$$

(3.4)

In terms of accuracy, the most successful model is the pseudo-2D model, but this model is too complex for usage in real-time battery management systems [61]. However, researchers have investigated simplification methods to reduce the order of governing equations [61].

3.2. Reduced Order Modeling

Modeling battery performance, especially SOC, in EV's accurately enables an indicator of battery condition and in some cases the future condition of the battery. EV specific models differ from the robustness of fully defined electrochemical models in that they need to consider speed rather than accuracy as well as capabilities at high C-rates for on-line usage in BMSs. Overall, the simplification of models for use in EVs incudes simplified or reduced order (ROM) electrochemical models and ECMs. The ROM methods essentially simplify the model through various discretization techniques to account for the most important contributors to the cell behavior [55] [111]. Discretization methods are represented by a few categories including: analytical methods, integral approximation, Padé approximation, finite element methods (FEM), and finite difference methods (FDM). Analytical reduction methods utilize Eigen function series expansion and Laplace transformation. Similarly, using power series expansion is a method called Padé approximation. Integral approximation converts the governing analytical equations from PDEs to simplified ODEs using integration. Also, specific for computational methods the FEM and FDM are used for multi-scale and multi-physics solving, but these methods are not applicable to real-time computation in BMSs because of the relatively long solution time. Alternatively, spectral method have been employed offering a 10-100 times increase in speed relative to FDMs [93].

Mathematical models can be segmented into simplified analytical models such as the Kinetic Battery Model (KiBAM) representing the battery with a relatively small number of equations

and stochastic models which are fast and accurate based on stochastic discrete-time Markov chains [55], [112].

When selecting a model, users must consider a balance of accuracy, calibration effort, and the ability to implement for the application [56]. This balance is especially useful for Battery Management Systems (BMS). In place to monitor and control the current state of the batter in terms of voltage, temperature, current and variables associated with the mutli-physics operation of the battery, BMSs are essential to maintaining safe battery operation. An example BMS flowchart with capabilities to monitor battery condition, control operation, manage thermal performance, and perform safety checks is shown in Figure 7.

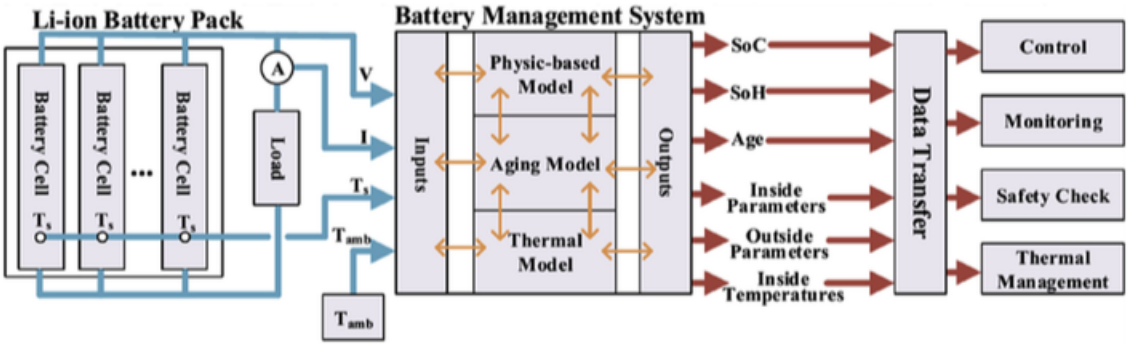

Figure 7. Example flowchart of a BMS [61]

Optimization of electrochemical models has been studied for real-time battery management systems [89].

With the battery performance changing with condition and over time, modeling in either category relies on determining condition- and time-variant model parameters empirically. Experimental methods of determining parameters depend on the model selection and generally include: Electrochemical Impedance Spectroscopy (EIS) [57]–[59], [113] and High Pulse Power Characterization (HPPC) cycle testing to determine a representative internal resistance and capacitance [57], [114]–[116]. Model parameters for the corresponding lookup tables are determined off-line from the experimental data. Alternatively, model parameters are determined by the coefficients of fitting functions to the experimental data. In both cases, the model parameters determined are associated with the operating conditions of the experiment used. Thus, in order to account for many SOC, temperatures, and C-rates, more experiments must be completed. Selection of parameter values is essential to accuracy optimization because the error of the EMC prediction relative to actual operation of the battery is considered. Methods of parameter optimization are Prediction-error minimization (PEM) and a Gauss-Newton search scheme [55]. Again, the downfall of ECMs is that they need experimental data for parameter lookup tables at operating ranges of SOC and temperatures. Also, they cannot predict internal variables (electrolyte potential) [55].

Recent modeling has reached a balance of complexity and accuracy for use in BMS computations through Equivalent Circuit Modeling (ECM) or (EC). A focus of this study, ECM methods are built on representative electrical circuits consisting of an ideal voltage source, resistance, and capacitance terms that vary in complexity. As such, these models offer the capability of real-time results [55], [117].

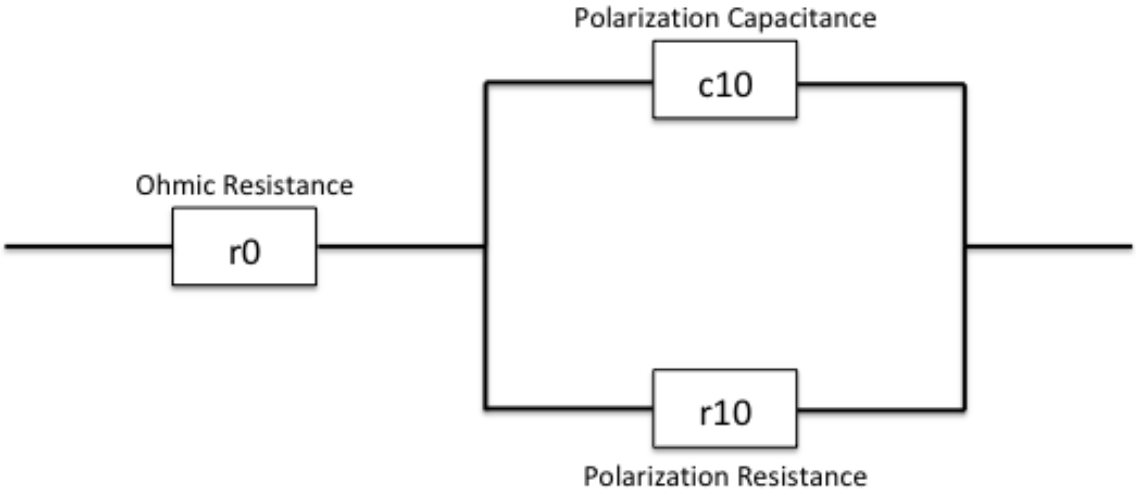

Figure 8. Example equivalent circuit model, 1RC Randles model

Figure 8, demonstrates a common ECM adding to it an RC network. Models of this type are known as Thevenin Models or 1RC models, containing parameters for a terminal voltage source (V_t), open circuit voltage (OCV), load current (I_L), internal resistance (R_0), equivalent polarization resistance (R_P), and equivalent polarization capacitance terms (C_P) [55], [118]. Parameters in Thevenin and other ECM must be determined experimentally by Electrochemical Impedance Spectroscopy (EIS), relating equivalent impedance to empirical data by applying pulses of AC voltage at steady state conditions of the battery. Examples of other commonly used equivalent circuit models are the Randles model [30], [54], [57], [59], [63], [119]–[122], Thevenin models [57], [121] simple resistance models [57], and variations there of [42], [113].

The drawbacks of determining parameters for ECM models is that the parameter is only applicable to its respective steady state condition, thus experiments at various SOCs and temperatures need to be completed in order to create the look-up tables for these types of models. In more detail of battery condition, SOC is used as a variable because it significantly affects

battery behavior. Considering other variables, temperature can damage the battery and C-rate dictates energy production and can increase internal resistance [55]. Aging is the characteristic battery condition changes over time which changes the model itself making the output less accurate. This can be captured in an additional State-of-Health (SOH) parameter [55], [123]. Although relatively more work is required up-front, this is a benefit discussed later in Section 3.4.

A common 1RC model used for EIS is the Randles model [54], using parameters similar to the Thevenin Model described previously including the resistance term as the bulk resistance (R_b) representing the electric conductivity of the electrolyte, separator, and electrodes, the charge transfer resistance (R_ct), double layer capacitance (C_dl), both representing the voltage drop due to activation polarization, and a term for the Warbug Impedance (Z_W) for the diffusion of Li-ions in the cell [47], [55], [84].

However, ROM usage in EV is not the same in all applications and should not be confused for use with HEVs because the model and parameter assumptions differ [111], [124]. Equivalent circuit models can be made for real-time EV applications with the balance between speed and accuracy. The selection of an appropriate EMC is a matter of 1) model structure selection, 2) experimental testing considerations and 3) error and fit criteria [55]. In EV applications, the goal of BMS design is to find a model structure with the correct balance between accuracy and simplicity. Optimization methods have been used in order to assist in the determination of precise and relatively simple RC network model structures [55] [125].

Battery models can be further segmented into model type (empirical look-up table or function solving), variables included (SOC, temperatures, C-rate, SOH, and combinations there of), and parameterization technique of model components [55]. ECM models have evolved to include thermal and SOC capabilities [126].

Models have evolved into streamlined combinations of isothermal, continuous, piecewise-linear, electrode-average models using optimization methods such as the knot placement technique for instance [89]. The work conducted by Farag et al reduced the CPU run time by 20% when compared to reduced-order, electrode- average models and predict cell voltage accurately with less than 2% error [89]. Computational speed is important for the control of or monitoring of model parameters live, also known as in-line monitoring. State-of-the-art modeling used to predict cell voltage and battery response for BMS's has evolved to use actual automotive driving profiles [63], [89], [113], [119].

Battery management systems are only as accurate as the model used. Non-linear monotonic correlation between State-of-Charge (SOC) and Open Circuit Voltage (OCV) is necessary for accurate battery state estimation [127]. The OCV has been studied and shown to be a function of aging, temperature, and previous history using various battery active material choices (C/NMC, C/LFP, LTO/NMC) through a temperature range from -20 C to 45 C [127]. After their studies, Fermann et al. concluded that the OCV and the OCV hysteresis change over the battery lifetime [127].

Battery modeling and SOC estimation has technical and commercial implications from an improved understanding of battery safety during charge and discharge, for optimizing battery usage, and for improved accuracy of EV battery pack range. Another area of work is studying how to include complex battery models into an onboard battery management system (BMS) which needs to operate in real-time [55]. Understanding the SOC provides BMS's an estimate of the remaining available energy in the battery, insight into charge/discharge strategy, and an ability to protect the battery from over charge/discharge. A review of SOC estimation methods is provided by Hannan et al. by comparison of benefits, drawbacks and estimation error [68]. Li-ion battery operation, aging, and ultimately safety, is highly dependent on temperature. At low temperatures aging and performance is effected and at high temperatures thermal runaway is a safety concern. Low temperatures reduce the available energy and increase internal impedance [66]. Even though li-ion EV batteries have shown advantages when compared to other chemistries, commercial disadvantages of Li-ion batteries reveal issues of safety, cost, charging time, and recycling [66].

Model reduction methods include those that simplify the solid-state concentration function as a polynomial profile [128], further simplifying the solid concentration equation of the P2D model with parabolic profile (PP) approximation [129]. Evolving into more advanced methods of simplification for the electrolyte concentration [130], solid material concentration, and potential in State Variable Models (SVM) first developed by Smith et al. [65], [131]. Improvements of the battery modeling include Electrode Averaged Models (EAM) [132], P2D models simplified with: proper orthogonal decomposition [62], polynomial profile (PP) approximations of x-direction dependent functions (pore wall flux, solid phase concentration, electrolyte

concentration), simplified PP profiles [133], SPM models including thermal considerations [134], reduced P2D models [135] also including temperature considerations [Klein, 2013], reduced SVM [92] into extended single particle models (ESPM) [104], and ESMP models that account for temperature [111].

Model reduction methods evolved over time and each simplification method has advantages and disadvantages [61]. The P2D model simplified using polynomial profiles by Subramanian et al. are dependent on pore-wall flux, ionic conductivity of the electrolyte, solid phase average concentration, and electrolyte concentration have advantages of speed in comparison to finite difference approximation methods of P2D's and disadvantages that the pore-wall flux is not a function of time causing increased error at high C-rates and when considering battery aging [96], [129]. The SPM model developed by Gou et al. has an advantage of accounting for temperature but a disadvantage of accuracy only at low C-rates [134]. The reduced P2D model proposed by Forman et al deemed accurate with other ROM techniques but the CPU time was inadequate for use in real-time applications. However, this was improved upon by Dao et al. by incorporating polynomial profiles and Galerkin approximation with an advantage of significantly reduced CPU time and a disadvantage of Li-ion wall flux particle parameters modeled as constant [136]. The reduced SVM model developed by Lee et al. changed fully physics based equations to computationally simple representations with advantages of decreasing the CPU time and providing relatively high C-rate capabilities up to 2C, but with disadvantages of the mathematical complexity[137]. The P2D model developed by Klein et al. used polynomial profiles of solid concentration, ignoring changes in electrolyte concentration, this provided advantages in being able to account for temperature considerations but this model has a

disadvantage in applicability at C-rates of 2C or less [138]. In 2013, Luo et al. accounted for non-uniform Li-ion wall flux in an Extended Single Particle Model (ESPM) providing advantages of accurate results with P2D models for C-rates larger than 4C while having a disadvantage of minimal errors in the cell potential curves [139]. Through Padré Approximation, Maracki et al, developed a P2D model having advantages in control and parameter identification [85]. Rahimian et al. used an ESPM to predict electrolyte potential as well as concentration both as a function of time proving advantageous in its accuracy relative to COMSOL P2D and SP models from 1C to 5C-rates, although having disadvantages that it does not account for temperature and aging [104]. More recently, to account for temperature, Tanim et al used an ESPM model obtaining the temperature variable as an input from sensors on-board the battery providing improved accuracy in comparison to P2D models and speed fast enough for control, however this method was not accurate above 5C rates or below -10 C, which is still a substantial improvement from earlier techniques [111]. An advanced simplified Electrochemical Multi-Particle (SEMP) model developed by Majdabadi et al is able to handle particles with various radii and properties with an advantage of improving accuracy with experiments up to C-rates of 5C, with a disadvantage that this verification only was conducted on a Li foil/LiFePO4 cathode half-cell [140].

In comparison of P2D, SPM, and PP approximations, there are differences for varying discharge rates and accuracy. The second order PP and SPM models are both useful for discharge rates at or below 1C while at higher discharge rates the second order PP is more accurate until characterizing pulse loads. The CPU time is 100 times smaller for the PP model in comparison to

the P2D model. However, to successfully reproduce the PD2 results, higher order models must be used [113].

The change of battery parameters over time has lead to advanced ROM techniques of real-time on-line parameter identification. With on-line parameter identification, the model parameters can be calculated real-time for calculation of battery performance. Methods of on-line parameter identification have been studied called adaptive battery models [61], [88]. Temperature and current can be measured on-line, but SOC cannot be measured directly and needs to be estimated. The accuracy of SOC estimation is important and can be obtained by common methods of 1) Coulomb-Counting, 2) look-up tables or polynomials relating SOC to OCV, or 3) recursive adaptive filters such as utilization of the Kalman filter. The Coulomb Counting (CC) method is powerful and can be used as a reference to evaluate other SOC estimation methods. However, if the initial SOC estimation is inaccurate, errors accumulate in the calculations. The most common group of SOC estimation method is to use recursive adaptive filters [142]. Filters such as the Kalman filter use the error between battery output and model prediction, which is initially large.

3.3. Numerical Modeling

Analytical models are necessary for characterizing battery behavior and ideal for 1D analysis, especially calculations for BMSs. However, Finite Element Analysis most suitably solves the scalability into two- and three-dimensions. Battery modeling for electric-vehicle safety is a multi-physics and multi-scale effort. The robust parametric capability and ability to solve large detailed systems makes Finite Element Modeling an appealing choice for understanding

batteries. As of 2014, work toward accurate finite modeling has focused on an automotive industry need for predictable and efficient methods for simulating battery deformation and failure in crash situations. State-of-the-art simulation efforts to aid in the design of improved battery safety encompass, studies of deformation, mechanical and electro-chemical failure.

Finite element simulations have been created by Jeon (Abaqus) [143], Yi (ANSYS) [144], Sun 2015 (Comsol) [145], and Sievers (Modelica) [69] for cylindrical and pouch cell geometries. The simulations utilize the Bernardi model or adaptations of it for application of heat generation. Jeon et al. used a conservation of energy model considering heat generations due to both joule heating and entropy change to solve a transient FEA problem in LiCoO2/C and LiNiCoMnO2/C cylindrical cells [143]. The resulting maximum temperature profile analyzed contributions of each heat sources at several discharge rates. It was found that Joule heating is significant contributor at high discharge rates, while at low discharge rates, entropy change was dominant [143]. Local heat generation is modeled with an enhanced single particle model. Furthermore, the ESP model is implemented into a two-way coupled electro-thermal simulation utilizing a 3D thermal solver with a quasi-3D porous electrode solver applied to the plane of spirally wound electrodes [82]. Additional simulation investigation of 3D spirally wound cylindrical cells with thermal capabilities has been conducted by Lee et al. [146] and other research groups [96], [147].

Simulation software with built in capabilities for lithium-ion battery specific modeling includes LS-Dyna [85], [116], [148]–[150], COMSOL [61], [62] and Abaqus [148].

3.4. Modeling Health of the Battery

Modeling techniques from analytical to ECM representations for li-ion batters have disadvantages and advantages for BMSs. Currently, a limiting drawback on long-term accuracy of models used in BMSs is the inability to account for cell SOH in terms of electrochemical aging, thermal damage, and structural damage. For example, in an ECM representation, the electrode performance is characterized by specific components of the circuit as well as the separator component of the battery contributing to the circuit embedded inside model parameters [115]. Aging of the battery has been shown to decrease the capacity, SOC, over time [68]. This decrease in performance is consolidated into what is called the State of Health (SOH) of the battery [63]. Although research has been conducted on electrochemical contributions over time to SOH, this study focuses on more physical phenomena such as thermal damage and mechanical damage of the battery. Thermal and Mechanical damage are risk factors especially in EV applications of Li-Ion batteries. Understanding how battery performance is affected by physical SOH influences can ultimately improve battery safety.

A disadvantage of empirical BMS models are that they do not account for the change in battery model parameters with aging and the model is only specific to one type of cell [61]. Simplified P2D models have been developed in attempt to remedy the problems of empirically based BMS models and more complicated models. As a compromise, the simplified models receive inputs such as voltage, current, battery temperature, and ambient temperature, with outputs such as SOC, SOH, aging status, parameters inside, parameters outside, and internal temperatures used for control, on-line monitoring, optimization, parameter estimation and age prediction [61].

Equivalent modeling of healthy batteries begins with identification of associated model parameters from empirical data. Variations of commonly used RC equivalent circuit models may take the form of Fractional-order Models (FOM) for which parameters are found with optimization methods and compared [113]. Furthermore, parameter sensitivity analysis in order to determine influence on the model output based on simulations under various conditions [151]. Sensitivity analysis and step-wise identification methods show very good results, such as a better fitting of the simulated cell voltage with experimental data [151]. With a modeling focus on estimation of SOC is explored deeply because the electro-chemical reactions and aging mechanisms are complex.

Li-ion batteries can be stressed by mechanical and non-mechanical methods that inhibit their healthy operation and can be chronic or acute dangers to the health of the battery. Non-mechanical stresses exhibited on the separator inside li-ion cells include intercalation stress and thermal stresses. The intercalation stress is a produced by the expansion and contraction of the electrodes [110]. With a composition made up of various materials, li-ion cells by design will contain thermal stresses. Heat generation [81], [152], [153] and heat transfer [79], [98], [101], [154]–[156] are understood, but the fatigue due to internal thermal stresses is not understood [110].

Chronic/Normal Aging

Even during normal operation, battery health is effected by aging. Conditions such as current imbalance can accelerate pack aging [64]. Current imbalance can be cause by cell-to-cell chemical variation or variation in operating conditions [64]. A failure mechanism caused by

normal aging of the battery is an internal short circuit caused by SEI layer growth dendrite formation. From an in-depth investigation of why this happens, Ashwin et al. concluded that he thermal imbalance has more impact than the change in inter-connecting resistance on the split current distribution, which accelerates the irreversible porous filling and ageing [64] . Research has shown a strong influence of cycling temperature on thermal stability [157]. The variations in performance are mainly attributed to aging effects on the anode side specifically, by the formation of an effective SEI during cycling for which the magnitude is temperature dependent [30], [157]. On the cathode side, decomposition of the cathode is main contributor to thermal runaway and the subsequent reactions with the electrolyte [157]. Reactions such as, evolving gases which confirmed the severe degradation of the electrolyte and active material during cycling at 20 C [157]. As for temperature dependence, the cells cycled at 45 C show an improved electrochemical performance over the lifetime of the cell than those cycled at 20 C [30].

Another example of a key performance indicator of aging is the lithium content. Experiments have studied the lithium content of/at the individual components of the cells for different states of charge (SOCs) by inductively coupled plasma-optical emission spectrometry (ICP-OES) and the lithium distribution as well as the loss of active lithium within the cells is calculated after cycling [158]. With increasing the SOC, the lithium contents decrease in the cathodes and simultaneously increase in the anodes [158]. The temperature increase shows a clear shift of the lithium content in the direction of the anode for the T-cells [158]. The comparison of the C-rate influence shows that the lower the C-rate, the more the lithium content on the electrodes is shifted into the direction of the anode [158]. Models for control and battery management are

designed to monitor the concentration and potential [63]. However, models lack more significant parameters such as variable double layer capacitance, the full current-over potential relation and over potentials due to mass transport limitations [63]. Srbik et al. developed an improved coupled electrochemical and thermal model accounting for capacity fade via a loss in active species and for power fade via an increase in resistive solid electrolyte passivation layers at both electrodes with a capability to simulate cell behavior under dynamic events. The model is validated against test procedures, such as standard battery testing load cycles for current rates up to 20 C, as well as realistic automotive drive cycle loads [63].

An additional model variable with significant influence is the separator. Although it is an inactive component in the electrochemical interactions inside a cell [159], the properties of the separator and its influence on other variables of the electrochemical response are represented in some analytical models such as the Pseudo-2D model developed by Jokar et al [61]. In the Psudo-2D model the separator is a variable in the liquid-phase positive Li-ion concentration (c_e) and liquid-phase potential (Φ_e) calculations. An ideal separator has infinite electrical resistance and zero ionic resistance. The presence of the separator in between the electrodes inherently increases the ionic resistance because the non-uniform surface of the separator restrict the contact area between the electrolyte and electrodes and the porous channels create an indirect pathway for the ionic current [61] [160]. Also, increasing the porosity and optimizing separator thickness reduced the conductivity of the liquid electrolyte [160]. Specifically, the separator parameters (porosity, thickness, pore size, pore diameter) influence the MacMullin number (N_M) and tortuosity ($\boldsymbol{\tau}$), both factors in the ionic conductivity of the separator [160]. Manufacturers of separator material seek a balance between porosity and mechanical strength. If a separator is too

think the lack of strength creates a risk for internal short circuits. Typical separators range between 20 and 30 um in thickness with porosities ranging from 40% to 70%. Further separator focused research has revolved around studying the thermal stability, wettability of the separator [159] and high rate charge-capacity [160]. The separator has been shown to have minimal effects on cell performance at discharge rates below 20C [160]. However, when the stability is compromised, the relationship between thermal response and aging response with respect to the separator specifically has not been studied in depth. Volck et al. has begun to investigate the matter with research on "dummy" pouch cells [39].

However, modeling lithium ion batteries using analytical models do not include a parameter for the separator porosity. Simplified equivalent circuit models are developed to use empirical data to accurately determine model parameters. First, these parameters are usually found for healthy, undamaged cells. Second, even robust equivalent circuit models do not have a parameter for separator porosity. Opportunity exists to develop a model to include the health of the separator and at this time, porosity is a physical indicator of the health.

The challenge of multi-physics modeling is to obtain the material properties and model parameters for the system [110]. We are using reduced order ECM based equations, which contain empirically derived parameters. This approach allows us to use temperature and damage dependent parameters; a first for ECM modeling and Li-ion battery simulations. The ECM equations are adapted in the LS-Dyna simulation environment allowing for the benefits of large deformation capability as well as the parallel processing capability on an HPC. A combination of the reduced order ECM model and ability to run simulations in parallel allows for new 3D

lithium-ion simulation capability to be utilized at its highest potential. We have the capability to build cells and run experiments, study uses 1D model where we use 3D LSDYNA and can run large format simulations, and we have a highly accurate structural simulation with calculated material properties.

Pingel et al., conducted an in-depth study of isolating separator damage to study the effect on battery performance. With complete control over battery manufacturing, 0.012 Ah coin cells were made using Celguard 2325 separator that was damaged by means of mechanical loading, heating near the melting temperature, or a combination of the two. The material was damaged prior to assembly of the coin cell; a unique capability for isolating damage effects on cell performance. Damaged material was used to manufacture the batteries as well as reserved for experimentation and characterization. The material serves the purpose of separating Cathodes and Anodes in a battery while allowing lithium ions to transport during energy producing chemical reactions. Porosity of the Celguard separator is a physical parameter of the material that dictates the quality of the electro-chemical reactions. The porosity of the undamaged and damaged material was characterized by studying measurements of pores with an SEM as well as a using Mercury intrusion porosimetry. Separator samples were mechanically loaded at 15 kN, 30 kN, 45 kN, and 60 kN and heated to 110 C and 135 C. Results correlated well, showing that as mechanical load increases, porosity size of pores decrease and porosity decreases. As temperature increases near the melting temperature the porosity decreases. Loads of 0 kN, 15 kN, 30 kN, 45 kN, and 60 kN corresponded to porosity values of 41±1%, 35±1%, 32±1%, 21±3%, 18±2% respectively. Temperatures of 110 C and 135 C corresponded to 27±1% and 19±5%

respectively. In comparison, 15 kN loads compared to110 C heated and 60 kN compared to 135 C heated resulted in similar porosity values.

Acute/Catastrophic

Other mechanisms of health degradation include acute/catastrophic failure and chronic longer-term degradation. Mechanical damage specifically contributes to significant risk for both failure mechanisms. Catastrophic failures due to mechanical damage are cell puncture, internal, and external short circuits. Chronic failure occurs from damage, which effects battery performance, but gradually over time. The influence of chronic health changes in battery modeling state-of-the-art. When applied to ECM, some parameter identification of un-healthy batteries has been investigated.

Advanced model accuracy under different conditions is compared with that of conventional Randles model and the parameter variations at different stage of the aging process are studied [161]. Characterizing battery model parameters has led to improvements from traditional pulse power characterization (PPC). Improving modeling accuracy and reduction in the experimentation time, per state-of-charge (SoC) and temperature, to several minutes compared to several hours for a PPC experiment [119]. Research into progressive improvement of BMS technology has lead to adaptive identification algorithm of model parameters on separate time scales showing validation with experimental results that the strategy performs better than the traditional RLS based identification methods [120].

4. Advancement in Lithium-Ion Coupled Field Simulation

Following the review of modeling methods by Jokar, suggested modeling improvements are outlined as follows: (1) an in-depth investigation into the effect of operating variables and polynomial profiles selected for approximation; (2) account for the nonlinearity of Li-ion internal parameters with more advanced functions, suggesting improvements for current density, electrolyte properties, and pore wall flux; (3) since current models accounting for temperature have only been used to model C-rates up to 1C rate, for applications in BMSs explore an improved understanding of internal heat generation, temperature-dependent properties and effects of pack geometry, (4) enhance the capabilities of P2D governing equations to account for aging sources, side reactions and Solid Electrolyte Interface (SEI) growth; (5) account for aging for improved battery control with a focus on age prediction as well as SOC and SOH estimations; and (6) further investigate reliable modeling for LiFePO4 cathodes for an improved understanding of Lithium insertion/extraction and micro/macroscopic models suggesting models that include variable cathode parameters [61].

In this study a numerical and experimental investigation addresses the recommended future work in the field of li-ion battery analysis in order to build a state-of-the-art modeling capability. Specifically, the recommendations from Jokar that have been addressed include: (3) model parameter temperature dependence by HPPC cycling at various temperatures and states-of-charge and aging or damage mechanisms of (4), and (5).

4.1. Overview

This work builds on modeling and structural characterization foundations by Gilaki [45], [46], [46], [150] as well as experimental characterization of separator material by Martinsen [48], [162] and Pingel with influence from prior research in the field in order to create an accurate model of the cell physics then building upon it to include novel capabilities of accounting for damage.

4.2. Structural Domain

The multi-scale groundwork of the simulation geometry was created by Gilaki et al [150]. A layered cylindrical cell model created in LS-Dyna was used to accurately model structural deformations of a 6P spirally wound cylindrical cell. Extensive work has been conducted by Avdeev/Gilaki [46] and Martinsen et al. [48], to build and validate an accurate structural finite element model of individual lithium-ion cells. Development of an accurate finite element model consisted of thorough material testing of individual battery material components in various environmental conditions the battery can be exposed to. Compression and impact testing on cells were conducted in order to investigate catastrophic deformation conditions and potential short circuit scenarios. We set out to answer how we might design battery cells for safety without conducting dangerous experiments. The battery cells used to develop structural parameters and geometry for the numerical model happened to be uncharged dummy cells. A unique defining characteristic of this work is the access to dummy cells. This allows for safe structural abuse analysis compared to the volatility of a charged cell. CT scanning was used to investigate and compare internal deformations and critical short circuit areas.

Being able to locate the precise location of a short circuit is one of the key objectives of this research. We have developed an algorithm to locate potential short-circuit locations based on stress/strain criteria derived from the finite element analysis results. The developed algorithm allows us to detect separator thinning and tearing – one of the key mechanisms leading to electric shorts and subsequent catastrophic failure. Identified elements of the short circuit algorithm become sources in the thermal and electrochemical simulation.

4.3. Thermal Domain

Using existing modeling results as a heat generation input load for the thermal simulation, the thermal effects on surrounding cells can be studied. Improved understanding of the temperature distribution and model accuracy for deformed cells is a valuable asset that current research is lacking.

With the groundwork in place, an explicit LSDYNA model was developed to study the transient heat generation of deformed battery cells, starting with a single cell model as a baseline. Ultimately, understanding of the single cell thermal response in a deformed and un-deformed state will be useful for battery module and pack simulations.

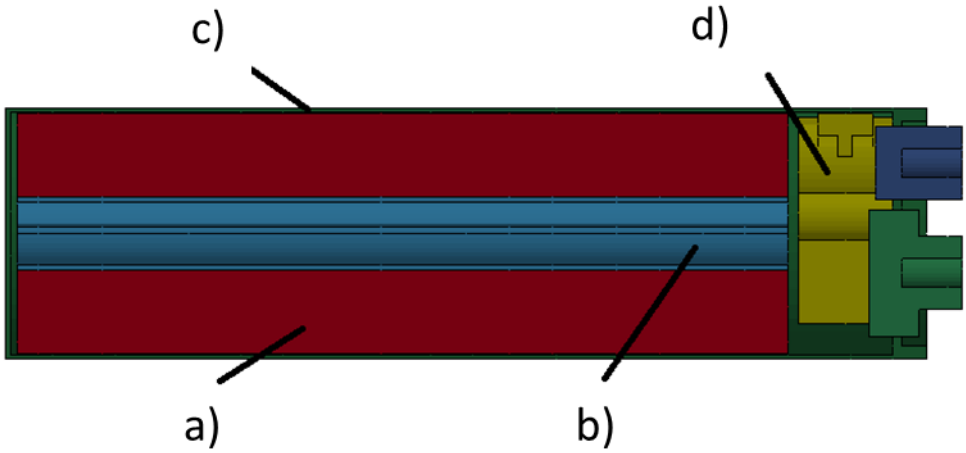

Figure 9. Baseline 6P cell geometry adapted from Avdeev et al. [46]: a) jellyroll, b) core, c) case, d) spacer.

First, the single cell model was created in LSDYNA with nodal-element information of un-deformed and deformed cells from the final deformed geometry after structural simulations performed by Avdeev and Gilaki [45], [46]. Their geometry is shown in Figure 9. The baseline un-deformed thermal model is constrained and loaded in accordance with studies by Sievers [69]. With an initial temperature of 298 K, the temperature of an un-deformed cell after 300 seconds reached 320 K; a 22 K increase; see Figure 10.

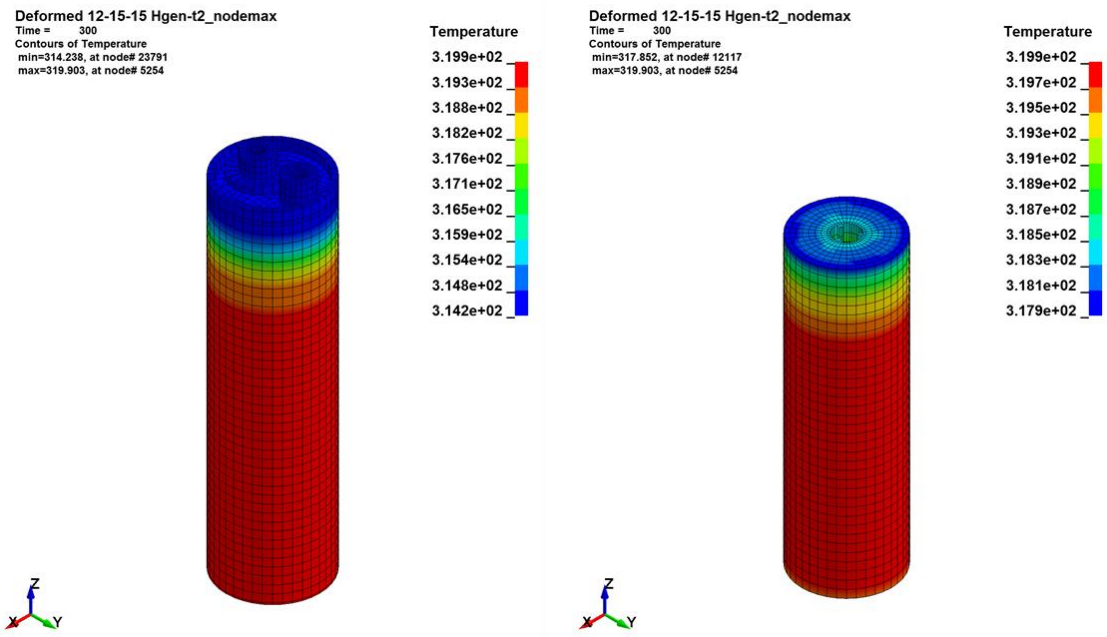

Figure 10. Undeformed thermal response of a cell: (a) outside casing and (b) homogenized jellyroll.

With an accurate baseline model, we can study the heat distribution of deformed cells; see

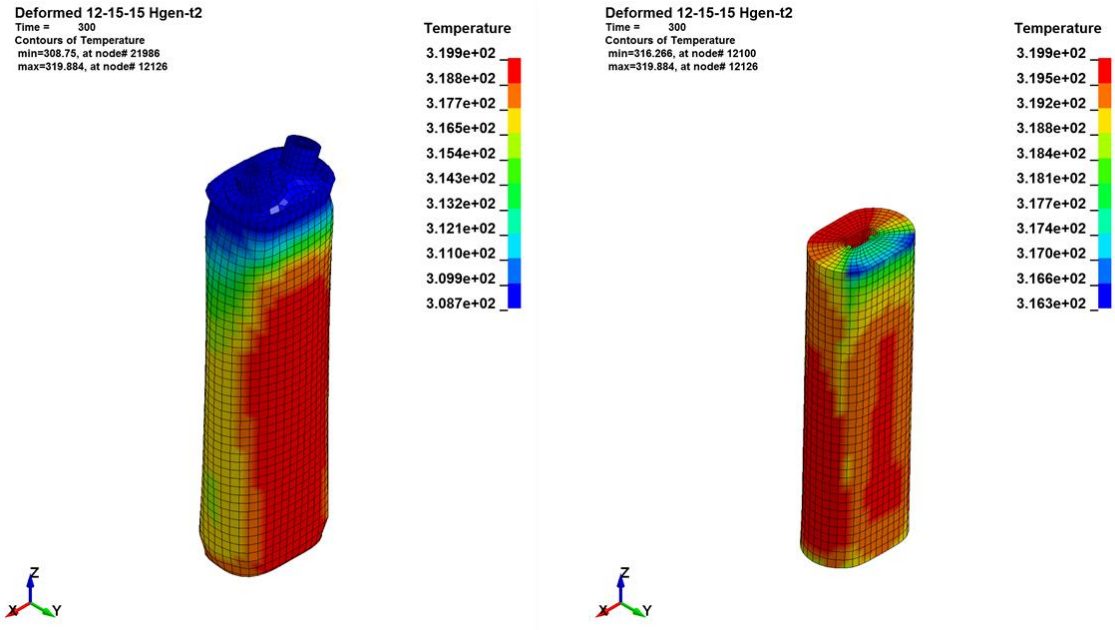

Figure 12 and Figure 13. Heat generation in a cell can be classified between two situations: those resulting from a short circuit and those that are due to normal operating conditions; see

Figure 11. Without a short circuit scenario, heat generation is a result of typical charge and discharge modes only with varied geometry.

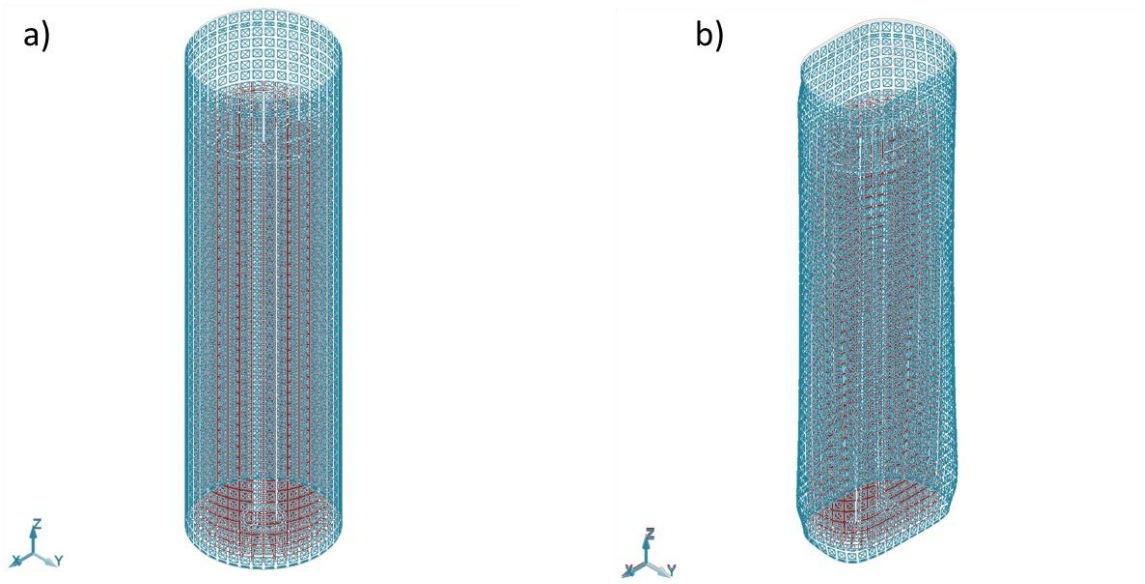

Figure 11. Boundary conditions of homogenized volumetric heat generation and convection: a) undeformed cell, b) deformed cell.

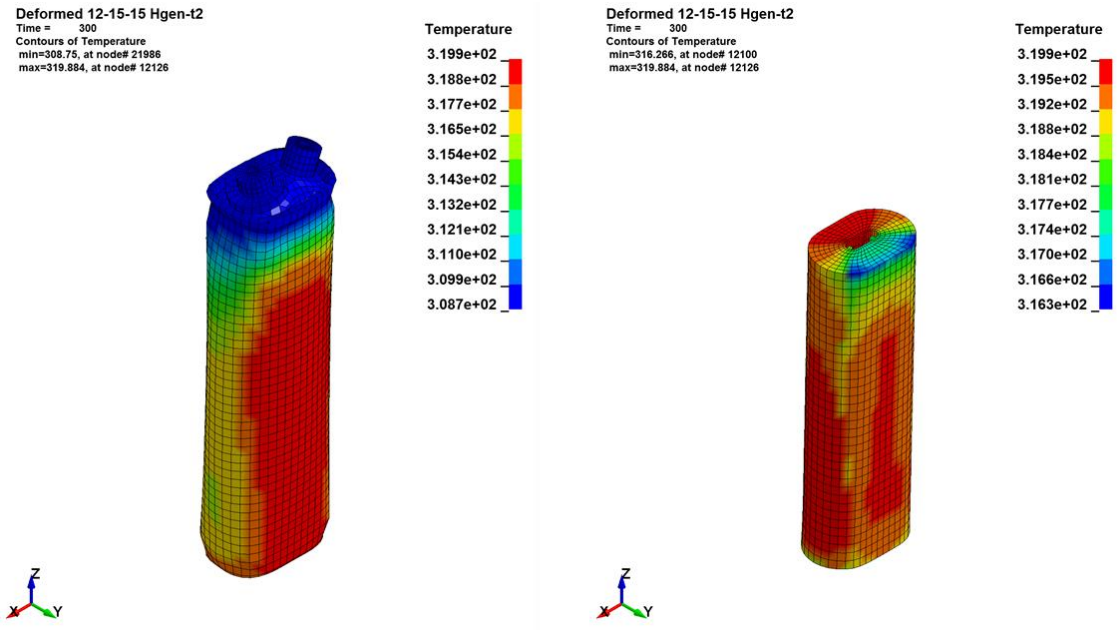

Figure 12. Thermal response of horizontal lug deformation with homogenous heat generation: (a) outside casing and (b) homogenized jellyroll.

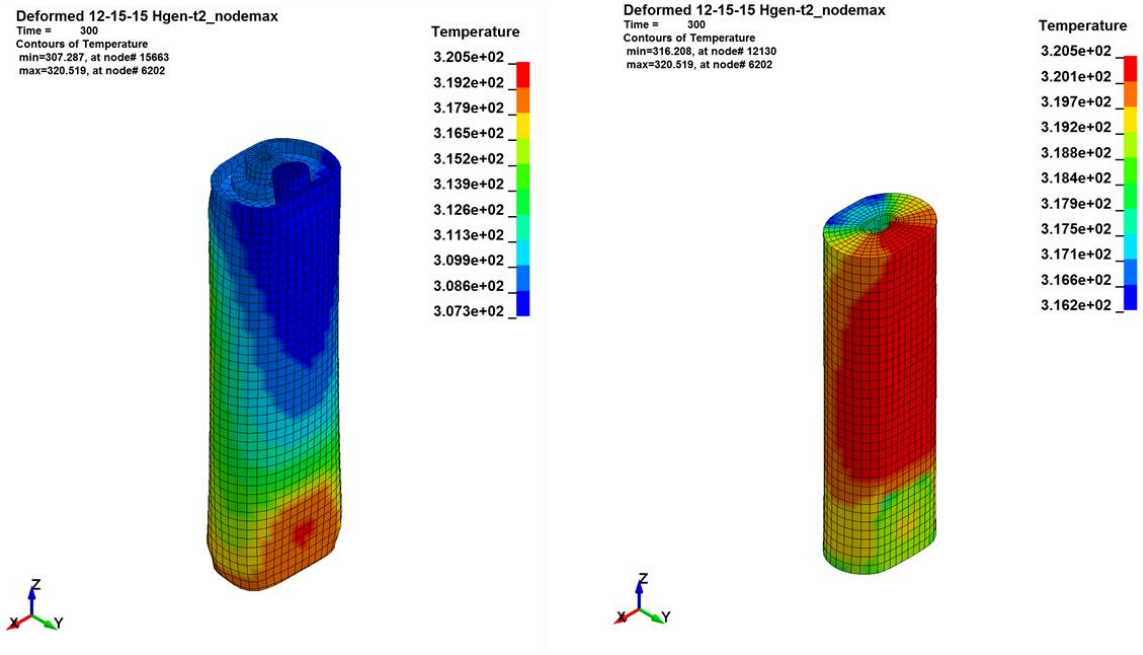

Figure 13. Deformed Thermal response of vertical lug deformation with homogenous heat generation, no short circuit: (a) outside casing and (b) homogenized jellyroll.

With a critical short circuit scenario, the heat generation response can lead to potential thermal runaway situations. Two examples of critical impact orientations are vertical and horizontal lug orientations. The source of heat generation after either short circuit situation was assumed to be at the point of the short. Short circuit locations included external lug contacts and for an internal short as locations of critical separator stresses above its ultimate strength; Figure 14 shows the two critical short circuit load conditions. Further investigation of cell orientation during internal short circuit is depicted by Figure 15 and Figure 16. The maximum temperature after 300 seconds reaches 298 K.

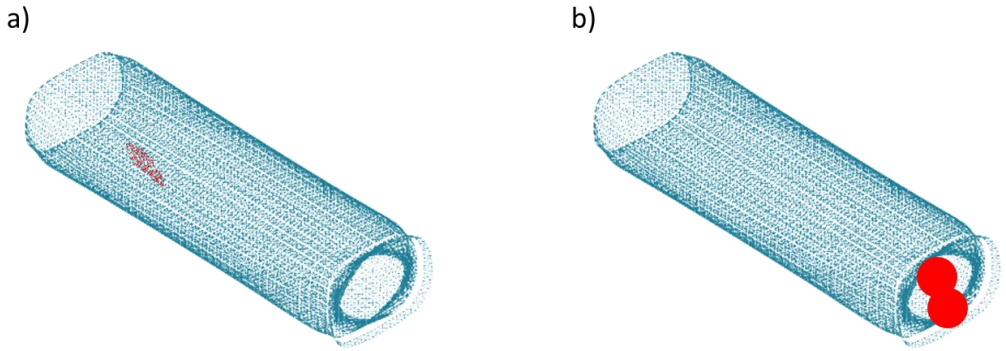

Figure 14. Volumetric heat generation in response to: (a) external lug contact and (b) internal short circuit.

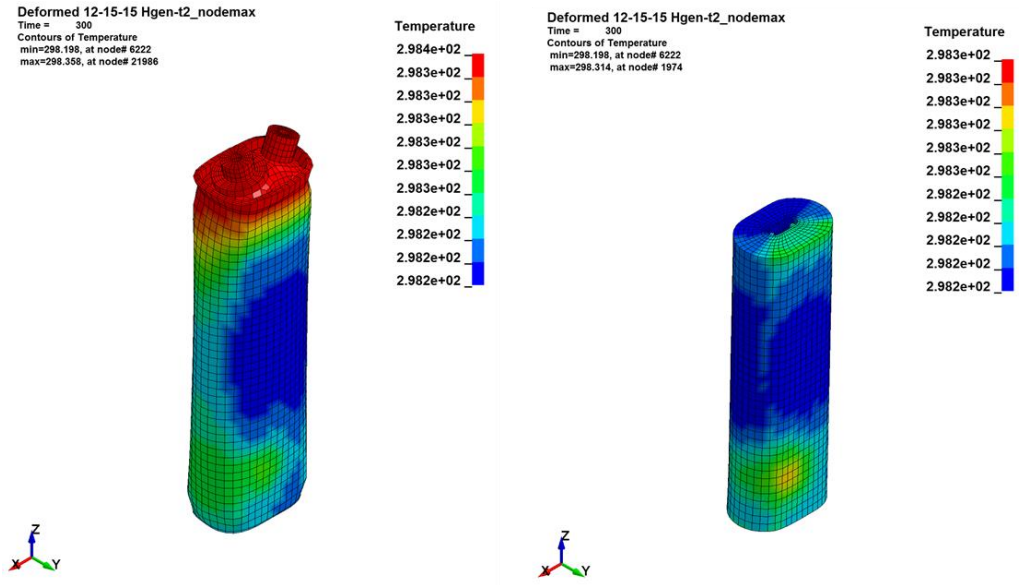

Figure 15. Thermal response of horizontal lug deformation after internal short circuit: (a) protective aluminum case and (b) homogenized jellyroll.

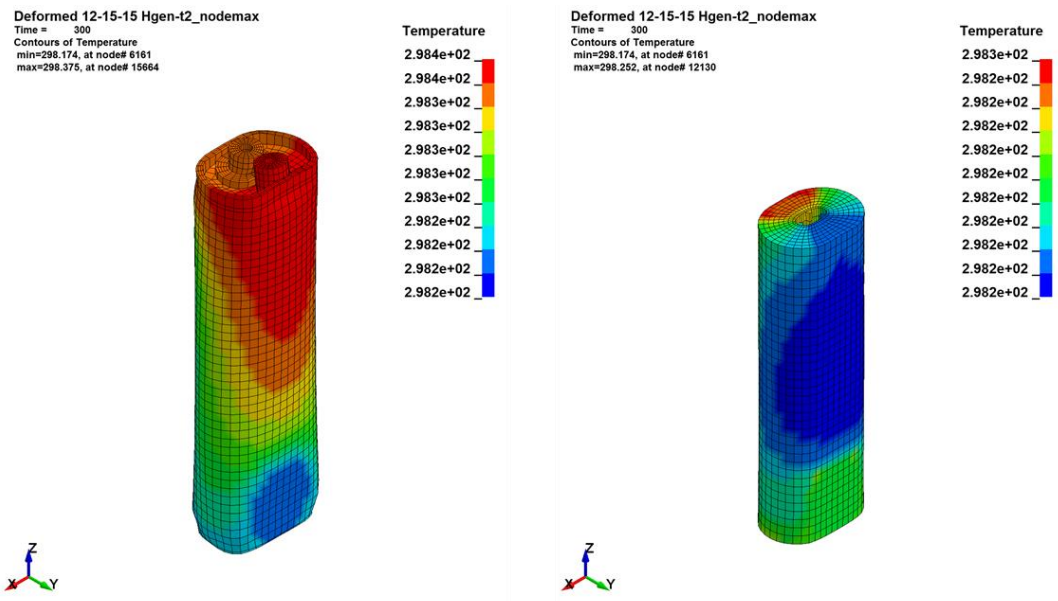

Figure 16. Thermal response of vertical lug deformation after internal short circuit: (a) protective aluminum case and (b) homogenized jellyroll.

The current assumption for short circuit simulations is that the heat generation value remains the same, but is applied only to the location of the short circuit in the deformed model. However, more investigation is needed to confirm the heat generation characteristics of a short circuit. The location of short circuit was determined by an algorithm monitoring external lug contact and maximum strain of internal jellyroll layers. Upon contact or a strain value above a critical threshold, the elemental data is saved and used as locations for future time steps where heat generation will be applied.

The thermal LSDYNA model cell model is a collection of inert and active materials for the battery cell. The inert material consists of the plastic spacer and inner tube. The active materials of the cell include all materials associated with the energy production processes; the jellyroll, the outer casing and lugs. The thermal properties for all materials are homogenous except for that of the jellyroll. The tightly wound collection of micro-scale layers results in orthotropic thermal

properties larger, i.e. more resistive, in the radial direction than in the axial direction. This assumption is adopted from Sievers [69]. A summary of the thermal material characteristics is shown below in Table 1.

Table 1. Thermal material properties.

		Thermal Conductivity [w/mmK] [sievers 2010]				
Component	Material	K_{xx}	K_{yy}	K_{zz}	Density [kg/mm3]	Specific heat capacity [J/kgK]
Case	Aluminum		.015		12.7×10^{-9}	903
Jellyroll	Homogenized	.001	.001	.028	28.7×10^{-6}	385
Spacer	ULTEM		0.2×10^{-4}		31.3×10^{-9}	.02

Thermal load of the lithium-ion battery is simplified as a constant value during the duration of the simulation. The thermal load produced within the jellyroll is assumed to be a homogenous volumetric heat generation of 300 kW/m^{-3}, derived from experimental and analytical findings [69], [76], [163], [164]. However, the heat generation in a cell is not constant, Somasundaram showed that the heat generation changes with respect to discharge rate, SOC and time [83]. Future models will use more complex heat generation curves. Heat is dissipated by natural convection with a convection coefficient (h) of 5 Wm-2K-1 [83] and an ambient temperature of 298.15 K.

Different from structural impact simulations using a time-scale on the order of micro-seconds, a longer timescale, on the order of seconds to minutes was used for the thermal simulations. Not only was this timescale selected to show long-term behavior of the thermal cell, but comparative

results in literature also used similar timescales [69], [83]]. A time step size of 0.05 seconds and total time of 300 seconds were selected for the simulation.

The solver for this simulation was selected to be the diagonal scaled conjugate gradient iterative solver among other options such as the bi-conjugate, Choleski, non-symmetric, and symmetric direct solvers because of its explicit performance for transient thermal simulations and moreover its ability to be used in multi-physics analysis.

4.4. Coupled Field Modeling

The simulation evolves into a fully coupled-field representation using outputs from both the structural and thermal simulations. Full multi-physics modeling introduces additional non-linearity into the computation of simulation results making the solution process more complex. There are various numerical methods and simulation practices to account for complex multi-physics problems. Additionally, in this study the benefits of a parametric model are exemplified by introducing SOC, temperature, and damage dependence related to the change in porosity variable of the separator.

A numerical investigation of battery model parameters was possible with the parametric abilities built into LS-Dyna with the ECM simulation capability. Specifically, the Randles model parameters for Ohmic Resistance (r0), Polarization Resistance (r10), and Polarization Capacitance (c10) have the ability to be included in a look-up table as a function of SOC and temperature. The simulation is fed by the empirically derived parameters at various States of Charge (SOC) from 10% to 90% at 10% increments and temperatures 25 C, 40 C and 50 C. The

specific cycling method and determination of parameters will be discussed in Section 5.1.2 – Parameter Characterization. With the capability to study damaged parameters, the simulation explored the influence of parameters changes in order of magnitude, dependence on SOC, temperature, and the parametric changes due to mechanical and thermal stresses. This is an initial framework to objectively and comparatively investigate the impact of design variables by following a method of isolating them in an analytical model. The simulation will require further investigation and validation to become an accurate stand-alone design tool.

4.4.1 Multi-physics LS-Dyna Cell Simulation

The multi-physics li-ion simulation model is primarily built upon an accurate example of the latest battery modeling capabilities in LS-Dyna performed by L'Eplattenier et al. [116]. Within the LS-Dyna modeling environment, "keywords" are established to prepare the geometry, boundary conditions, loads, run the analysis, and specify what data to save. Pouch cell geometry was used to establish this capability beginning from early exploration of a single layer model isolating numerical and design variables individually. A progression of more than one hundred simulation iterations was created to achieve the current capability of a fully parametric 2.5 Ah, 30 layer pouch cell.

A representative three-layer pouch cell was used an iterative model to learn the robust capabilities of the LS-Dyna environment and objectively compare results and ECM modeling parameters. Specific LS-Dyna keywords and input files can be found in the Appendix. In more detail, the cell geometry dimensions were adopted from a Johnson Controls Inc. 140105 pouch cell having anode dimensions (129 mm x 77 mm) and cathode dimensions (127 mm x 73 mm),

40 mm wide tabs, with layer thicknesses as follows: aluminum current collector (12 **μm**), cathode (54 **μm**), separator (17 **μm**), anode (58 **μm**), and copper current collector (14 **μm**). In all, the 3-layer geometry was meshed an element size of 2 mm totaling 32,430 solid elements and 67,596 nodes where the 30-layer geometry contains 565,950 solid elements and 1,179,564 nodes; Figure # and Figure # show the element size distribution in the x-dir/x-dir and thickness respectively.

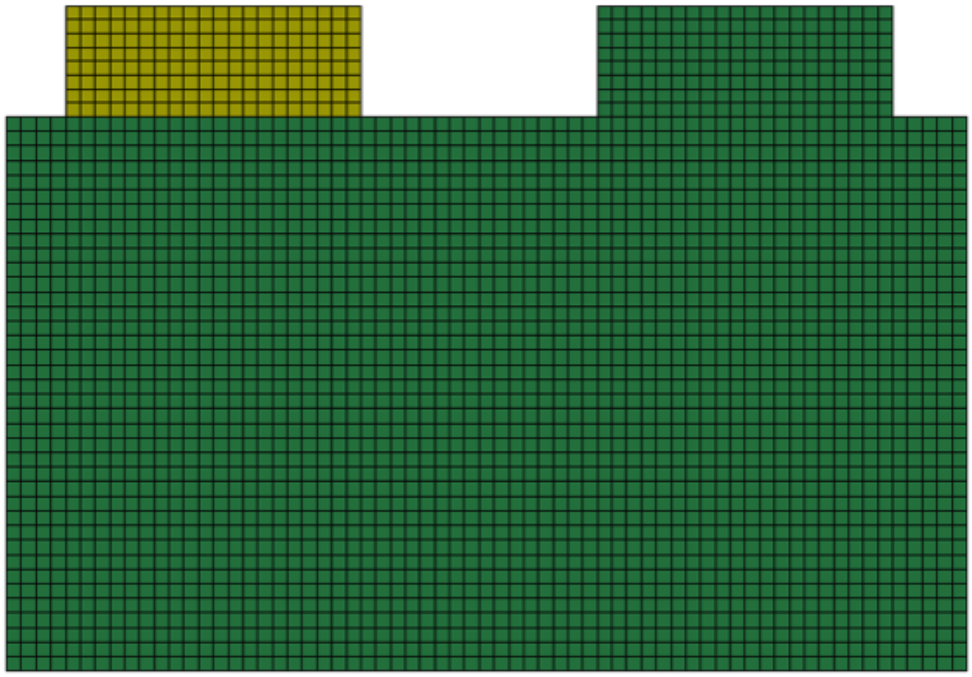

Figure 17. Top view of pouch cell geometry and element size

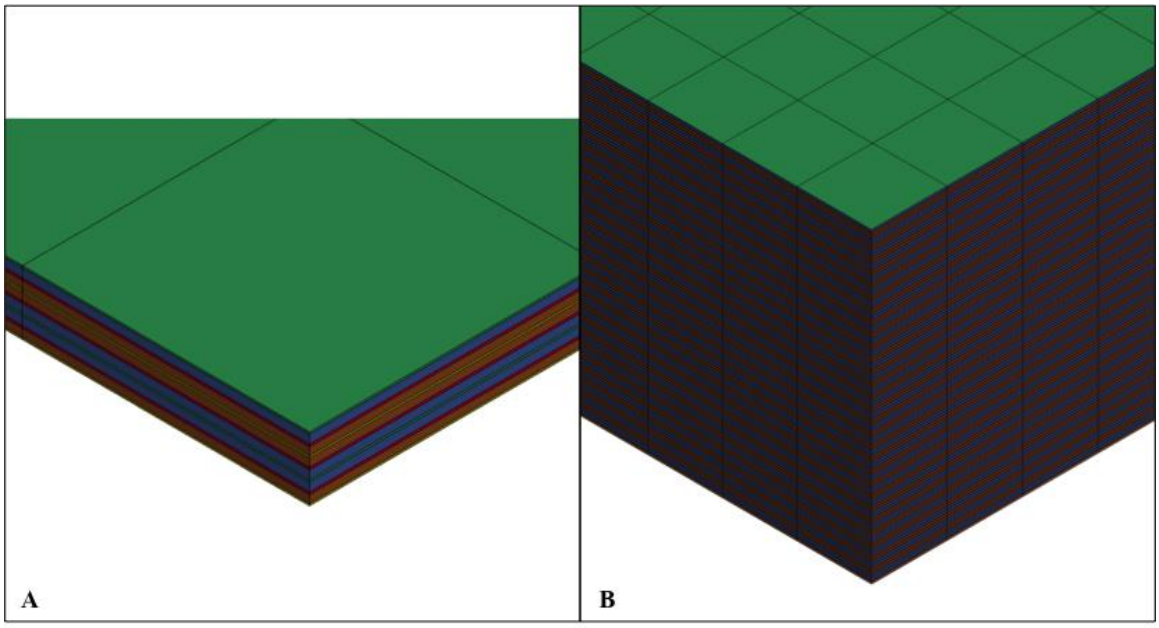

Figure 18. Cross-sectional views of pouch cell layer thickness. A) 3-layer geometry, B) 30-layer geometry

The multi-physics capability of the simulation is introduced from utilization of a Randles Circuit ECM battery module in the LS-Dyna software. A steady state 7.5 A (3C) current was applied to the top row of elements on the positive tab and a negative 7.5 A (3C) current was applied to the top row of elements on the negative tab. Input variables for ECM circuit parameters can be a function of SOC and Temperature. It is important to use accurate parameters, especially those corresponding to the damaged cells of this study, reinforcing the need for the R0 charge/discharge, R10 charge/discharge, C10 charge/discharge parameter determination study. Additional ECM parameters needed are the Randles unit area, initial SOC, SOC as a function of voltage and initial temperature.

The solution was completed by both the electromagnetism and resistive heating solvers for a maximum simulation time of 20 seconds and a time-step of 0.5 seconds.

4.4.2 Simulation results

The simulation is able to predict three dimensional distributions of parameters such as electrical potential, charge distribution, ohmic heating power, and temperature distribution as well as determine scalar values over time such as voltage and temperature Figure 19. The current density and ohmic heating power, shown in

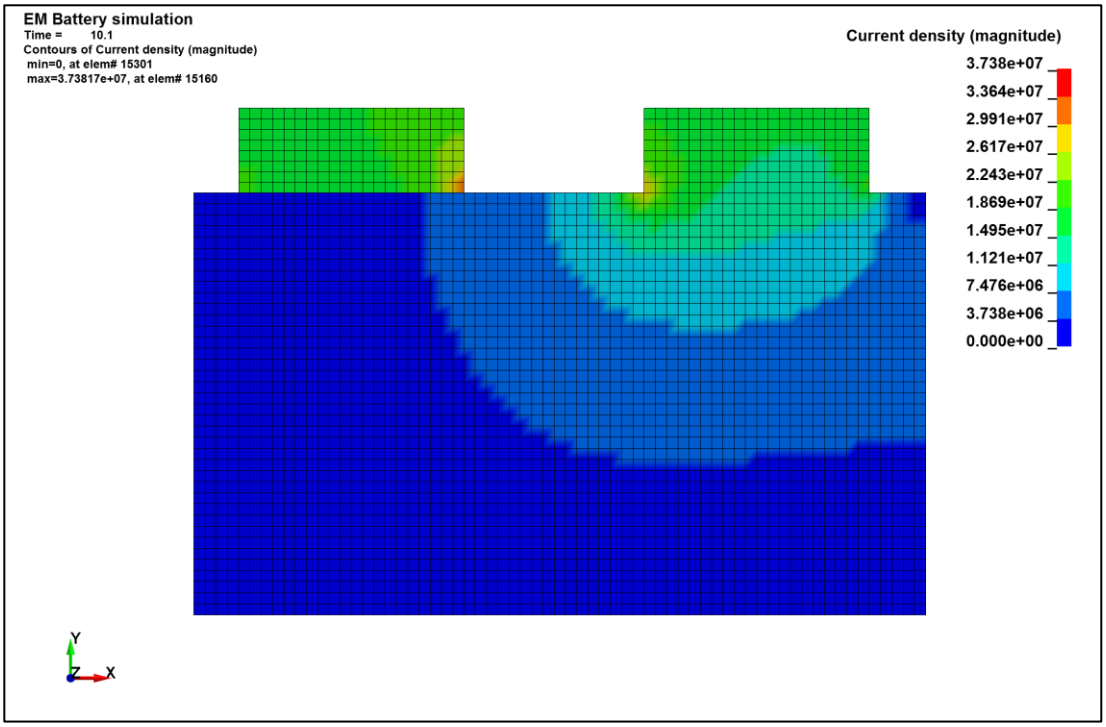

Figure **20** and

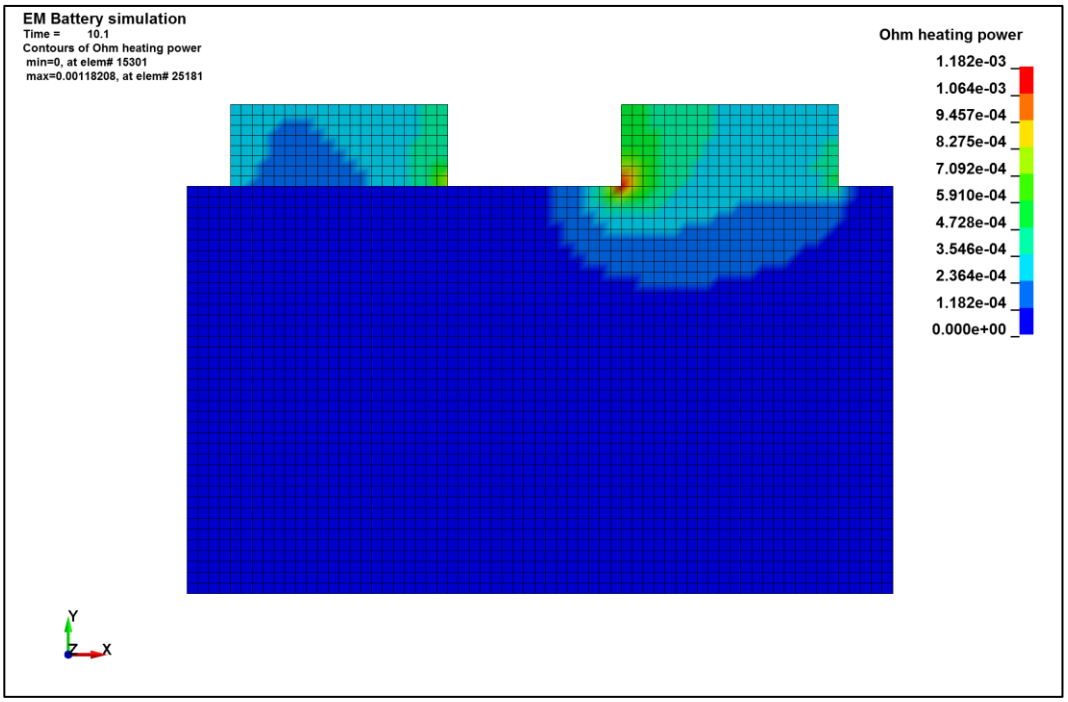

Figure 21 respectively, are isolated near the tabs. At these conditions, the temperature at the center of the cell, corresponding to a location monitored during thermal experiments, reached 30.0 °C, Figure 22.

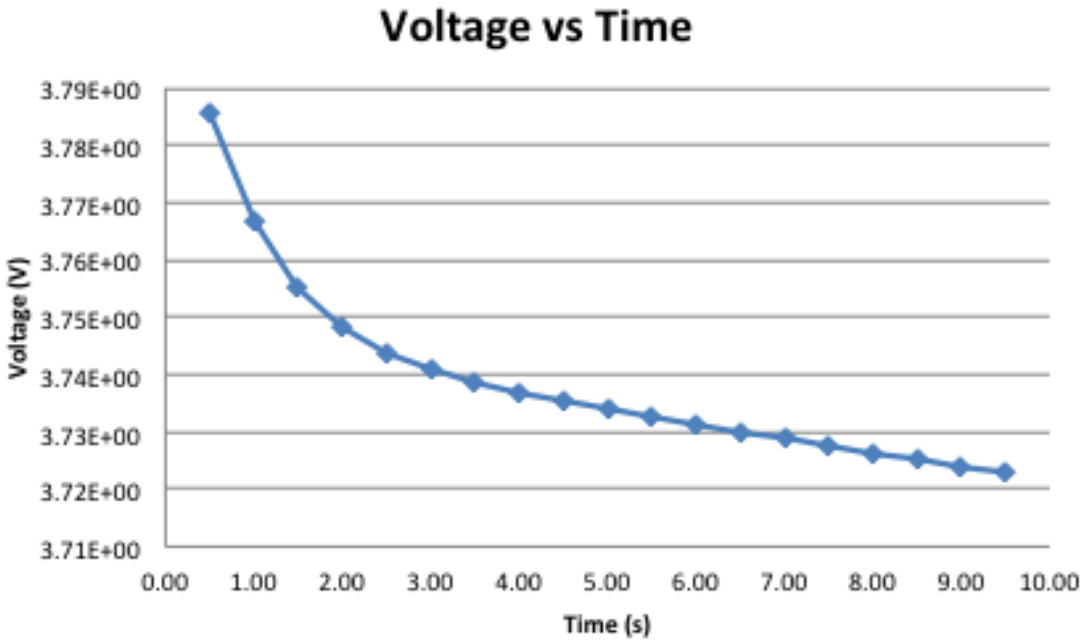

Figure 19. Example voltage output of simulation

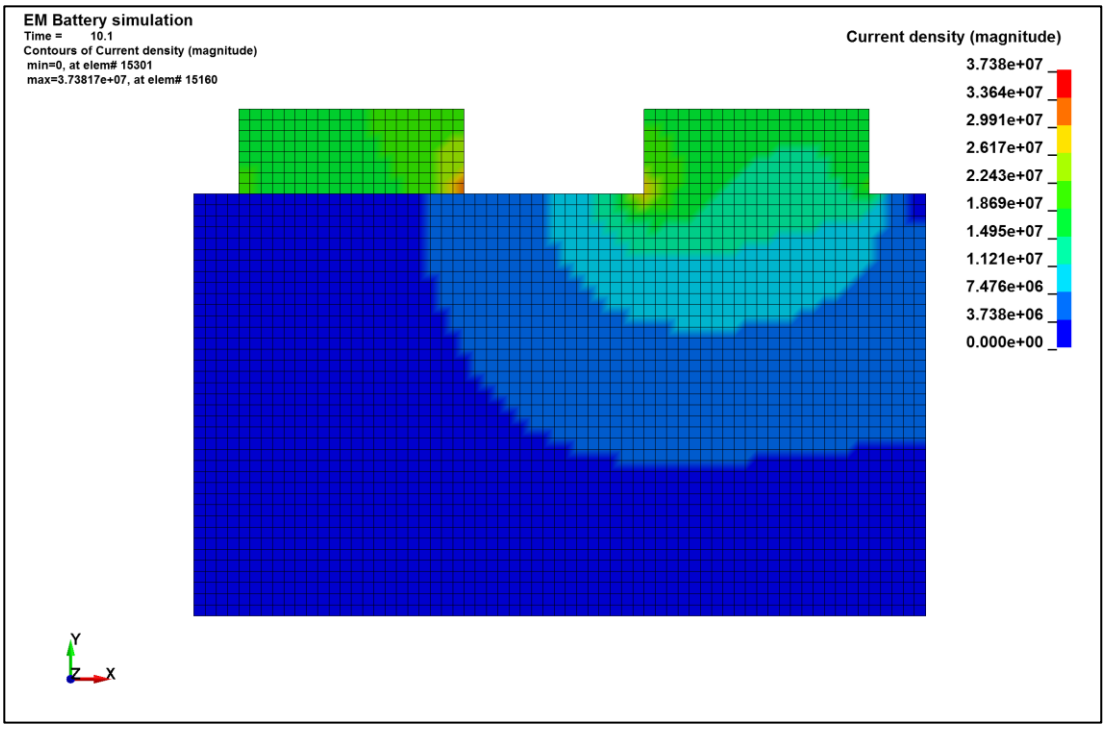

Figure 20. Example Current Density output of simulation

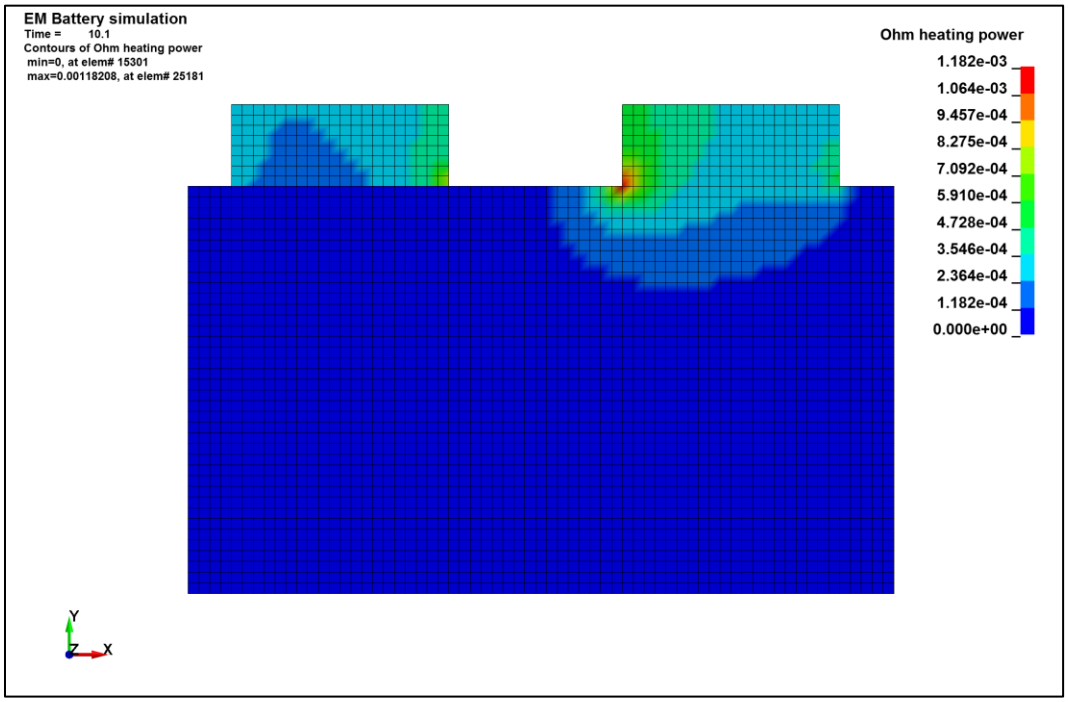

Figure 21. Example Ohmic Heating Power output of simulation

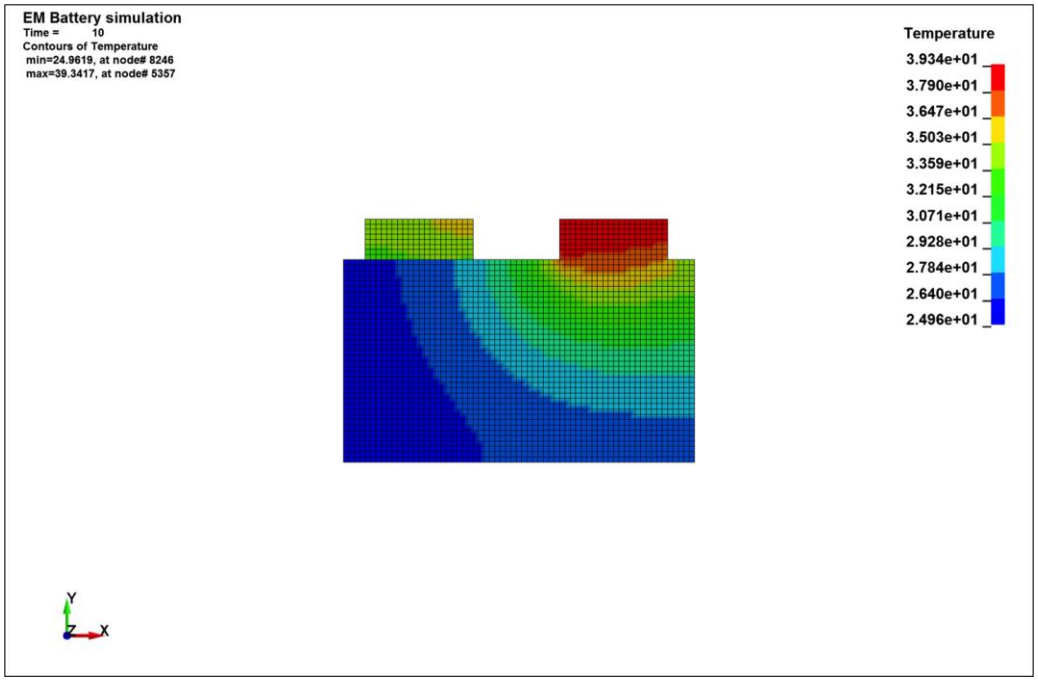

Figure 22. Example Temperature distribution output of simulation

5. Experimental validation

The validity of computational modeling depends on the accuracy of model parameters such as the choice of a material model and material properties. In collaboration with Avdeev and Gilaki, some of the work in this study is conducted to validate structural deformations of crushed lithium-ion cells. The electro-chemical and thermal experimental benchmarking for the models in this study are primarily adopted from studies performed previously by researchers in literature.

The experimental work in this study is conducted in order to develop an accurate representation of the multi-physics phenomena of a cell with and without damage. A macroscale analysis of full cell damage is carried out on a spirally wound 6P cell geometry by 3D image segmentation of CT scan data. The effect of mechanical damage on the separator is studied through electro-chemical experiments on 12.5 mAh 2023 coin cells and thermal effects are studied using 2.5 Ah 30 layered pouch cell geometry.

5.1. Multi-physics Validation

Modeling of any system requires validation; the ECM and Numerical models used to characterize li-ion cell response in this study are validated by electrochemical and thermal testing of custom manufactured cells.

It is our intent to verify simulation numerical and analytical mathematical models used in the study with experimental data either taken independently conducted at UWM or used from existing drawn from published research. Experimental data for smaller 18,650 cylindrical cells

exists for charge/discharge, thermal, structural, and abuse behavior. Although this data is available, the viability of using 18,650 cell data for a 6P cell results hasn't been studied. It is possible that 18,650 data is inadequate for determining an acceptable input for our simulation model that we are confident will best represent the system. We hope to obtain experimental validation for the 6P cell geometry or as an alternative, develop a case study for acceptable repurposing of thermal, electrical, and chemical parameters between different battery geometries. The approach taken is to verify the characteristic chemistry of the lithium-ion cell in pouch form because of the availability and relative ease of manufacturing compared to the 6P cylindrical cell. Once the pouch cell computation model is experimentally verified, the 6P model is developed with trust in the accuracy of the model and parameters.

Experiments conducted on similar lithium-ion cells can be categorized in terms of monitoring charge/discharge aging, thermal, structural, and abuse behavior. The state-of-charge (SOC) is important for understanding the reliability of battery operation [14], [165], [166]. An experimental procedure for determining the state-of-charge (SOC) of a lithium-ion cell is to monitor the residual capacity relative to the maximum capacity [165]. Knowing the SOC for a cell can provide insight into cell performance, efficiency and help identify aging [165]. Thermal behavior is closely associated with the exothermic electrochemical response of the cell. Thermal experiments include researchers seeking baseline heat generation values using calorimeters [71] as well as some studying extreme environmental conditions following the UN testing manual [167]. Predicting thermal phenomenon is essential to understanding battery failure and a critical focus of this study. When a battery fails, extreme heat is dissipated through flammable internal fluids creating a danger to the user. The outside casing of the battery protects the volatile

internal components from structural failure and is tested by puncture, impact, drop, and crush experiments [76], [167].

During abuse testing of lithium-ion batteries, the goal is to learn from controlled failure at extreme conditions. This type of testing is dangerous. Most researcher labs, including ours, do not have the capability to induce a structural failure on an over charged battery as it is engulfed in flame. Yet again, the benefit of an all-encompassing simulation model can allow for safer, more accessible, and more capable battery design. It is not meant to replace experimental testing, which is essential to an accurate model, but it may be able to be used by taking information from safer and more common testing results.

5.1.1 Custom Cell Manufacturing

The experimental investigation uses custom coin and pouch cells manufactured for characterization of cell response to mechanical damage. In general, coin cells are made up of an electrode, electrolyte, Lithium metal cathode, separator and anode. The electrolyte solution is a combination of carbonate or combination (for example Ethylene Carbonate, Dimethyl Carbonate, or Ethyl Methyl Carbonate) plus LiPF6 salt at a concentration of 1.0 M to 1.2 M. The electrodes of the battery are the Cathode and Anode. The Cathode, often on an Aluminum foil substrate, contains a coating of the active material. The active material slurry is often characteristic for the type of application: LiCoO2 (laptops, cell phones), LiNiCoMnO2 or "NMC" (hybrid vehicles), LiMn2O4 or "Spinel" (hybrid vehicles), LiNiCoAlO2 or "NCA" (hybrid vehicles), and LiFePO4 or "Olivine" (used by A123). The Anode, often on a Copper foil substrate, contains a coating of Graphite or Carbon. Between electrodes, a polymer separator that is ~40% porous allowing for

Li-ion transfer between Cathode and Anode while preventing a short circuit between the two. The polymer used to create the separator can be Polyolefin Polyethylene, Polyolefin Polypropylene, or tri-layered Polyethylene/ Polypropylene/ Polyethylene.

In this study, coin cells made with a copper anode coated with graphite, aluminum cathode coated with 92% NMC111, and a Celgard 2325 separator between; see Figure 23.

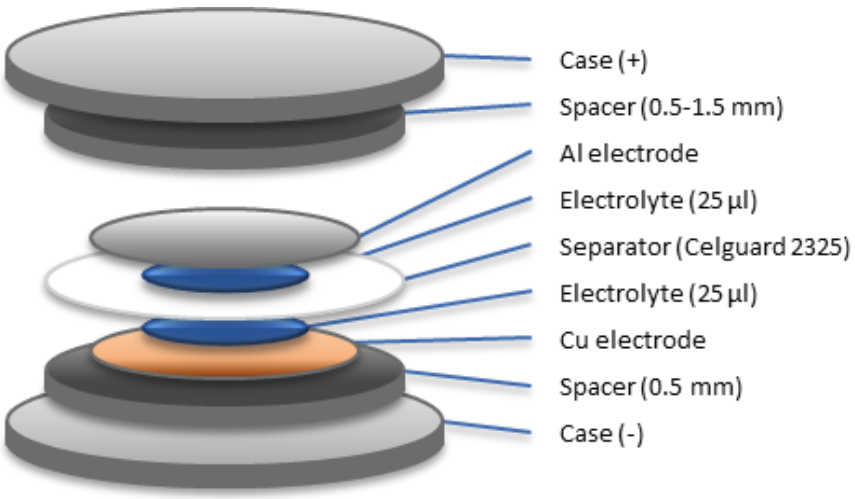

Figure 23 Diagram of Coin Cell using Celgard 2325 Separator

For studying specific effects of battery components, for instance the effects of chemical changes in the Cathode or Anode, special cells are manufactured for research purposes called "Half-cells." Although useful, for this investigation of the separator effects, full cells with uniform Anode and Cathode parameters are manufactured with separator materials in various states of health in terms of mechanical and thermal abuse. The mechanical integrity of the separator

material is put at risk by applying range of loads: 33.71 MPa, 67.42MPa, 101.13MPa and 134.84 MPa. The load sequence will be nominally referred to as 33 Mpa, 66 Mpa, 100 Mpa, and 133 Mpa respectively. The selection a maximum stress corresponds to the point at which the separator can be ruptured and create an internal short circuit; results verified by Giliaki's accurate simulation model. The intermediate sections of stress are even increments from no load to the maximum load. Thermal damage is induced by heating the separator material to the point at which cells are at risk of thermal runaway at 110C and the designed melting/5 temperature of 135 C.

5.1.2 Parameter Characterization

The ECM model parameters were determined using Hybrid Pulse Power Characterization (HPPC). To determine the Randles parameters specific to the battery chemistry of this representative 2032 coin cell with a capacity of 12.5 mAh was cycled using the same HPPC method. The first twenty cycles were used for formation at a 1C charge/discharge rate. formation, the test method chosen followed a charge/discharge cycle as follows in

Table 2.

Table 2. HPPC cycle method.

Step	Description
1	8 hr rest
2	charge, 0.0013 A (1C) up to 4.1 V
3	charge, 4.1 V constant, 7.457e-5 A cut-off
4	1 hr rest
5	10% discharge, -0.0013 A (1C) 6 min (0.001295 Ah = 10%)
6	Rest 1 hr
7	HPPC Charge Pulse 10 sec, 0.013 A (10 C)
8	40 sec rest, constant current (0 A), 0V
9	HPPC Discharge Pulse 10 sec, -0.0065 A (5 C)
10	60 sec (1 min) rest, constant current (0 A)
11	50 sec, constant current discharge (-1 C, -0.00130A)
12	Back to step 5 if counter is < 9 (Repeat step 5 – step 11 for SOC 90, 80, 70, 60, 50, 40 , 30, 20 , 10)
13	charge, 0.0013 A (1C) up to 4.1 V

The EMC parameters of Ohmic resistance (R0), charge-transfer resistance (R10), and interfacial capacitance (C10) are derived in a similar manner as described by [114]–[116], from the single-degree RC circuit shown in **Figure 8**. Ohmic resistance (R10) is determined by calculating the

resistance from the immediate change in voltage at the end of Step 6 and the first point of Step 7; Figure 24 and

Figure **25**. In order to find the charge-transfer resistance (R10) and interfacial capacitance (C10), both variables of polarization and sometimes called polarization resistance and polarization capacitance respectively, the voltage data from Step 8 and Step 10 are used respectively by using a linear least squares fit. The curve fit determines parameters of a standard exponential function used to model the RC circuit; example data shown in Figure 26.

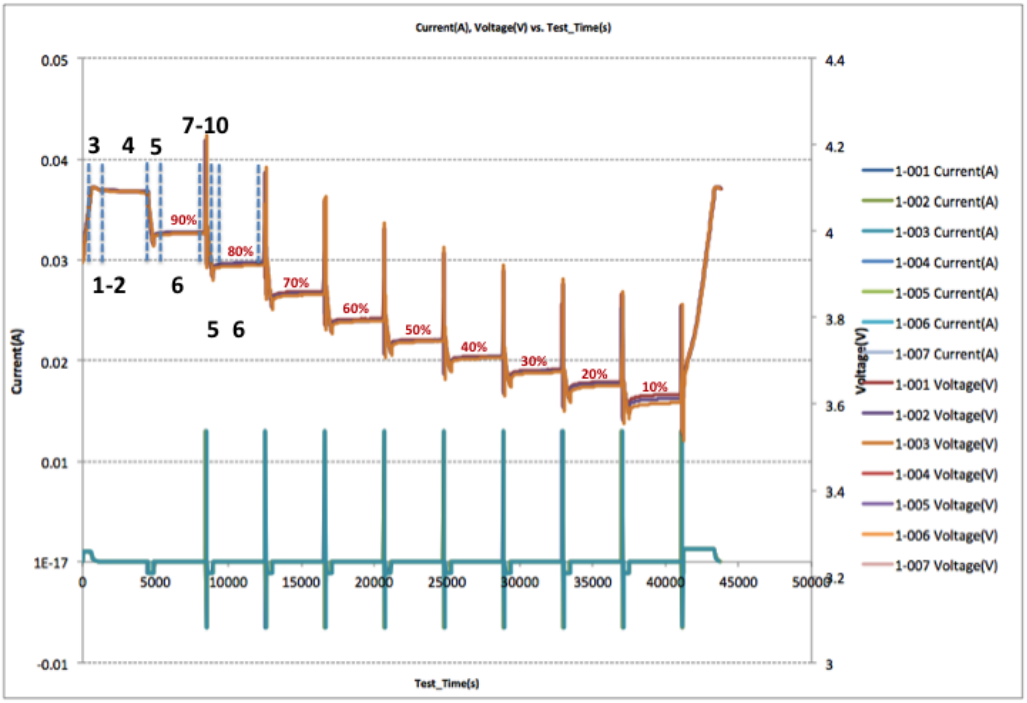

Figure 24. HPPC voltage and current pulse correlation

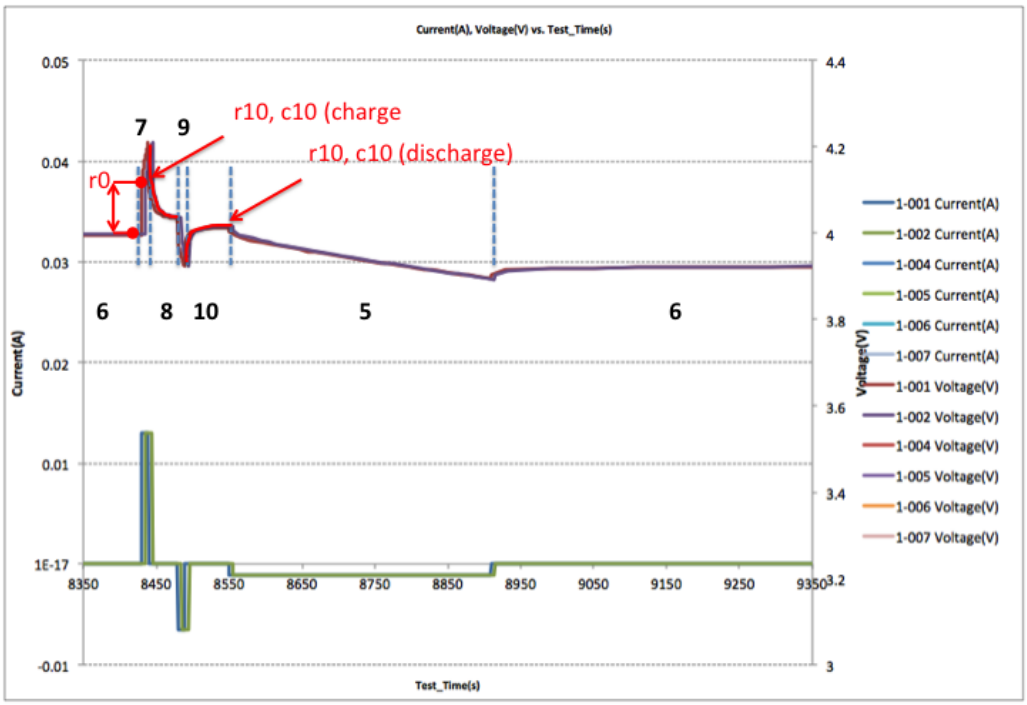

Figure 25. Depiction of ECM parameter derivations

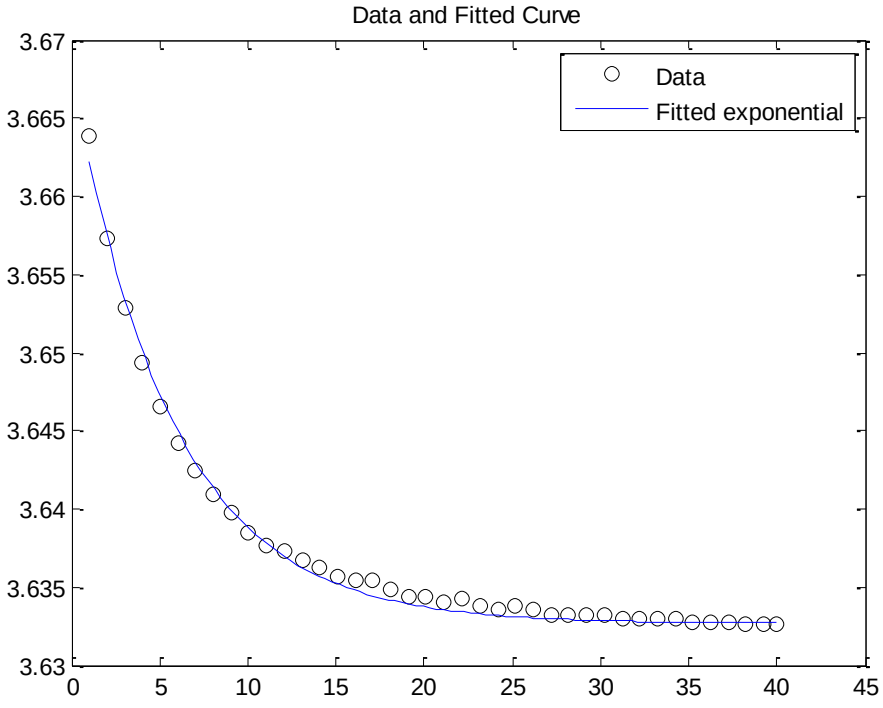

Figure 26. Curve fit of data for parameter calculation.

5.2. Structural Validation

Cylindrical Cells

Cylindrical cells for use in EV applications are the primary focus of this research. The other coin and pouch geometries are used to find ECM parameters and verify response, but characterizing a cylindrical cell, module, and pack is the strategic goal of this work. It is focused on the Johnson Controls Inc. 6P cell geometry with a 37 mm diameter, 137 mm height, and nominal capacity of 3.6V/6.8 Ah, NCA/Graphite.

The experiments conducted with Avdeev and Gilaki included compression and impact testing of structural abuse scenarios leading to a short circuit condition. The impact testing was conducted on a custom drop test apparatus. Two situations of flat plate and rigid rod impact were studied. Detailed experimental setup and results were shared by Avdeev et al [46]. However, this series of tests did not reliable lead to short circuit conditions. Thus, compression testing was conducted on the cells until short circuit detection was apparent. The cell was loaded into the experimental test equipment with a rigid rod in the center of the cell and monitoring equipment attached to each battery lead to detect a short; see **Figure 27**. In summary, Gilaki found the short circuits were detected by monitoring voltage and resistance of the cell. A short resulted from a rise in voltage and decrease in resistance. This response consistently occurred at approximately 60 kN of load.

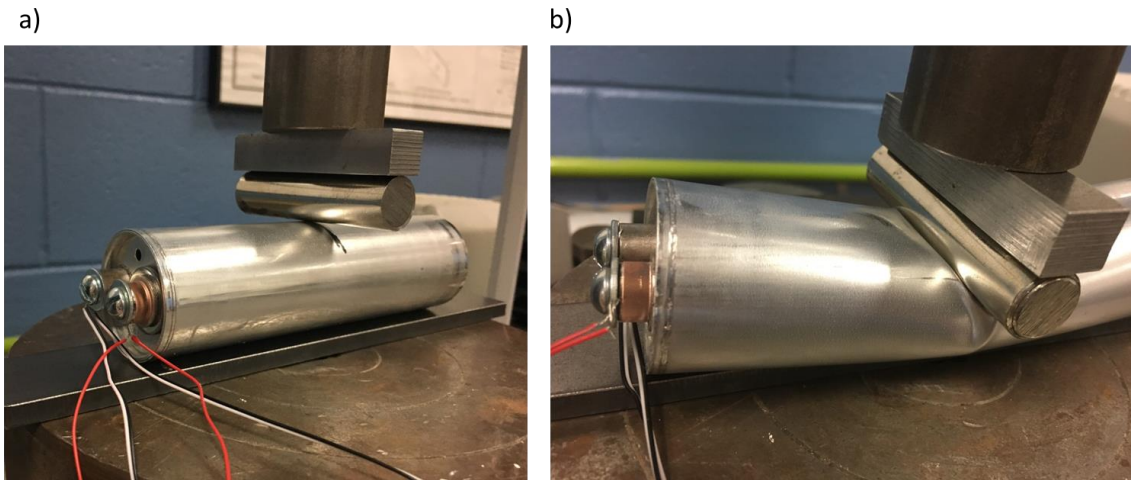

Figure 27. Compression test setup while monitoring cell electrical response: a) undeformed, b) deformed.

5.2.1. Failure Analysis - CT Scanning

CT scanning of a single cell is an important step in the battery failure analysis. It provides verification of existing structural results and an insight into how the cell is structurally failing. The underlying assumption is that structural deformation/failure in the cell causes either a short circuit or a localized area of current discharge that starts an abnormal thermal heat transfer process through the cell.

CT scan images give us a non-invasive look inside cell failure. We are looking for structural casing fractures, layer cracking, especially indications of separator failure, as well as any other visual queues that there could be a potential problem. The images below show the internal deformations after a rod indentation experiment for which a short circuit is likely to occur. Two distinct areas of interest are (A) highly distorted layers buckling against each other and (B)

electrode fracture near the aluminum core (see Figure 28). This information can be used to compare and verify structural simulation deformation results. Notice, in the comparison in Figure 29 and Figure 30, the areas of the heterogeneous simulation with highest deformation correspond to the regions highly deformed layers in the CT scan image (*note to reader: this is an assumption that will later be verified or denied*). It also provides verification of internal short circuit assumptions used in the multi-physics model.

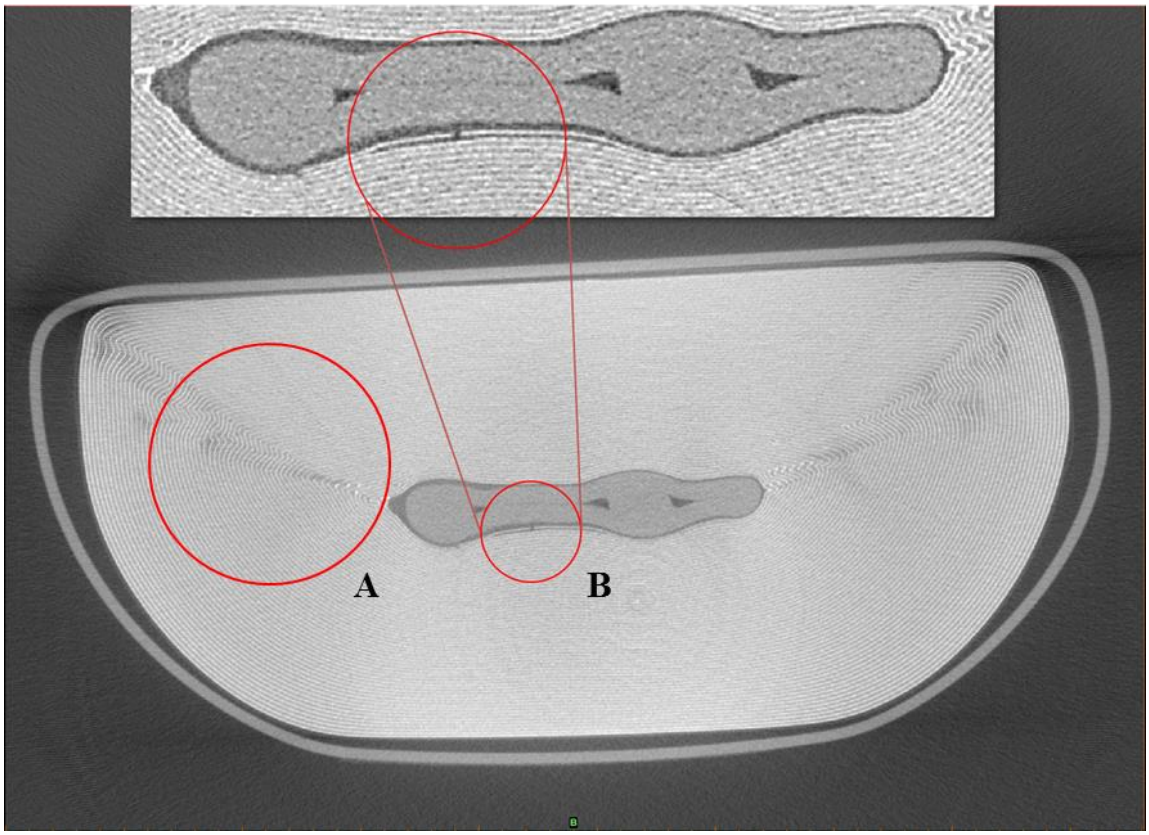

Figure 28. Internal failure location and analysis: (A) highly distorted layers, and (B) electrode fracture.

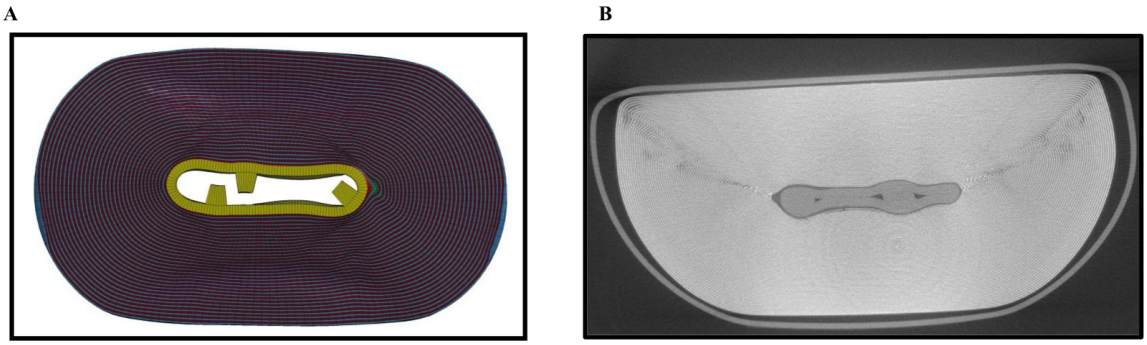

Figure 29. Comparison of (A) structural simulation deformation contour and (B) CT scan image distorted layers.

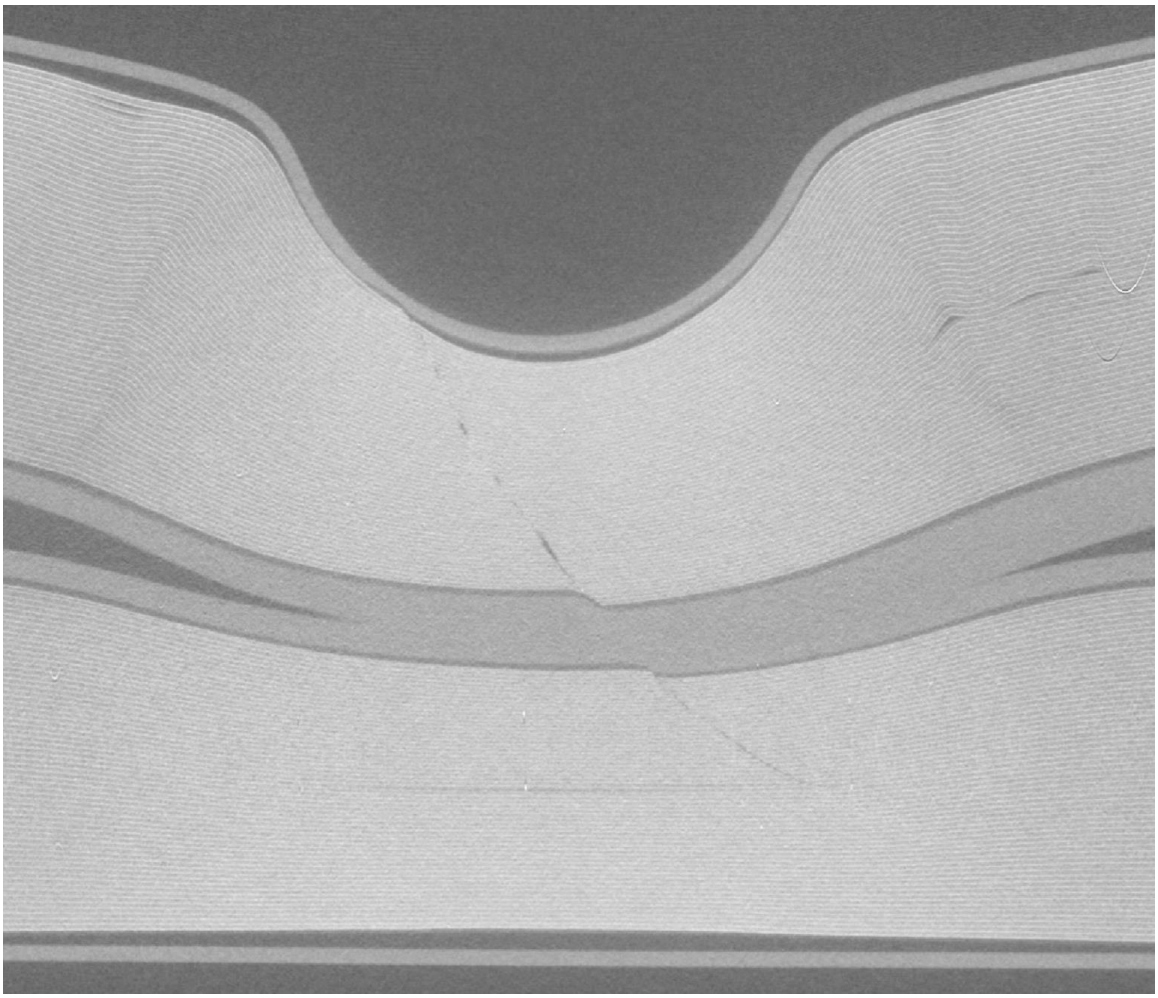

Figure 30. Rod compression internal failure analysis.

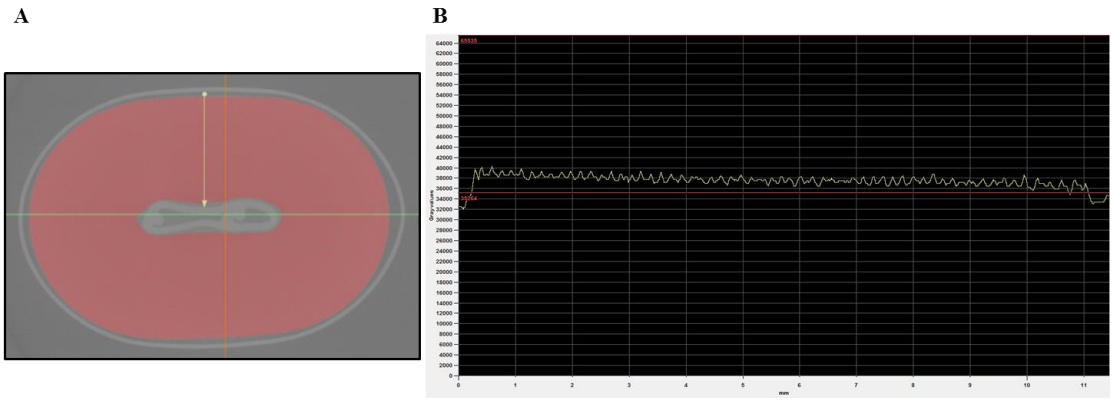

Figure 31. Quality control using Mimics software: (A) measurement line, and (B) layer differentiation.

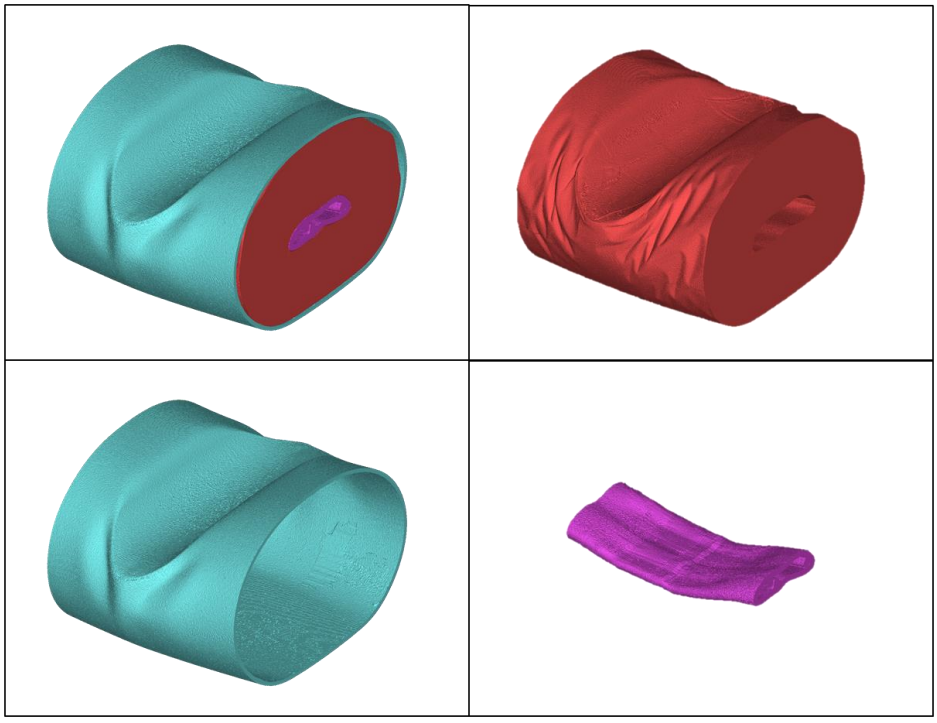

Figure32. 3D CT reconstruction of rod compression

The technique can also be used for quality control purposes. Mimics can differentiate between individual layers through grey value interpretation allowing for an accurate count of the layers; see Figure 31. For the scanned cell of interest, there are about 58 distinct peaks which correspond to layers in the cell.

A North Star Imaging scanner was used to perform the CT scanning of the battery cells. For this specific type of cell, the scan parameters were optimized for highest scan resolution while maintaining the full diameter of the cell within view of the detector. Scan parameters included: the source voltage, source current, detector magnitude, table magnitude, detector acquisition rate, filter thickness, number and angle of radiographs. The source voltage and current controls the amount of power output from the source. The table magnitude (TM) is the distance between the scanned object, in our case a battery cell, and the x-ray source. The detector magnitude (DM) is the distance between the detector and the source. A depiction of the scan setup and a list of scan parameters values are shown in Figure 33 and Table 3 respectively. This set of scanning parameters resulted in scans with a calculated resolution of 30.9 μm while keeping the entire cell within the field of view. The scan resolution is sufficient to depict individual layers of the jellyroll and is calculated by (5.1.

$$Resolution = pitch \times \frac{TM}{DM} \quad \textbf{(5.1)}$$

In order to obtain accurate segmentation with sufficient level of fine detail representation, we have chosen spatial scan increments of 0.25 degrees, which corresponds to 1,440 scans per cell

covering a 360 degree rotation of the target. Each scan (slice) was saved as a DICONDE (.dcm) image for nondestructive evaluation, containing not only information about the image but optional fields for saving object and scan parameter information [168]. The DICONDE format is a common file type for medical imaging that is an acceptable file type for the reconstruction software we have chosen.

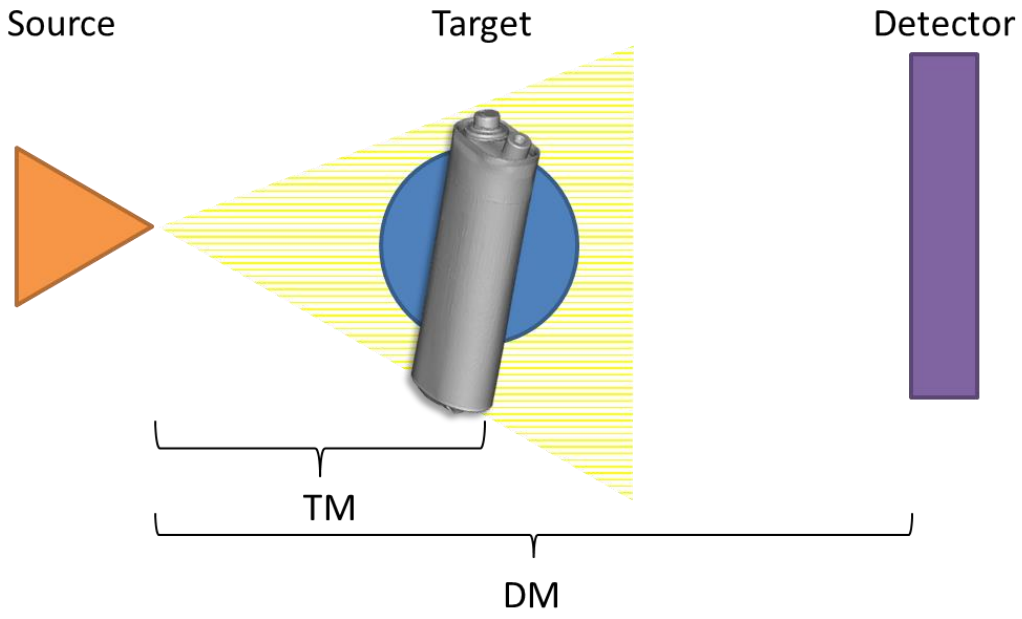

Figure 33. CT scan diagram: source producing x-rays, target of interest, detector, target magnitude (TM), and detector magnitude (DM).

Table 3. Scan parameters.

Scan Parameter	Value [units]
Source voltage	200 kV
Source current	90 µA
Detector acquisition rate	1 fps
Filter thickness	0.094" Cu
Detector magnitude (DM)	550 mm
Table magnitude (TM)	135 mm
# of radiographs	1440
Rotation angle	0.25 °
Calculated scan resolution	30.9 µm
Pixel pitch (constant)	127 µm

For scans of localized critical areas, such as the deformations around rod indentations, this setup is ideal. However, for a full cell reconstruction at the same resolution, multiple scans need to be pieced together since the full cell does not fit within the field of view. To make assembling multiple scans together easier, a steel reference marker was attached near the top and bottom section beings scanned. This positional reference marker was placed so that it appears in every scan; thus, it could be located and aligned properly with neighboring scans. After alignment of each scan with its neighbor and post-processing, the separate pieces make up a high-resolution full cell scan.

We used the commercial software package Mimics (Materialise) to build a 3-D layered model from the CT-scan data. The reconstruction process consisted of three major steps: (1) scan data import, (2) segmentation, and (3) 3-D model creation (see Figure 34).

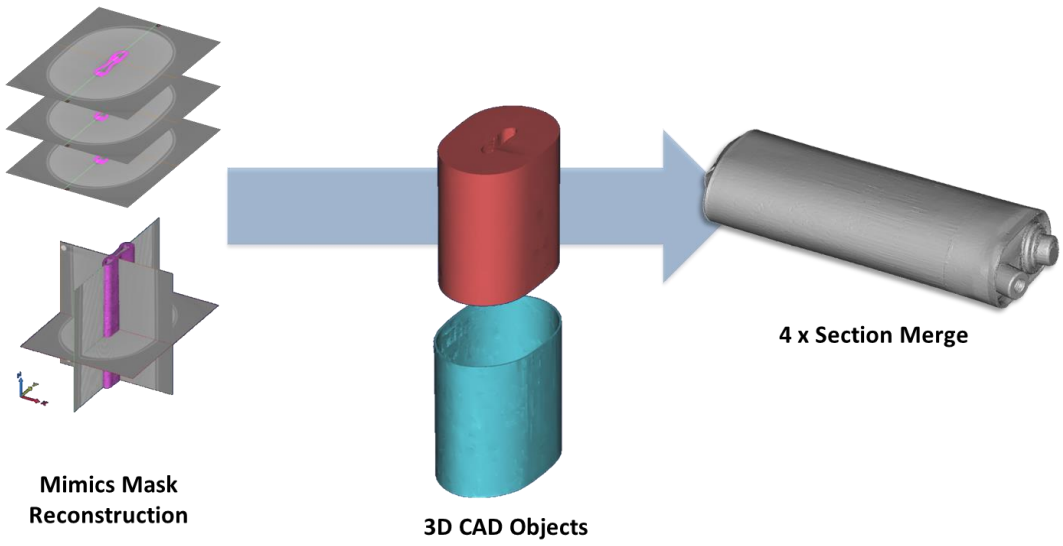

Figure 34. Mimics reconstruction process: (A) data scan and mask construction, (B) individual 3-D model components, and (C) full cell model (aligned and merged).

Importing the CT scan data is an automated process, only requiring information about the, image size, the pixel resolution, and the header information. The size of each image should be the same for each scan but can vary between the scans. Each pixel in the scan corresponds to spatial dimensions in the x-, y-, and z-directions. In the example below, the scan resolution was set to 0.3 mm in the x-, y-, and z-directions. The header size can drastically effect the representation of image data and for our case it is set to a value of zero.

After the images were arranged sequentially in a stack, a selection mask was used to segment individual battery components by setting specific density thresholds. This process is depicted in Figure 35 and Figure 36. A CT scan image contains information in the form of greyscale values corresponding to different densities. In the case of a lithium-ion battery scan, the dense copper current collector appears as bright white on the scan while the aluminum casing and current collectors appear as less intense and the polymer separator layers cannot be perceived at all since they do not absorb x-rays. The corresponding threshold range used for each material can be

found in Table 4. Grey value thresholding upper and lower limits were selected for the mask based on accuracy and ease of post processing. After the mask was created, we manually post processed the images in order to eliminate some noise outside the region of interest.

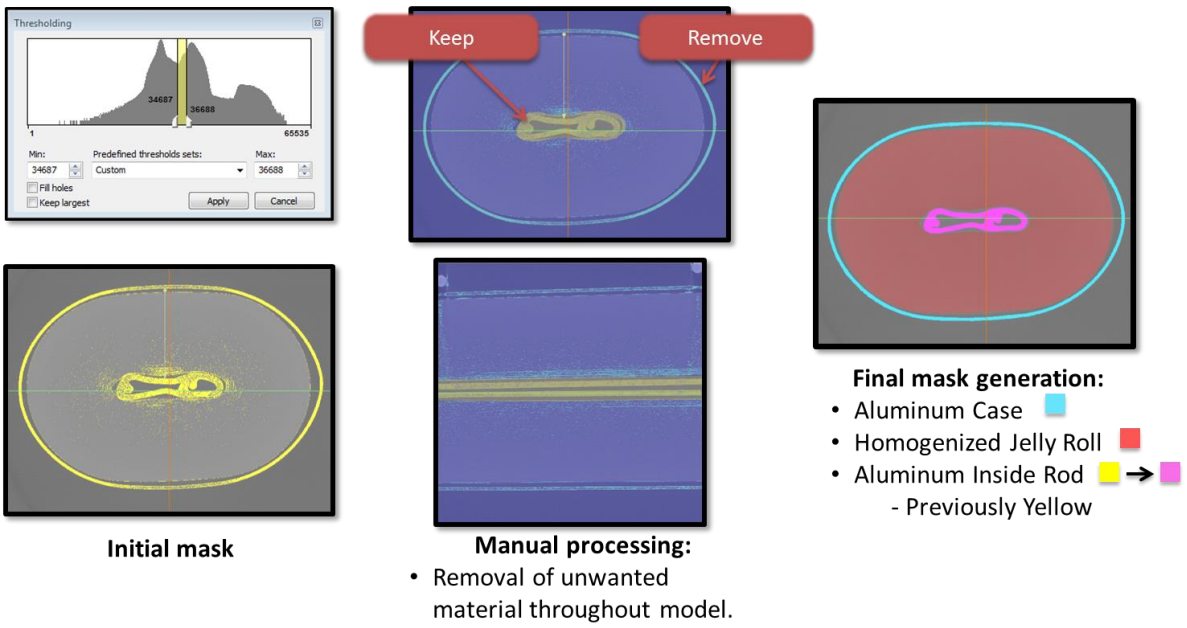

Figure 35. Layer processing procedure: (A) initial mask segmentation, (B) cleaning and post processing, and (C) final mask segmentation and separation.

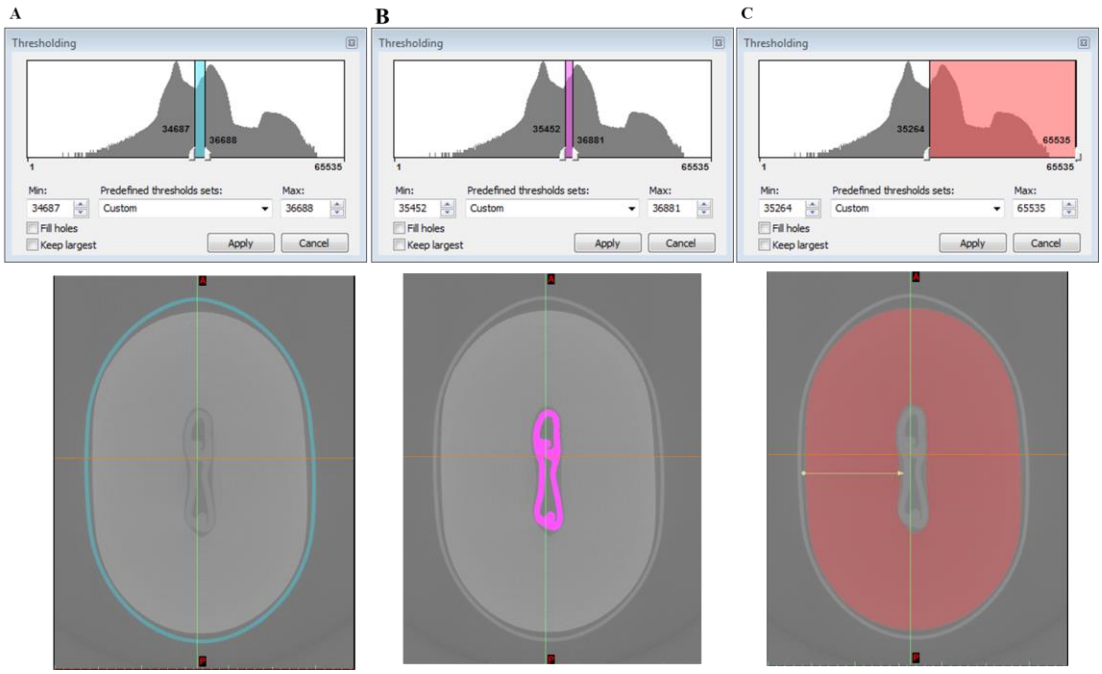

Figure 36. Thresholding images corresponding to cell components: (A) Aluminum Case, (B) Aluminum Rod, and (C) Jellyroll.

Table 4. Grey value selection thresholds

Component	Lower Grey Value	Upper Grey Value
Aluminum Case	34687	36688
Aluminum Rod	35452	36881
Jellyroll	35264	65535

The CT scan results were used by Gilaki et al to verify simulation accuracy. Additionally, the 2D and 3D segmentation capability is useful for further analysis of internal and external short circuit risk areas of acute damage such as internal short circuits and verifying the deformation of the internal structure especially the separator layer.

5.2.2. Porosity effects on ECM parameters

Increasing mechanical loading and operating temperatures were shown by Mason et al to decrease the measured porosity of the separator material. The results summarized in Table 5 show the porosity correlated to a change in the mechanical integrity.

Table 5. Mercury Intrusion Porosity results

Stress	Undamaged	15K	30K	45K	60K	110°C	135°C
Porosity	41±1%	35±1%	32±1%	21±3%	18±2%	27±1%	19±5%

The ECM model parameters display a dependence on SOC, temperature, and damage/porosity. As the SOC increases from 10% to 90%, take the undamaged results at 25C for example, R0 increases slightly from 7.44 **Ω** to 8.36 **Ω**, an 11.0% change. As for the R10 and C10 parameters, the values remain within 2.15% and 4.33% respectively, showing less of a significant correlation to SOC. Temperature dependence is more of a factor than SOC. As the temperature increases from 25C to 50C averaged parameter values across SOC change by: R0 decreases by 48.9% from 5.51 **Ω** to 2.70 **Ω** , R10 decreases by 56.0% from 7.68 **Ω** to 3.38 **Ω** , and C10 increases by 54.0% from 1.26 F to 1.94 F. Specifically to C10 only, the capacitance values are consistently higher during discharge. Comparisons R0, R10, and C10 of SOC and temperature dependence for an undamaged condition can be found by inspection of Figure 37, Figure 38, and Figure 39 respectively. The results show inconsistencies at 80% SOC for R0 at 25C during charge, R0 at 40C during discharge, R10 at 25C, 40C, and 50C during charge and discharge, as well as 25C

during charging. Investigation of the data does not reveal a likely cause of this discrepancy, thus in order to better understand the validity or invalidity of the outliers, more data must be obtained.

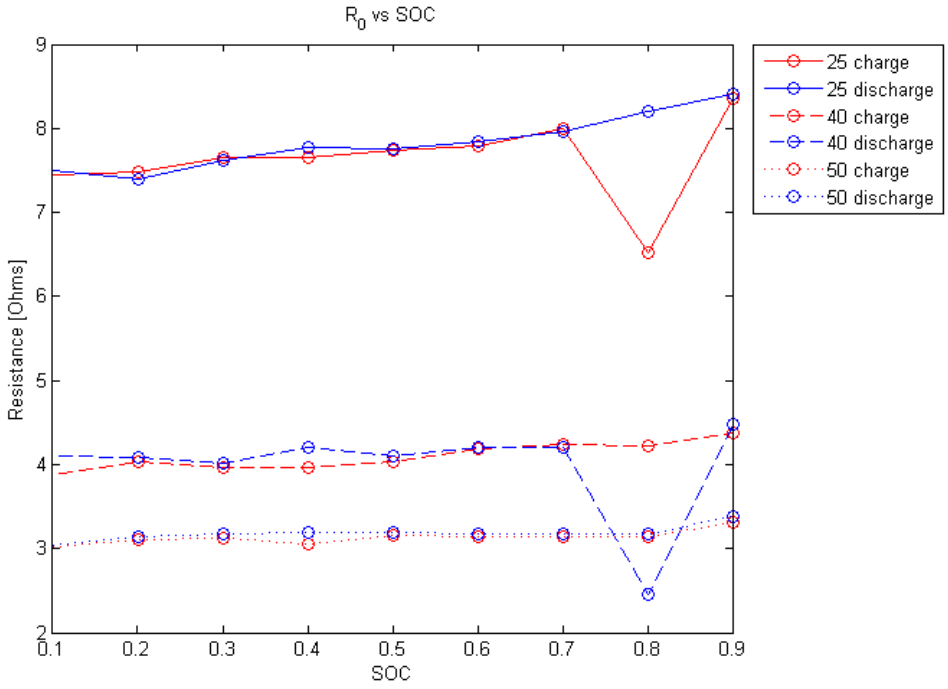

Figure 37. R0 vs SOC Temperature dependence

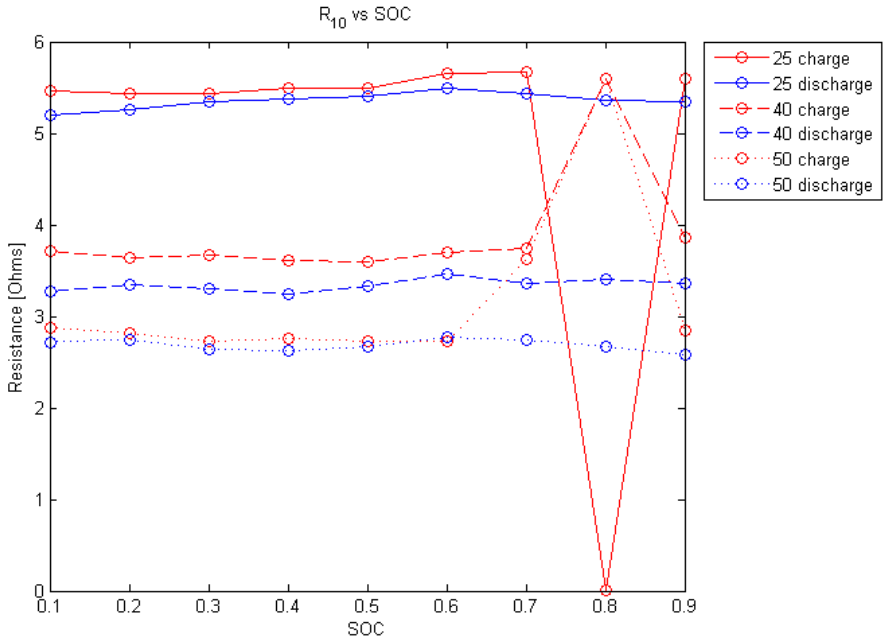

Figure 38. R10 vs SOC Temperature dependence

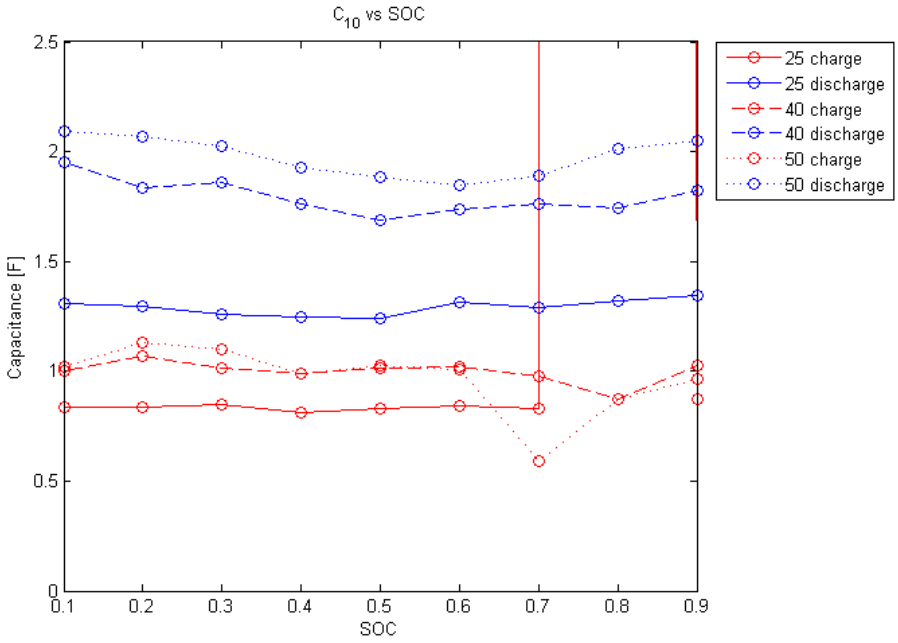

Figure 39. C10 vs SOC Temperature dependence

The resulting parameters for damaged cells showed a correlation to the negative impact of combined damage conditions, 100% of cells cycled at 25C regardless of damage completed the HPPC experiment, while only 75% of cells completed the test at 40C, and 50% of cells completed the test at 50C. Mechanical stress on the separator contributed to the malfunction of the cells with a significant impact on likelihood of failure above the 100 MPa condition at 40C and above the 66 MPa condition at 50C. A comparison of those cells that passed and failed is illustrated in Table 6. All other cells did not complete the HPPC experiment. Although not all damage increments have associated date to find parameters, it is apparent that any amount of damage can significantly limit cell performance and increase risk of malfunction.

Table 6. Effect of combined damage on cell reliability (green = pass, red = fail)

Channel	25C	40C	50C
0 kN 081	1	1	1
0 kN 082	1	1	1
0 kN 083	1	1	1
15 kN 084	1	1	1
15 kN 085	1	1	1
30 kN 086	1	1	
30 kN 087	1	1	
45 kN 091	1	1	1
45 kN 092	1		
60 kN 093	1	1	
60 kN 094	1		
60 kN 095	1		

Results for the cells that did pass the HPPC test can be seen in the comparative figures below of the negatively correlated trend of R0, R10, and C10 when damaged. The Ohmic Resistance (R0) dependently increases with mechanical stress; Error! Reference source not found.**. The charge-transfer resistance (R10) and the internal capacitance (C10) do not have a significant correlation based on stresses except for at the 133MPa condition; Figure 40. Damage effect on Ohmic resistance (R0)**

and **Error! Reference source not found.**.

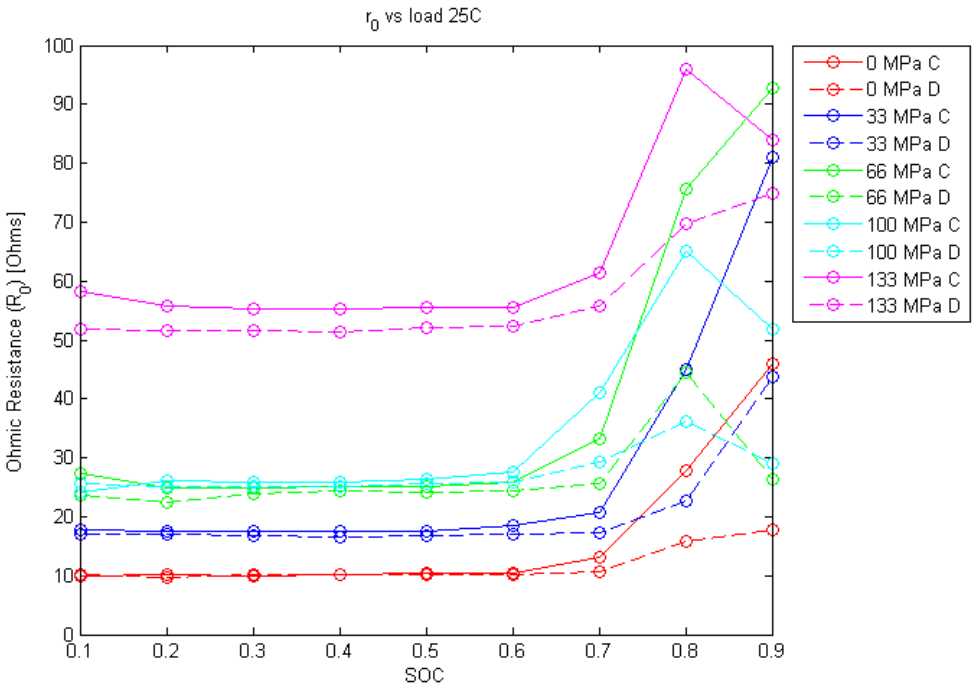

Figure 40. Damage effect on Ohmic resistance (R0)

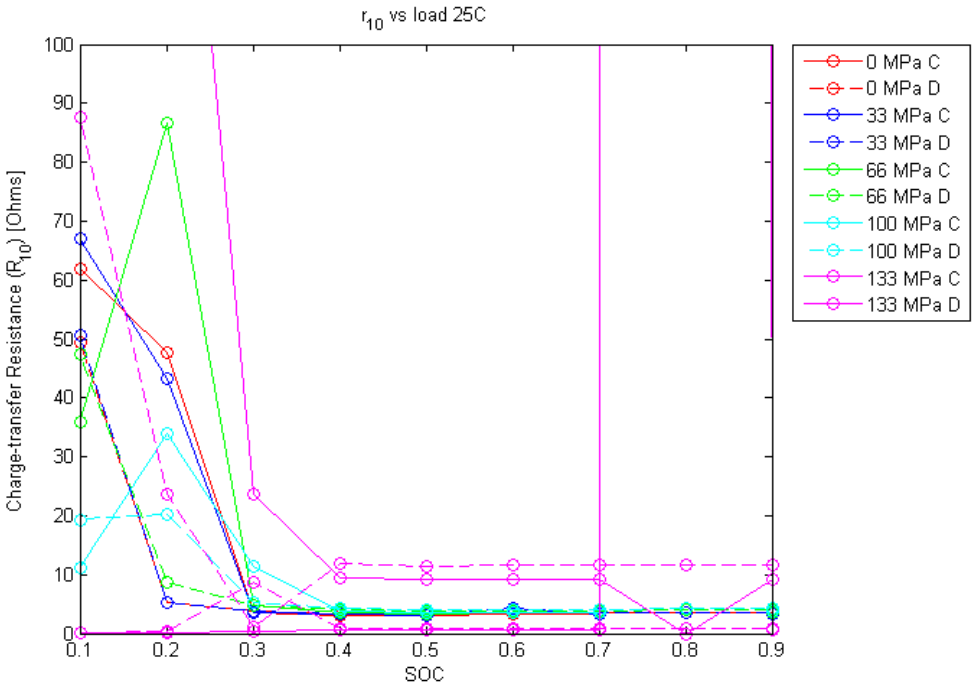

Figure 41. Damage effect on charge-transfer resistance (R10)

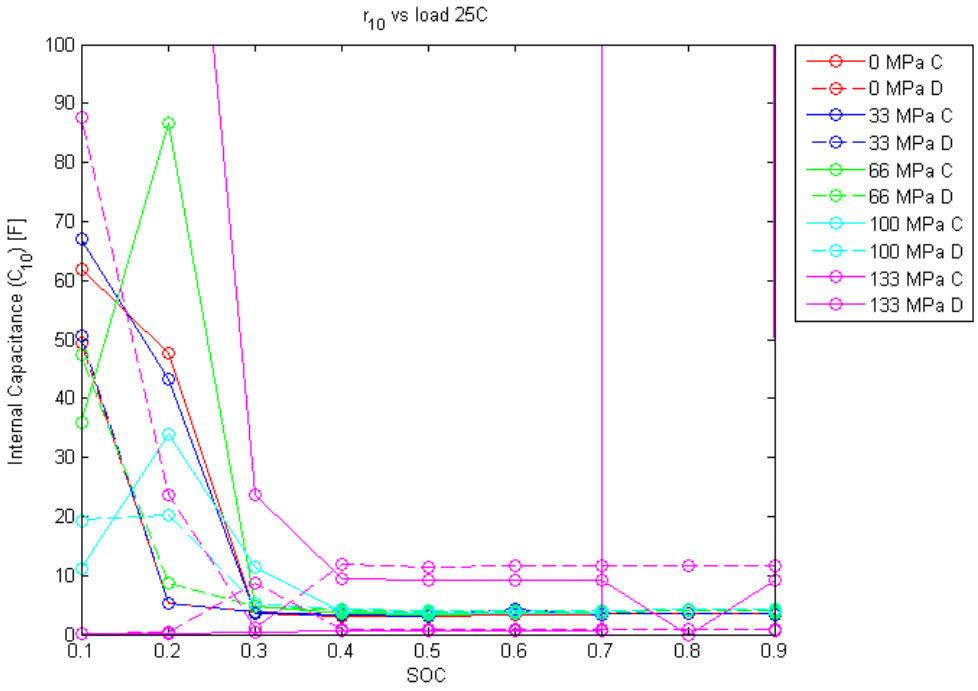

Figure 42. Damage effect on internal capacitance (C10)

Additional Figures and data can be found in the Appendix.

5.3. Thermal Validation

Thermal validation of li-ion cell performance was conducted by monitoring the temperature of a pouch cell while cycling over time and at various C-rates using a Xenics Gobi 640 thermal camera and an Arbin BT-2000 battery cycler.

5.3.1 Pouch Cell Manufacturing

The pouch cell manufactured for this study is a 2500 mAh or 2.5 Ah li-ion cell were manufactured in a vacuum chamber and consist 30 active layers using a 129 mm wide x 77 mm tall copper anode coated with graphite, a 127 mm wide x 73 mm tall aluminum cathode coated with NCA, a Celgard 2325 polymer separator and 1.0M LiPF6 (lithium hexafluorophosphate) in EC/PC/EMC/DMC (25/5/40/30) by weight percent using battery grade solvents.

Three pouch cells were manufactured, a baseline and two cells with compressed separator material. A compressed area of approximately 120 mm x 45 mm centered on each piece of the separator. Only the first two increments of nominal compressive stress (33 MPa and 66 MPa) were selected for pouch cell thermal validation because more robust safety precautions for cycling pouch cells with stress levels of 100 Mpa and 133 Mpa were not established at the time. After the layers were assembled, the stack was placed inside the pouch, filled with electrolyte and sealed. The seal was monitored for leaks before cycling. Since the pouch material is reflective to infrared radiation, the outside of the cell was painted matte black to observe the temperature distribution on the surface of the pouch.

5.3.2 Pouch Cell Cycling

The cycling procedure for pouch cells was designed to study the thermal response due to various C-rates (1C, 3C, and 5C). The first three cycles were used for formation at a 1C/1C charge/discharge rate up to 4.1 V down to 2.7 V, followed by cycle number 4 to 18 at 3C/3C, finishing with cycles 19 and 20 at 1C/5C both of which have a cut-off voltage of 2.1 V.

Specific locations on the pouch cell were monitored with digital markers in the Xenics Xeneth software. Markers placement included the center of the cell, each of the four corners of the cell, an average of the area created by the four corners, and one marker on each positive and negative tab; as shown in Figure 43.

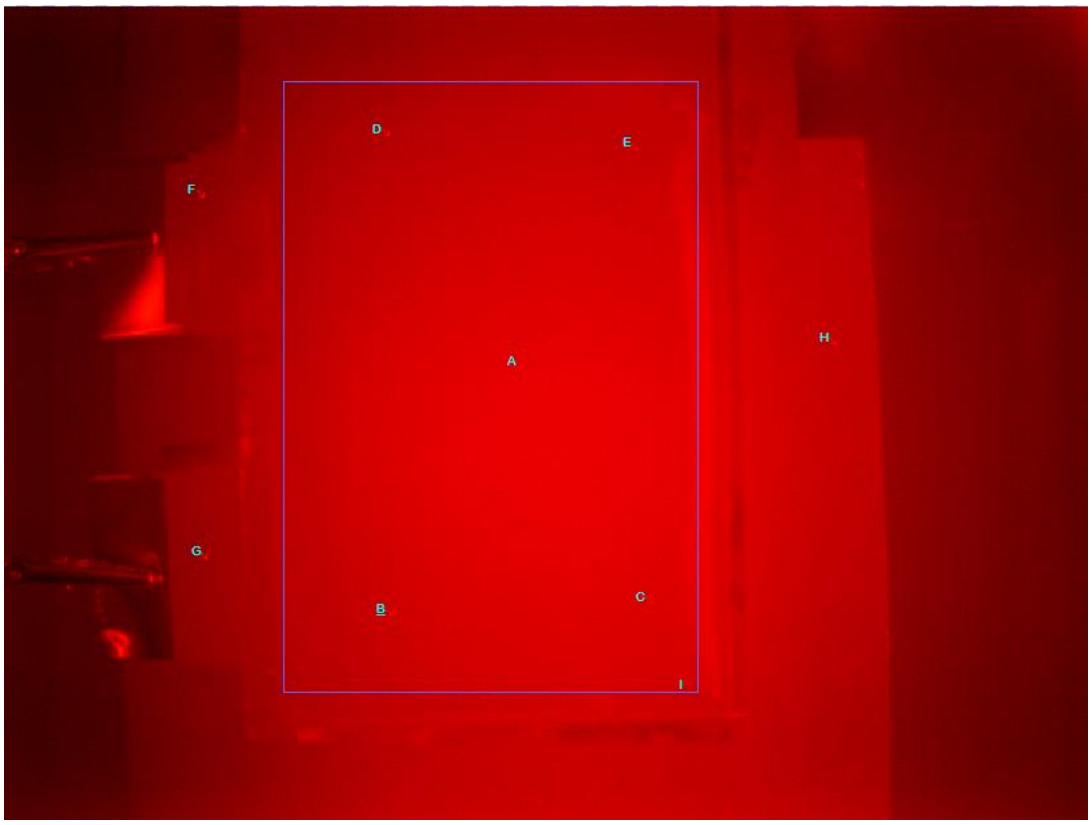

Figure 43. Xeneth Tool Locations (A) center of cell, (B) bottom left, (C) bottom right, (D) top left, (E) top right, (F) positive tab, (G) negative tab, (H) ambient

5.3.3 Pouch Cell Results

After comparatively cycling cells with and without damaged separator material, observations were made of how damaged separator material effects the maximum temperature of the cell and at what periods of charge/discharge the maximum temperature is observed. The maximum cell

temperatures occurred at the center of the cell reaching 26.8 C, 28.7 C, 31.7 C corresponding to the baseline, 33 MPa, (15 Kn) and 66 MPa(30 Kn) respectively. For a complete list of experimental temperatures with predicted maximum temperatures for 100 Mpa and 133 Mpa compression corresponding to the numerical simulation results, see Table 7. The thermal trend during a representative series of cycles can be seen in Figure 44.

Table 7. Pouch Cell Maximum Temperatures (where * = predicted values)

Load	0 MPa	33 MPa	66 MPa	100 MPa	133 Mpa
T [°C]	26.7	28.7	31.7	36.0*	42.2*

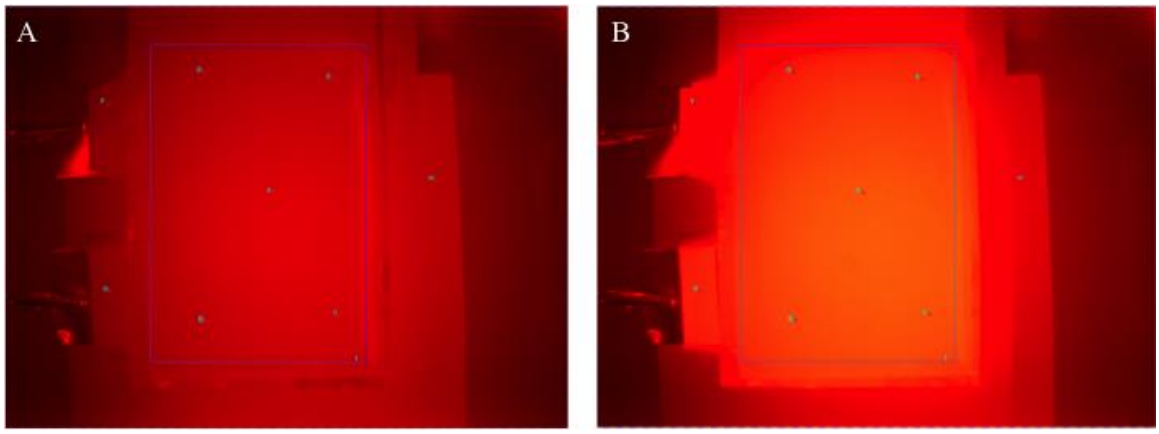

Figure 44. Temperature distribution (A) at rest and (B) during discharge

Through observation, the cell produces the most heat by the exothermic reactions during discharge to reach a maximum temperature. During the charge cycle the reaction is slightly endothermic as the temperature decreases back to steady state and rapidly decreases near the end of the charge cycle. This rapid increase in temperature is attributed to the relaxation polarization phenomenon while cycling from negative to positive current (positive heat flux) and from

positive to negative current (negative heat flux). The increases in maximum temperature with increases in mechanical stress can be contributed to the decrease in porosity of the separator. The change in porosity relates to heat generation by influencing the change in internal resistance and the ability of Li-ion charge transfer between the active layers, decreasing the charge capacity.

6. Summary of Results and Contributions

6.1. Review of Conclusions

Emerging needs for multi-physics and multi-scale simulation tools and mathematical models that can inform the battery design are addressed by this work. Up to this point, we have defined the addressable need for improved lithium-ion battery design procedures focusing on safety. As an extension of structural treatment of battery packs by Avdeev et al. [45], [46], the focus of this study is on multi-field analysis, adding thermal, electrical, and chemical analysis capabilities to the existing structural model with a focus on studying the impact of damage on battery variables and performance. This is a relatively new concept in the study of lithium-ion battery modeling and management. Contributing to an improved understanding of a numerical tools used for battery design is not the only implication of this work; it extends beyond current knowledge with a study of scalability and battery design characteristics that are critical to battery safety.

Structural integrity of the battery cell is one primary concern. The hypothesis was that structural damage will change the electrochemical and thermal response of the battery. CT scanning was used for improved accuracy of a structural model by investigating internal deformation

measurements and for failure analysis by locating short circuit problem areas. The experimental procedure and detailed post-processing information is shared.

Relative to the numerical model, a comparison of thermal response is conducted of both the un-deformed and the deformed battery cells. First, thermal simulations under normal operating heat generation and convection conditions were completed. Additional analysis includes a study if the cell's response to structural changes exhibiting internal/external short circuits and preliminary analysis of thermal runaway.

Under normal thermal load and boundary conditions, the battery cell generated a maximum temperature of 320 K, increasing 22 degrees from an initial temperature of 298 K after 300 seconds, which is similar to the maximum temperatures and predicted temperatures reached for the pouch cell thermal experiment. Further experimental investigation of the temperature response of a live 6P cell is required for best accuracy and confirmation of the model validity before confirming that the simulation method is an adequate design tool.

Short circuit conditions were assumed to be a localized source of heat generation, expelling the same amount of heat generation but at a single location. The maximum cell temperature after 300 seconds was 298.4 K, a 0.3 K change from the initial temperature of 298.1 K. This number is surprisingly low for a structural failure that often leads to catastrophic thermal runaway. After our initial findings we understand that modeling the thermal response of a short circuit condition will require additional investigation. Specifically, to focus into the heat generation details: duration of discharge, discharge rate through short

A short circuit is created from the electrical nature of in the cell and ultimately leads to thermal issues. Preliminary development for incorporating thermal physics in the structural model have been conducted using existing heat generation data from literature. The heat generation was provided as an input to the deformed cell geometry obtained from the refined structural simulation. Irregular temperature distributions from a transient simulation indicate the importance of understanding the behavior of a full electric vehicle battery pack in a post-crash scenario.

A robust multi-scale and multi-physics tool is powerful for battery design. Such a resource provides an opportunity to design new batteries and optimize existing designs with a focus on safety. Optimization of cell strength, cooling characteristics, and charge capacity are all potential possibilities for applications of this tool.

A comprehensive study of a lithium-ion modeling, experimental, and numerical approach for the isolation of design variables is achieved. Specifically, the porosity of the separator is studied with empirical modeling techniques in a multi-physics and multi-scale simulation environment, LS-Dyna.

Our research showed that the structural and thermal stability of the separator in terms of porosity has an impact on the cycling performance. Mechanical load and heat near the melting temperature of the separator closes pores, decreasing cycle life, capacity, and reliability of the cell. Physical damage increases the risk of catastrophic failure and decreases the long-term performance of the cell. The data obtained in this study can be used to adjust existing models for

use in battery design and battery management systems. Also, and understanding of unhealthy operation can add value for condition monitoring of individual cells in the battery pack. For example, the trends observed for mechanical damage can add a predictive component to the SOH and useful life of the battery. Specific parameters characterized for SOC, temperature and damage dependence in a single network ECM are the ohmic resistance (R0), charge-transfer resistance (R10), and the internal capacitance (C10). The SOC and thermal dependence align with trends and nominal values found previously by other researchers, such as the nominal ohmic resistance found to be approximately 20 mΩ [57], [63], [67], [115], [122]. The damage dependence is a new relationship for ECM parameters. The trend of internal resistance (R0) increases with damage while the other parameters R10 and C10 remain consistent. It is the hypothesis that the parameters change with damage and that the risk of a performance decrease or electrochemical malfunction is attributed to a reduction in li-ion intercalation in the volume of the bulk electrolyte due to a decrease in porosity; ultimately, increasing the ohmic resistance, cell temperature and risk of thermal runaway when using constant charge/discharge cycling currents.

It has been shown that mechanical and thermal damage to the cell, especially the separator layer, can create a risk of chronic and acute changes in battery response. The separator porosity is a design variable that is experimentally studied and isolated in modeling efforts. The focus on one design variable's impact on the electrochemical-thermal response of the cell is a framework for future studies. Additional design variables of the separator which would make a logical next step and important contribution to the field are: separator thickness and pore size.

The extensive experimental investigation did not completely verify the simulation results. The electrochemical results of voltage and temperature correlated within 12% of the experimental results.

Even though the results did not closely correlate to experimental validation, future work can be done to improve the accuracy and capability of the simulation.

6.2. Future Work

Future researchers can use this method as a guide for studies isolating damage effect of other components within the cell to improve upon the simulation model can include additional investigation of damaged parameters in the parametric environment with close attention to validating the parameters by other means than only HPPC itself, such as EIS.

Additional parameter characterization experiments should be conducted in the future for validation of results. When comparing the two sets of baseline HPPC experiments, the data used in this study cannot be compared at HPPC pulse steps below 30% SOC because some cells failed to operate under normal conditions. For an illustration of the difference, see Figure 45 and Figure 46 of voltage during two sets of baseline (0 MPa) HPPC data.

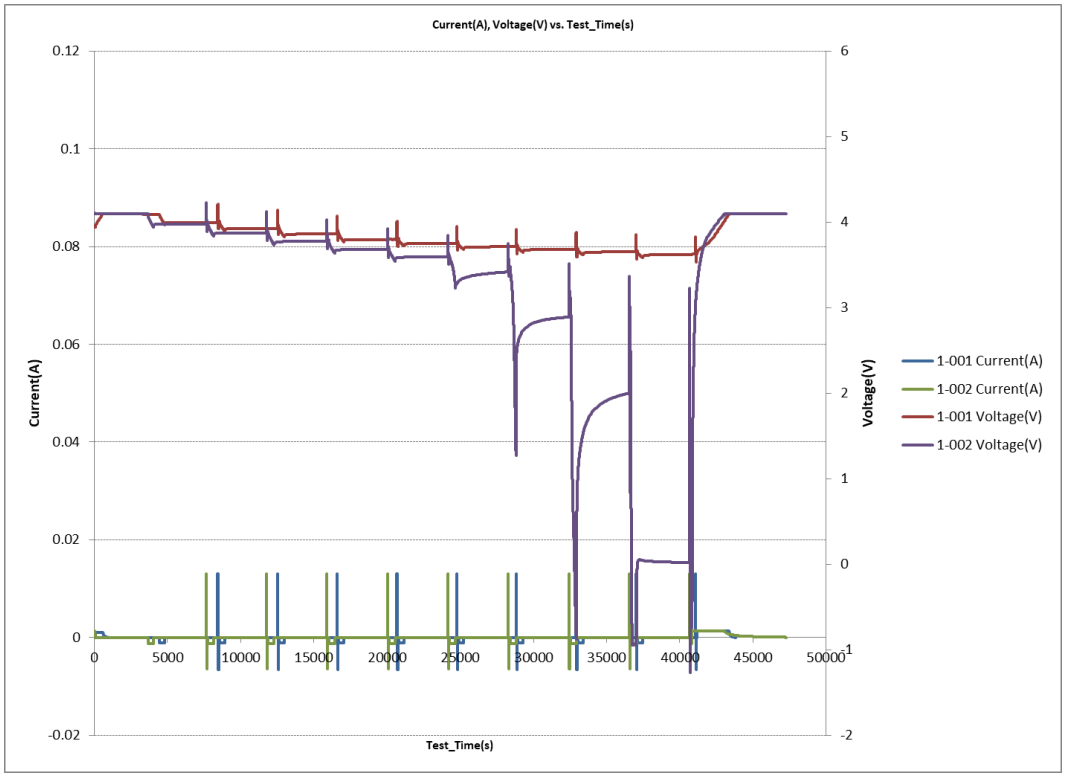

Figure 45. Voltage vs SOC comparison of baseline HPPC experiments.

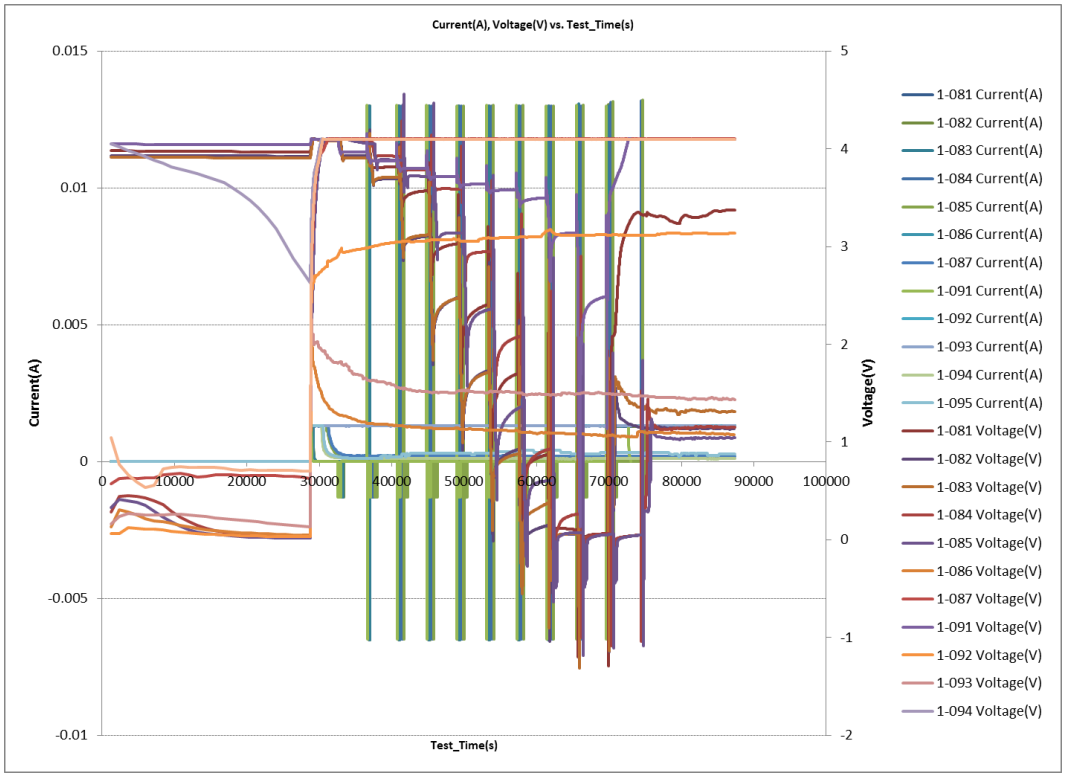

Figure 46. Raw HPPC data for all damaged cells. Some cells do not have reliable data.

In order to validate the thermal response fully, cycling representative cells manufactured with 100 MPa and 133 MPa or equivalent mechanically damaged separators can provide missing thermal information. Experimental electro-thermal data was obtained with 0kN, 15kN, and 30kN pouch cells, but for safety concerns the 45kN and 60kN cells were never created. In the future, additional cells must be cycled for an accurate assessment of simulation results. Another set of future experiments would be to verify simulation results of 45 kN and 60 kN crushed pouch cells and a cylindrical spirally wound cell.

REFERENCES

[1] V. Woollaston, "New blow for Tesla: Fire in the 'world's safest electric car' began in vehicle's battery," Daily Mail, 03-Oct-2013. [Online]. Available: http://www.dailymail.co.uk/sciencetech/article-2442392/New-blow-Tesla-Fire-worlds-safest-electric-car-began-vehicles-battery.html.

[2] S. Abada, G. Marlair, A. Lecocq, M. Petit, V. Sauvant-Moynot, and F. Huet, "Safety focused modeling of lithium-ion batteries: A review," *J. Power Sources*, vol. 306, pp. 178–192, Feb. 2016.

[3] L. Brown, "Press Release – FAA Statement," 16-Jan-2013.

[4] N. Williard, W. He, C. Hendricks, and M. Pecht, "Lessons Learned from the 787 Dreamliner Issue on Lithium-Ion Battery Reliability," *Energies*, vol. 6, no. 9, pp. 4682–4695, Sep. 2013.

[5] J. M. Kolly, J. Panagiotou, and B. A. Czech, "The Investigation of a Lithium-Ion Battery Fire Onboard a Boeing 787 by the US National Transportation Safety Board," Technical Report. Available at: http://www. isasi. org/Documents/library/technical-papers/2013/ISASI% 20NTSB% 20Kolly. pdf, 2013.

[6] S. Hollister, "Here's why Samsung Note 7 phones are catching fire," *CNET*, 10-Oct-2016. [Online]. Available: https://www.cnet.com/news/why-is-samsung-galaxy-note-7-exploding-overheating/.

[7] F. Larsson, P. Andersson, and B.-E. Mellander, "Lithium-Ion Battery Aspects on Fires in Electrified Vehicles on the Basis of Experimental Abuse Tests," *Batteries*, vol. 2, no. 2, p. 9, Apr. 2016.

[8] T. Gryta, "Americans Keep Their Cellphones Longer," *Wall Street Journal*, 18-Apr-2016. [Online]. Available: http://www.wsj.com/articles/americans-keep-their-cellphones-longer-1461007321.

[9] CADEX, "BU-808: How to Prolong Lithium-based Batteries," *Battery University*, 2016. [Online]. Available: http://batteryuniversity.com/learn/article/how_to_prolong_lithium_based_batteries.

[10] R. Barrett, "This Saab story is one in a million," *Journal Sentinel*, 06-Dec-2006. [Online]. Available: http://archive.jsonline.com/business/29181064.html.

[11] "FreedomCAR and Fuel Partnership Plan." FreedomCAR, Mar-2006.

[12] E. Musk, "Infinite Mile Warranty," *Tesla*, 15-Aug-2004. [Online]. Available: https://www.tesla.com/en_GB/blog/infinite-mile-warranty?redirect=no.

[13] D. Doughty and E. P. Roth, "A general discussion of Li ion battery safety," *Electrochem. Soc. Interface*, vol. 21, no. 2, pp. 37–44, 2012.

[14] L. Lu, X. Han, J. Li, J. Hua, and M. Ouyang, "A review on the key issues for lithium-ion battery management in electric vehicles," *J. Power Sources*, vol. 226, pp. 272–288, Mar. 2013.

[15] B. Wojdyla, "The Straight Story On the Chevy Volt Battery Fire," *Popular Mechanics*, Nov 28. [Online]. Available: http://www.popularmechanics.com/cars/hybrid-electric/a11865/the-straight-story-on-the-chevy-volt-battery-fire-6601217/.

[16] "SAFO 15010." Federal Aviation Administration, 08-Oct-2015.

[17] "SAFO 16001." Federal Aviation Administration, 19-Jan-2016.

[18] "SAFO 16004." Federal Aviation Administration, 06-May-2016.

[19] "SAFO 16011." Federal Aviation Administration, 16-Sep-2016.
[20] "SAFO 16012." Federal Aviation Administration, 09-Sep-2016.
[21] A. Ng, "Samsung pins explosive Galaxy Note 7 on battery flaw," *CNET*, 14-Sep-2016. [Online]. Available: https://www.cnet.com/news/samsung-galaxy-note-7-explosion-battery-manufacturing-error/.
[22] A. Shedletsky, "Beyond the Teardown: How we think about failure analysis, Samsung Galaxy Note 7 edition," *Instrumental.ai*, 12-Dec-2016. [Online]. Available: https://www.instrumental.ai/blog/2016/12/beyond-the-teardown-galaxy-note-7.
[23] A. Shedletsky, "Aggressive design caused Samsung Galaxy Note 7 battery explosions," *Instrumental.ai*, 02-Dec-2016. [Online]. Available: https://www.instrumental.ai/blog/2016/12/1/aggressive-design-caused-samsung-galaxy-note-7-battery-explosions.
[24] "Samsung Expands Recall to All Galaxy Note 7 Devices," *Samsung*, 09-Dec-2016. [Online]. Available: http://www.samsung.com/us/note7recall/.
[25] "Statement on Conclusion of Chevy Volt Investigation." National Highway Traffic Safety Administration, 20-Jan-2012.
[26] A. Peseran, "NREL Multiphysics Modeling Tools and ISC Device for Designing Safer Li-Ion Batteries," presented at the 33rd Annual International Battery Seminar and Exhibit, Fort Lauderdale, FL, 24-Mar-2016.
[27] C. Zhang, S. Santhanagopalan, A. Pesaran, E. Sahraei, and T. Wierzbicki, "Coupling of Mechanical Behavior of Lithium Ion Cells to Electrochemical-Thermal Models for Battery Crush," NREL (National Renewable Energy Laboratory (NREL), Golden, CO (United States)), 2015.
[28] S. Park, A. Savvides, and M. Srivastava, "Battery capacity measurement and analysis using lithium coin cell battery," in *Proceedings of the 2001 international symposium on Low power electronics and design*, 2001, pp. 382–387.
[29] T. Marks, S. Trussler, A. J. Smith, D. Xiong, and J. R. Dahn, "A Guide to Li-Ion Coin-Cell Electrode Making for Academic Researchers," *J. Electrochem. Soc.*, vol. 158, no. 1, p. A51, 2011.
[30] A. Friesen, X. Mönnighoff, M. Börner, J. Haetge, F. M. Schappacher, and M. Winter, "Influence of temperature on the aging behavior of 18650-type lithium ion cells: A comprehensive approach combining electrochemical characterization and post-mortem analysis," *J. Power Sources*, vol. 342, pp. 88–97, Feb. 2017.
[31] J. Liu, Z. Wang, J. Gong, K. Liu, H. Wang, and L. Guo, "Experimental Study of Thermal Runaway Process of 18650 Lithium-Ion Battery," *Materials*, vol. 10, no. 3, p. 230, Feb. 2017.
[32] S. Al-Hallaj, J. Prakash, and J. R. Selman, "Characterizaton of commercial Li-ion batteries using electrochemical-calorimetric measurements," *J. Power Sources*, vol. 87, pp. 186–194, 2000.
[33] A. Mills and S. Al-Hallaj, "Simulation of passive thermal management system for lithium-ion battery packs," *J. Power Sources*, vol. 141, no. 2, pp. 307–315, Mar. 2005.
[34] G. Zhang, L. Cao, S. Ge, C.-Y. Wang, C. E. Shaffer, and C. D. Rahn, "In situ measurement of radial temperature distributions in cylindrical li-ion cells," *J. Electrochem. Soc.*, vol. 161, no. 10, pp. A1499–A1507, 2014.

[35] E. Sahraei, R. Hill, and T. Wierzbicki, "Calibration and finite element simulation of pouch lithium-ion batteries for mechanical integrity," *J. Power Sources*, vol. 201, pp. 307–321, Mar. 2012.
[36] S. J. Drake, D. A. Wetz, J. K. Ostanek, S. P. Miller, J. M. Heinzel, and A. Jain, "Measurement of anisotropic thermophysical properties of cylindrical Li-ion cells," *J. Power Sources*, vol. 252, pp. 298–304, Apr. 2014.
[37] T. Wierzbicki and E. Sahraei, "Homogenized mechanical properties for the jellyroll of cylindrical Lithium-ion cells," *J. Power Sources*, vol. 241, pp. 467–476, Nov. 2013.
[38] J. Schmalstieg, S. Käbitz, M. Ecker, and D. U. Sauer, "A holistic aging model for Li(NiMnCo)O2 based 18650 lithium-ion batteries," *J. Power Sources*, vol. 257, pp. 325–334, Jul. 2014.
[39] T. Volck *et al.*, "Method for Determination of the Internal Short Resistance and Heat Evolution at Different Mechanical Loads of a Lithium Ion Battery Cell Based on Dummy Pouch Cells," *Batteries*, vol. 2, no. 2, p. 8, Apr. 2016.
[40] F. Larsson, P. Andersson, and B.-E. Mellander, "Lithium-Ion Battery Aspects on Fires in Electrified Vehicles on the Basis of Experimental Abuse Tests," *Batteries*, vol. 2, no. 2, p. 9, Apr. 2016.
[41] E. Sahraei, J. Campbell, and T. Wierzbicki, "Modeling and short circuit detection of 18650 Li-ion cells under mechanical abuse conditions," *J. Power Sources*, vol. 220, pp. 360–372, Dec. 2012.
[42] D. Andre, M. Meiler, K. Steiner, H. Walz, T. Soczka-Guth, and D. U. Sauer, "Characterization of high-power lithium-ion batteries by electrochemical impedance spectroscopy. II: Modelling," *J. Power Sources*, vol. 196, no. 12, pp. 5349–5356, Jun. 2011.
[43] M. Chatiri, T. Gull, A. Matzenmiller, and A. Opel, "An assesment of the new LS-DYNA layered solid element: basics, patch simulation and its potential for thick composite structure analysis," *7th Eur. -DYNA Conf.*, 2009.
[44] J. N. Reddy, *Mechanics of Laminated Composite Plates and Shells*. CRC Press LLC, 2004.
[45] I. V. Avdeev and M. Gilaki, "Explicit Dynamic Simulation of Impact in Cylindrical Lithium-Ion Batteries," in *ASME 2012 International Mechanical Engineering Congress and Exposition*, 2012, pp. 461–467.
[46] I. Avdeev and M. Gilaki, "Structural analysis and experimental characterization of cylindrical lithium-ion battery cells subject to lateral impact," *J. Power Sources*, vol. 271, pp. 382–391, Dec. 2014.
[47] P. Arora and Z. (John) Zhang, "Battery Separators," *Chem. Rev.*, vol. 104, no. 10, pp. 4419–4462, Oct. 2004.
[48] I. Avdeev, M. Martinsen, and A. Francis, "Rate- and Temperature-Dependent Material Behavior of a Multilayer Polymer Battery Separator," *J. Mater. Eng. Perform.*, vol. 23, no. 1, pp. 315–325, Jan. 2014.
[49] A. Topa, *LS-Dyna: Car Crash*. YouTube, 2013.
[50] J. G. Michopoulos, C. Farhat, and J. Fish, "Survey on Modeling and Simulation of Multiphysics Systems," *J. Comput. Inf. Sci. Eng.*, vol. 5, pp. 198–213, 2005.
[51] P. N. Doval, "Aerodynamic Analysis and Drag Coefficient Evaluation of Time-Trial Bicycle Riders," 2012.

[52] M. Gyimesi, I. Avdeev, and D. Ostergaard, “Finite-Element Simulation of Micro-Electromechanical Systems (MEMS) by Strongly Coupled Electromechanical Transducers,” *IEEE Trans. Magn.*, vol. 40, no. 2, pp. 557–560, Mar. 2004.
[53] F. Bay, V. Labbé, Y. Favennec, and J.-L. Chenot, “A numerical model for induction heating processes coupling electromagnetism and thermomechanics,” *Int. J. Numer. Methods Eng.*, vol. 58, no. 6, pp. 839–867, 2003.
[54] J. E. B. Randles, “Kinetics of rapid electrode reactions,” *Discuss. Faraday Soc.*, vol. 1, pp. 11–19, 1947.
[55] A. Fotouhi, D. J. Auger, K. Propp, S. Longo, and M. Wild, “A review on electric vehicle battery modelling: From Lithium-ion toward Lithium–Sulphur,” *Renew. Sustain. Energy Rev.*, vol. 56, pp. 1008–1021, Apr. 2016.
[56] Y. Hu and S. Yurkovich, “Linear parameter varying battery model identification using subspace methods,” *J. Power Sources*, vol. 196, no. 5, pp. 2913–2923, Mar. 2011.
[57] E. Samadani *et al.*, “Empirical Modeling of Lithium-ion Batteries Based on Electrochemical Impedance Spectroscopy Tests,” *Electrochimica Acta*, vol. 160, pp. 169–177, Apr. 2015.
[58] Y. Xie, J. Li, and C. Yuan, “Mathematical modeling of the electrochemical impedance spectroscopy in lithium ion battery cycling,” *Electrochimica Acta*, vol. 127, pp. 266–275, May 2014.
[59] D. Andre, M. Meiler, K. Steiner, C. Wimmer, T. Soczka-Guth, and D. U. Sauer, “Characterization of high-power lithium-ion batteries by electrochemical impedance spectroscopy. I. Experimental investigation,” *J. Power Sources*, vol. 196, no. 12, pp. 5334–5341, Jun. 2011.
[60] S. Buller, M. Thele, R. W. A. A. DeDoncker, and E. Karden, “Impedance-Based Simulation Models of Supercapacitors and Li-Ion Batteries for Power Electronic Applications,” *IEEE Trans. Ind. Appl.*, vol. 41, no. 3, pp. 742–747, May 2005.
[61] A. Jokar, B. Rajabloo, M. Désilets, and M. Lacroix, “Review of simplified Pseudo-two-Dimensional models of lithium-ion batteries,” *J. Power Sources*, vol. 327, pp. 44–55, Sep. 2016.
[62] L. Cai and R. E. White, “Mathematical modeling of a lithium ion battery with thermal effects in COMSOL Inc. Multiphysics (MP) software,” *J. Power Sources*, vol. 196, no. 14, pp. 5985–5989, Jul. 2011.
[63] M.-T. von Srbik, M. Marinescu, R. F. Martinez-Botas, and G. J. Offer, “A physically meaningful equivalent circuit network model of a lithium-ion battery accounting for local electrochemical and thermal behaviour, variable double layer capacitance and degradation,” *J. Power Sources*, vol. 325, pp. 171–184, Sep. 2016.
[64] T. R. Ashwin, A. McGordon, and P. A. Jennings, “Electrochemical modelling of Li-ion battery pack with constant voltage cycling,” *J. Power Sources*, vol. 341, pp. 327–339, Feb. 2017.
[65] K. Smith and C.-Y. Wang, “Power and thermal characterization of a lithium-ion battery pack for hybrid-electric vehicles,” *J. Power Sources*, vol. 160, no. 1, pp. 662–673, Sep. 2006.
[66] J. Jaguemont, L. Boulon, and Y. Dubé, “A comprehensive review of lithium-ion batteries used in hybrid and electric vehicles at cold temperatures,” *Appl. Energy*, vol. 164, pp. 99–114, Feb. 2016.

[67] S. Nejad, D. T. Gladwin, and D. A. Stone, “A systematic review of lumped-parameter equivalent circuit models for real-time estimation of lithium-ion battery states,” *J. Power Sources*, vol. 316, pp. 183–196, Jun. 2016.
[68] M. A. Hannan, M. S. H. Lipu, A. Hussain, and A. Mohamed, “A review of lithium-ion battery state of charge estimation and management system in electric vehicle applications: Challenges and recommendations,” *Renew. Sustain. Energy Rev.*, vol. 78, pp. 834–854, Oct. 2017.
[69] M. Sievers, U. Sievers, and S. S. Mao, “Thermal modelling of new Li-ion cell design modifications,” *Forsch. Im Ingenieurwesen*, vol. 74, no. 4, pp. 215–231, Dec. 2010.
[70] L. L. Gaines and R. M. Cuenca, “Costs of Lithium-Ion Batteries for Vehicles,” 2000. .
[71] M. Chen *et al.*, “A Thermal Runaway Simulation on a Lithium Titanate Battery and the Battery Module,” *Energies*, vol. 8, no. 1, pp. 490–500, Jan. 2015.
[72] Q. Wang, P. Ping, X. Zhao, G. Chu, J. Sun, and C. Chen, “Thermal runaway caused fire and explosion of lithium ion battery,” *J. Power Sources*, vol. 208, pp. 210–224, Jun. 2012.
[73] T. Han, G.-H. Kim, and L. Collins, “Development of Computer-Aided Design Tools for Automotive Batteries-CAEBAT,” presented at the Automotive Simulation World Congress, 30-Oct-2012.
[74] A. Pesaran, M. Keyser, G.-H. Kim, S. Santhanagopalan, and K. Smith, “Tools for designing thermal management of batteries in electric drive vehicles,” in *Large Lithium Ion Battery Technology & Application Symposia Advanced Automotive Battery Conference Pasadena*, 2013.
[75] K. Shah *et al.*, “An experimentally validated transient thermal model for cylindrical Li-ion cells,” *J. Power Sources*, vol. 271, pp. 262–268, Dec. 2014.
[76] T. M. Bandhauer, S. Garimella, and T. F. Fuller, “A Critical Review of Thermal Issues in Lithium-Ion Batteries,” *J. Electrochem. Soc.*, vol. 158, no. 3, p. R1, 2011.
[77] H. Khasawneh, “Analysis of Heat-Spreading Thermal Management Solutions for Lithium-Ion Batteries,” in *ResearchGate*, 2011.
[78] K. Onda, H. Kameyama, T. Hanamoto, and K. Ito, “Experimental Study on Heat Generation Behavior of Small Lithium-Ion Secondary Batteries,” *J. Electrochem. Soc.*, vol. 150, no. 3, p. A285, 2003.
[79] S. C. Chen, C. C. Wan, and Y. Y. Wang, “Thermal analysis of lithium-ion batteries,” *J. Power Sources*, vol. 140, no. 1, pp. 111–124, Jan. 2005.
[80] X. Zhang, “Thermal analysis of a cylindrical lithium-ion battery,” *Electrochimica Acta*, vol. 56, no. 3, pp. 1246–1255, Jan. 2011.
[81] D. Bernardi, E. Pawlikowski, and J. Newman, “A general energy balance for battery systems,” *J. Electrochem. Soc.*, vol. 132, no. 1, pp. 5–12, 1985.
[82] N. Baba, H. Yoshida, M. Nagaoka, C. Okuda, and S. Kawauchi, “Numerical simulation of thermal behavior of lithium-ion secondary batteries using the enhanced single particle model,” *J. Power Sources*, vol. 252, pp. 214–228, Apr. 2014.
[83] K. Somasundaram, E. Birgersson, and A. S. Mujumdar, “Thermal–electrochemical model for passive thermal management of a spiral-wound lithium-ion battery,” *J. Power Sources*, vol. 203, pp. 84–96, Apr. 2012.
[84] L. Lam, P. Bauer, and E. Kelder, “A practical circuit-based model for Li-ion battery cells in electric vehicle applications,” in *2011 IEEE 33rd International Telecommunications Energy Conference (INTELEC)*, 2011, pp. 1–9.

[85] J. Marcicki *et al.*, "Battery Abuse Case Study Analysis Using LS-DYNA," presented at the 14th International LS-DYNA Users Conference, 2016.
[86] R. Zhao, S. Zhang, J. Liu, and J. Gu, "A review of thermal performance improving methods of lithium ion battery: Electrode modification and thermal management system," *J. Power Sources*, vol. 299, pp. 557–577, Dec. 2015.
[87] R. Benger, H. Wenzl, H.-P. Beck, M. Jiang, D. Ohms, and G. Schaedlich, "Electrochemical and thermal modeling of li-ion cells for use in HEV or EV application," *World Electr. Veh. J.*, vol. 3, May 2009.
[88] X. Han, M. Ouyang, L. Lu, and J. Li, "Simplification of physics-based electrochemical model for lithium ion battery on electric vehicle. Part II: Pseudo-two-dimensional model simplification and state of charge estimation," *J. Power Sources*, vol. 278, pp. 814–825, Mar. 2015.
[89] M. Farag, M. Fleckenstein, and S. Habibi, "Continuous piecewise-linear, reduced-order electrochemical model for lithium-ion batteries in real-time applications," *J. Power Sources*, vol. 342, pp. 351–362, Feb. 2017.
[90] L. Song and J. W. Evans, "Electrochemical-thermal Model of Lithium Polymer Batteries," *J. Electrochem. Soc.*, vol. 147, no. 6, pp. 2086–2095, 2000.
[91] V. Srinivasan and C. Y. Wang, "Analysis of Electrochemical and Thermal Behavior of Li-Ion Cells," *J. Electrochem. Soc.*, vol. 150, no. 1, p. A98, 2003.
[92] Y. Ye, Y. Shi, N. Cai, J. Lee, and X. He, "Electro-thermal modeling and experimental validation for lithium ion battery," *J. Power Sources*, vol. 199, pp. 227–238, Feb. 2012.
[93] A. M. Bizeray, S. Zhao, S. R. Duncan, and D. A. Howey, "Lithium-ion battery thermal-electrochemical model-based state estimation using orthogonal collocation and a modified extended Kalman filter," *J. Power Sources*, vol. 296, pp. 400–412, Nov. 2015.
[94] W. Fang, O. J. Kwon, and C.-Y. Wang, "Electrochemical-thermal modeling of automotive Li-ion batteries and experimental validation using a three-electrode cell," *Int. J. Energy Res.*, vol. 34, no. 2, pp. 107–115, Feb. 2010.
[95] L. H. Saw, Y. Ye, and A. A. O. Tay, "Electrochemical–thermal analysis of 18650 Lithium Iron Phosphate cell," *Energy Convers. Manag.*, vol. 75, pp. 162–174, Nov. 2013.
[96] P. W. Northrop, M. Pathak, D. Rife, S. De, S. Santhanagopalan, and V. R. Subramanian, "Efficient simulation and model reformulation of two-dimensional electrochemical thermal behavior of lithium-ion batteries," *J. Electrochem. Soc.*, vol. 162, no. 6, pp. A940–A951, 2015.
[97] C. R. Pals and J. Newman, "Thermal modeling of the lithium/polymer battery I. Discharge behavior of a single cell," *J. Electrochem. Soc.*, vol. 142, no. 10, pp. 3274–3281, 1995.
[98] C. R. Pals and J. Newman, "Thermal modeling of the lithium/polymer battery II. Temperature profiles in a cell stack," *J. Electrochem. Soc.*, vol. 142, no. 10, pp. 3282–3288, 1995.
[99] V. Ramadesigan, P. W. Northrop, S. De, S. Santhanagopalan, R. D. Braatz, and V. R. Subramanian, "Modeling and simulation of lithium-ion batteries from a systems engineering perspective," *J. Electrochem. Soc.*, vol. 159, no. 3, pp. R31–R45, 2012.
[100] K. Kumaresan, G. Sikha, and R. E. White, "Thermal Model for a Li-Ion Cell," *J. Electrochem. Soc.*, vol. 155, no. 2, p. A164, 2008.
[101] M. Chen *et al.*, "A Thermal Runaway Simulation on a Lithium Titanate Battery and the Battery Module," *Energies*, vol. 8, no. 1, pp. 490–500, Jan. 2015.

[102] K. A. Murashko, A. V. Mityakov, J. Pyrhönen, V. Y. Mityakov, and S. S. Sapozhnikov, "Thermal parameters determination of battery cells by local heat flux measurements," *J. Power Sources*, vol. 271, pp. 48–54, Dec. 2014.
[103] H. Maleki and A. K. Shamsuri, "Thermal analysis and modeling of a notebook computer battery," *J. Power Sources*, vol. 115, no. 1, pp. 131–136, Mar. 2003.
[104] S. Khaleghi Rahimian, S. Rayman, and R. E. White, "Extension of physics-based single particle model for higher charge–discharge rates," *J. Power Sources*, vol. 224, pp. 180–194, Feb. 2013.
[105] C. Gu, "Model order reduction of nonlinear dynamical systems," University of California, Berkeley, 2011.
[106] S. Golmon, K. Maute, and M. L. Dunn, "Numerical modeling of electrochemical–mechanical interactions in lithium polymer batteries," *Comput. Struct.*, vol. 87, no. 23–24, pp. 1567–1579, Dec. 2009.
[107] X. Zhang, W. Shyy, and A. Marie Sastry, "Numerical Simulation of Intercalation-Induced Stress in Li-Ion Battery Electrode Particles," *J. Electrochem. Soc.*, vol. 154, no. 10, p. A910, 2007.
[108] M. Doyle, T. F. Fuller, and J. Newman, "Modeling of Galvanostatic Charge and Discharge of the Lithium/Polymer/Insertion Cell," *J. Electrochem. Soc.*, vol. 140, no. 6, pp. 1526–1533, Jun. 1993.
[109] M. Doyle, J. Newman, A. S. Gozdz, C. N. Schmutz, and J.-M. Tarascon, "Comparison of Modeling Predictions with Experimental Data from Plastic Lithium Ion Cells," *J. Electrochem. Soc.*, vol. 143, no. 6, pp. 1890–1903, Jun. 1996.
[110] W. Wu, "A multiphysics model for the stress analysis of the separator in lithium-ion battery," Michigan State University, 2013.
[111] T. R. Tanim, C. D. Rahn, and C.-Y. Wang, "A temperature dependent, single particle, lithium ion cell model including electrolyte diffusion," *J. Dyn. Syst. Meas. Control*, vol. 137, no. 1, p. 011005, 2015.
[112] R. Rao, S. Vrudhula, and D. N. Rakhmatov, "Battery modeling for energy aware system design," *Computer*, vol. 36, no. 12, pp. 77–87, 2003.
[113] B. Wang, S. E. Li, H. Peng, and Z. Liu, "Fractional-order modeling and parameter identification for lithium-ion batteries," *J. Power Sources*, vol. 293, pp. 151–161, Oct. 2015.
[114] H.-G. Schweiger *et al.*, "Comparison of Several Methods for Determining the Internal Resistance of Lithium Ion Cells," *Sensors*, vol. 10, no. 6, pp. 5604–5625, Jun. 2010.
[115] L. Zhang, H. Peng, Z. Ning, Z. Mu, and C. Sun, "Comparative Research on RC Equivalent Circuit Models for Lithium-Ion Batteries of Electric Vehicles," *Appl. Sci.*, vol. 7, no. 10, p. 1002, Sep. 2017.
[116] P. L'Eplattenier *et al.*, "A Distributed Randle Circuit Model for Battery Abuse Simulations Using LS-DYNA," in *Electromagnetic*, 2016.
[117] B. Pattipati, C. Sankavaram, and K. Pattipati, "System Identification and Estimation Framework for Pivotal Automotive Battery Management System Characteristics," *IEEE Trans. Syst. Man Cybern. Part C Appl. Rev.*, vol. 41, no. 6, pp. 869–884, Nov. 2011.
[118] Z. M. Salameh, M. A. Casacca, and W. A. Lynch, "A mathematical model for lead-acid batteries," *IEEE Trans. Energy Convers.*, vol. 7, no. 1, pp. 93–98, 1992.
[119] W. D. Widanage *et al.*, "Design and use of multisine signals for Li-ion battery equivalent circuit modelling. Part 1: Signal design," *J. Power Sources*, vol. 324, pp. 70–78, Aug. 2016.

[120] H. Dai, T. Xu, L. Zhu, X. Wei, and Z. Sun, "Adaptive model parameter identification for large capacity Li-ion batteries on separated time scales," *Appl. Energy*, vol. 184, pp. 119–131, Dec. 2016.
[121] A. Li, S. Pelissier, P. Venet, and P. Gyan, "Fast Characterization Method for Modeling Battery Relaxation Voltage," *Batteries*, vol. 2, no. 2, p. 7, Apr. 2016.
[122] S. Orcioni, L. Buccolini, A. Ricci, and M. Conti, "Lithium-ion Battery Electrothermal Model, Parameter Estimation, and Simulation Environment," *Energies*, vol. 10, no. 3, p. 375, Mar. 2017.
[123] A. Papazoglou, S. Longo, D. Auger, and F. Assadian, "Nonlinear Filtering Techniques Comparison for Battery State Estimation," *J. Sustain. Dev. Energy Water Environ. Syst.*, vol. 2, no. 3, pp. 259–269, Sep. 2014.
[124] K. A. Smith, C. D. Rahn, and C.-Y. Wang, "Control oriented 1D electrochemical model of lithium ion battery," *Energy Convers. Manag.*, vol. 48, no. 9, pp. 2565–2578, Sep. 2007.
[125] X. Hu, S. Li, and H. Peng, "A comparative study of equivalent circuit models for Li-ion batteries," *J. Power Sources*, vol. 198, pp. 359–367, Jan. 2012.
[126] J. Gomez, R. Nelson, E. E. Kalu, M. H. Weatherspoon, and J. P. Zheng, "Equivalent circuit model parameters of a high-power Li-ion battery: Thermal and state of charge effects," *J. Power Sources*, vol. 196, no. 10, pp. 4826–4831, May 2011.
[127] A. Farmann and D. U. Sauer, "A study on the dependency of the open-circuit voltage on temperature and actual aging state of lithium-ion batteries," *J. Power Sources*, vol. 347, pp. 1–13, Apr. 2017.
[128] C. Y. Wang, W. B. Gu, and B. Y. Liaw, "Micro-macroscopic Coupled Modeling of Batteries and Fuel Cells," *J. Electrochem. Soc.*, vol. 145, no. 10, pp. 3407–3417, Oct. 1998.
[129] V. R. Subramanian, V. Boovaragavan, V. Ramadesigan, and M. Arabandi, "Mathematical Model Reformulation for Lithium-Ion Battery Simulations: Galvanostatic Boundary Conditions," *J. Electrochem. Soc.*, vol. 156, no. 4, p. A260, 2009.
[130] G. H. Kim and K. Smith, "Three-Dimensional Lithium-Ion Battery Model (Presentation)," National Renewable Energy Laboratory (NREL), Golden, CO., 2008.
[131] G.-H. Kim and K. Smith, "Multi-Scale Multi-Dimensional Li-Ion Battery Model for Better Design and Management (Presentation)," National Renewable Energy Laboratory (NREL), Golden, CO., 2008.
[132] D. Di Domenico, G. Fiengo, and A. Stefanopoulou, "Lithium-ion battery state of charge estimation with a Kalman filter based on a electrochemical model," in *Control Applications, 2008. CCA 2008. IEEE International Conference on*, 2008, pp. 702–707.
[133] V. Ramadesigan, V. Boovaragavan, J. C. Pirkle, and V. R. Subramanian, "Efficient Reformulation of Solid-Phase Diffusion in Physics-Based Lithium-Ion Battery Models," *J. Electrochem. Soc.*, vol. 157, no. 7, p. A854, 2010.
[134] C. R. Gould, C. M. Bingham, D. A. Stone, and P. Bentley, "New Battery Model and State-of-Health Determination Through Subspace Parameter Estimation and State-Observer Techniques," *IEEE Trans. Veh. Technol.*, vol. 58, no. 8, pp. 3905–3916, Oct. 2009.
[135] J. C. Forman, S. Bashash, J. L. Stein, and H. K. Fathy, "Reduction of an Electrochemistry-Based Li-Ion Battery Model via Quasi-Linearization and Padé Approximation," *J. Electrochem. Soc.*, vol. 158, no. 2, p. A93, 2011.
[136] T.-S. Dao, C. P. Vyasarayani, and J. McPhee, "Simplification and order reduction of lithium-ion battery model based on porous-electrode theory," *J. Power Sources*, vol. 198, pp. 329–337, Jan. 2012.

[137] J. L. Lee, A. Chemistruck, and G. L. Plett, "One-dimensional physics-based reduced-order model of lithium-ion dynamics," *J. Power Sources*, vol. 220, pp. 430–448, Dec. 2012.
[138] R. Klein, N. A. Chaturvedi, J. Christensen, J. Ahmed, R. Findeisen, and A. Kojic, "Electrochemical Model Based Observer Design for a Lithium-Ion Battery," *IEEE Trans. Control Syst. Technol.*, vol. 21, no. 2, pp. 289–301, Mar. 2013.
[139] W. Luo, C. Lyu, L. Wang, and L. Zhang, "An approximate solution for electrolyte concentration distribution in physics-based lithium-ion cell models," *Microelectron. Reliab.*, vol. 53, no. 6, pp. 797–804, Jun. 2013.
[140] M. Mastali Majdabadi, S. Farhad, M. Farkhondeh, R. A. Fraser, and M. Fowler, "Simplified electrochemical multi-particle model for LiFePO 4 cathodes in lithium-ion batteries," *J. Power Sources*, vol. 275, pp. 633–643, Feb. 2015.
[141] S. Santhanagopalan, Q. Guo, P. Ramadass, and R. E. White, "Review of models for predicting the cycling performance of lithium ion batteries," *J. Power Sources*, vol. 156, no. 2, pp. 620–628, Jun. 2006.
[142] G. L. Plett, "Sigma-point Kalman filtering for battery management systems of LiPB-based HEV battery packs," *J. Power Sources*, vol. 161, no. 2, pp. 1369–1384, Oct. 2006.
[143] D. H. Jeon and S. M. Baek, "Thermal modeling of cylindrical lithium ion battery during discharge cycle," *Energy Convers. Manag.*, vol. 52, no. 8–9, pp. 2973–2981, Aug. 2011.
[144] J. Yi, B. Koo, and C. Shin, "Three-Dimensional Modeling of the Thermal Behavior of a Lithium-Ion Battery Module for Hybrid Electric Vehicle Applications," *Energies*, vol. 7, no. 11, pp. 7586–7601, Nov. 2014.
[145] Q. Sun, Q. Wang, X. Zhao, J. Sun, and Z. Lin, "Numerical study on lithium titanate battery thermal response under adiabatic condition," *Energy Convers. Manag.*, vol. 92, pp. 184–193, Mar. 2015.
[146] K.-J. Lee, K. Smith, and G.-H. Kim, *A Three-Dimensional Thermal-Electrochemical Coupled Model for Spirally Wound Large-Format Lithium-Ion Batteries*. National Renewable Energy Laboratory, 2011.
[147] X. Hu and S. Stanton, "A Total Li-Ion Battery Simulation Solution," 04-Jun-2014.
[148] S. Kim, Y. S. Lee, H. S. Lee, and H. L. Jin, "A study on the behavior of a cylindrical type Li-Ion secondary battery under abnormal conditions. Über das Verhalten eines zylindrischen Li-Ionen Akkumulators unter abnormalen Bedingungen," *Mater. Werkst.*, vol. 41, no. 5, pp. 378–385, Jun. 2010.
[149] M. Gilaki and I. Avdeev, "Impact modeling of cylindrical lithium-ion battery cells: a heterogeneous approach," *J. Power Sources*, vol. 328, pp. 443–451, Oct. 2016.
[150] I. V. Avdeev and M. Gilaki, "Dynamic Simulation of Impact In Cylindrical Lithium-Ion Batteries," in *Proceedings of the ASME 2012 International Mechanical Engineering Congress and Exposition*, Houston, TX, 2015.
[151] C. Edouard, M. Petit, C. Forgez, J. Bernard, and R. Revel, "Parameter sensitivity analysis of a simplified electrochemical and thermal model for Li-ion batteries aging," *J. Power Sources*, vol. 325, pp. 482–494, Sep. 2016.
[152] H. Rao, Z. Huang, H. Zhang, and S. Xiao, "Study of fire tests and fire safety measures on lithiumion battery used on ships," in *Transportation Information and Safety (ICTIS), 2015 International Conference on*, 2015, pp. 865–870.
[153] Y. Zhang and K. Chou, "A parametric study of part distortions in fused deposition modelling using three-dimensional finite element analysis," *Proc. Inst. Mech. Eng. Part B J. Eng. Manuf.*, vol. 222, no. 8, pp. 959–968, Aug. 2008.

[154] Y. Chen and J. W. Evans, “Heat Transfer Phenomena in Lithium/Polymer-Electrolyte Batteries for Electric Vehicle Application,” *J. Electrochem. Soc.*, vol. 140, no. 7, pp. 1833–1838, Jul. 1993.
[155] K. Chen, G. Unsworth, and X. Li, “Measurements of heat generation in prismatic Li-ion batteries,” *J. Power Sources*, vol. 261, pp. 28–37, Sep. 2014.
[156] D. Chen, J. Jiang, G.-H. Kim, C. Yang, and A. Pesaran, “Comparison of different cooling methods for lithium ion battery cells,” *Appl. Therm. Eng.*, vol. 94, pp. 846–854, Feb. 2016.
[157] M. Börner *et al.*, “Correlation of aging and thermal stability of commercial 18650-type lithium ion batteries,” *J. Power Sources*, vol. 342, pp. 382–392, Feb. 2017.
[158] B. Vortmann-Westhoven, M. Winter, and S. Nowak, “Where is the lithium? Quantitative determination of the lithium distribution in lithium ion battery cells: Investigations on the influence of the temperature, the C-rate and the cell type,” *J. Power Sources*, vol. 346, pp. 63–70, Apr. 2017.
[159] X. Huang, “Separator technologies for lithium-ion batteries,” *J. Solid State Electrochem.*, vol. 15, no. 4, pp. 649–662, Apr. 2011.
[160] D. Djian, F. Alloin, S. Martinet, H. Lignier, and J. Y. Sanchez, “Lithium-ion batteries with high charge rate capacity: Influence of the porous separator,” *J. Power Sources*, vol. 172, no. 1, pp. 416–421, Oct. 2007.
[161] S. E. Li, B. Wang, H. Peng, and X. Hu, “An electrochemistry-based impedance model for lithium-ion batteries,” *J. Power Sources*, vol. 258, pp. 9–18, Jul. 2014.
[162] M. Martinsen, “Material Behavior Characterization of a Thin Film Polymer Used in lithium-ion batteries,” University of Wisconsin Milwaukee, 2012.
[163] I. Krüger, M. Sievers, and G. Schmitz, “Thermal Modeling of Automotive Lithium Ion Cells using the Finite Elements Method in Modelica,” 2009, pp. 1–8.
[164] G.-H. Kim, A. Pesaran, and R. Spotnitz, “A three-dimensional thermal abuse model for lithium-ion cells,” *J. Power Sources*, vol. 170, no. 2, pp. 476–489, Jul. 2007.
[165] M. Dubarry, C. Truchot, A. Devie, and B. Y. Liaw, “State-of-charge determination in lithium-ion battery packs based on two-point measurements in life,” *J. Electrochem. Soc.*, vol. 162, no. 6, pp. A877–A884, 2015.
[166] M. U. Cuma and T. Koroglu, “A comprehensive review on estimation strategies used in hybrid and battery electric vehicles,” *Renew. Sustain. Energy Rev.*, vol. 42, pp. 517–531, Feb. 2015.
[167] “Recommendations on the Transport of Dangerous Goods.” United Nations, 2011.
[168] C. Voelker, “If a picture is Worth 1,000 words, then Pervasive, Ubiquitous Imaging is Priceless,” *Standardization News*, 2003. [Online]. Available: https://www.astm.org/SNEWS/OCTOBER_2003/voelker_oct03.html.

APPENDIX

Table 8. Thermal modeling research matrix.

Author	Year	Batt. Geometry	T,crit. (°C)	T, amb (°C)	Heat gen. (g) (kWm^{-3})	Heat-trans coeff. ($Wm^{-2}K^{-1}$)	Thermal conductivity (K) ($Wm^{-1}K^{-1}$)	Math. Model
Spotnitz	2007	Cyl. (18650)	175	25	N/A	10, 20, 100 (pack)	N/A	
Bandhauer	2011	various types	90-120	20-25	2.3e6*	see Table VIII	see Table XVI	Yes**
Guo	2009	Pouch (VLP 50/62/100S)	246	140-160	N/A	8.7	0.334-398, see Table 1	
Sievers	2010	Cyl.	60-70	30	300	10	0.22-395, see Table 2	
Chen	2004	Plate	N/A	26.85*	N/A	natural conv, 100	0.334-398, see Table 4	Yes**
Kim	2007	Cyl. (18650, D50H90, D18H65)	155	35	~300 (C/min), g(t,T)	7.17, 5	N/A	
Krueger	2009	Cyl.	70	20-25	200, 300	N/A	0.22-395	
Argonne	N/A	N/A	N/A	0, 25, 50	*	N/A	N/A	
Lee	1986	N/A	N/A	N/A	N/A	N/A	N/A	
Somasundaram	2012	N/A	N/A	N/A	N/A	N/A	N/A	
Maleki	2002	Cyl. (18650)	N/A	45	N/A	N/A	N/A	Yes
Pals	1995	N/A	N/A	190	50-600*	6-30 (natural), 30-300 (forced)	see Table A-II	Yes**
Pals	1995	N/A	N/A	N/A	N/A	N/A	N/A	
Bernardi	1985	N/A	N/A	N/A	N/A	N/A	N/A	Yes
Chen	1994	Pouch (Li-Poly)	N/A	24.85	10-90, g(t,T)	6.0-25.0	see Table I	Yes
Chen	1993	Pouch (Li-Poly)	N/A	N/A	N/A	N/A	N/A	Yes
Newman	1995	Pouch (Li-Poly)	N/A	N/A	3.1e3	N/A	see Table II	Yes**
Song	2000	Pouch (Li-Poly)	N/A	N/A	N/A	N/A	0.5-395, see Table I	
Ye	2014	Cyl. (26650)	N/A	N/A	10, 100, 200	5	N/A	
Yi	2014	N/A	N/A	N/A	N/A	N/A	N/A	
Chen	2015	Cyl. (Li-Titanate)	177	N/A	~10, 90*	N/A	0.344-398, see Table 1	Yes

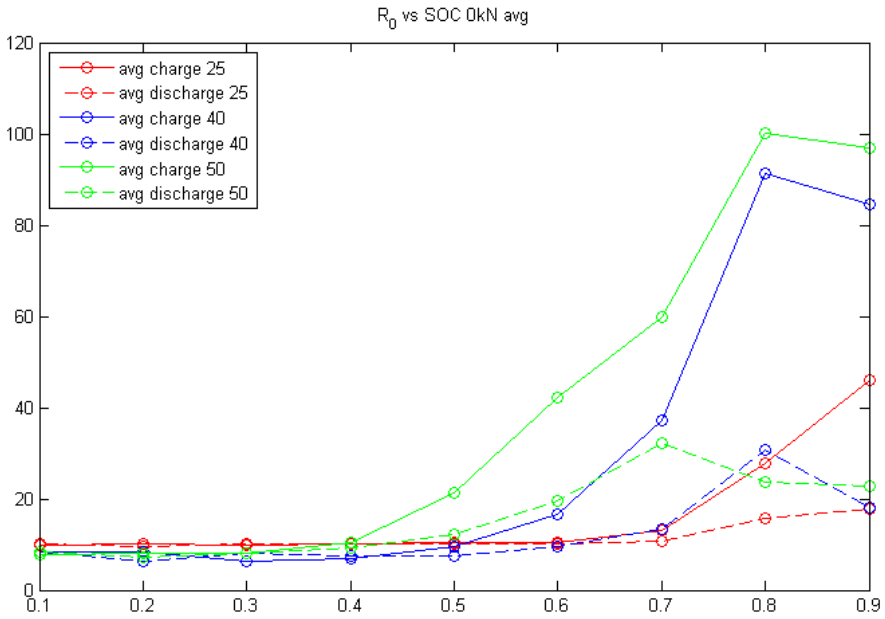

Figure 47. R0 vs SOC 0kN

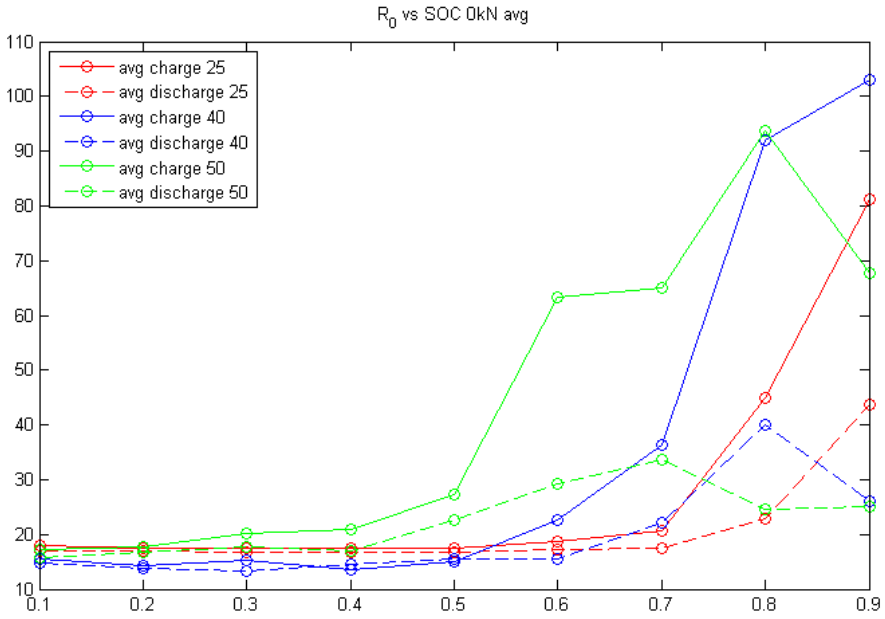

Figure 48. R0 vs SOC 15kN

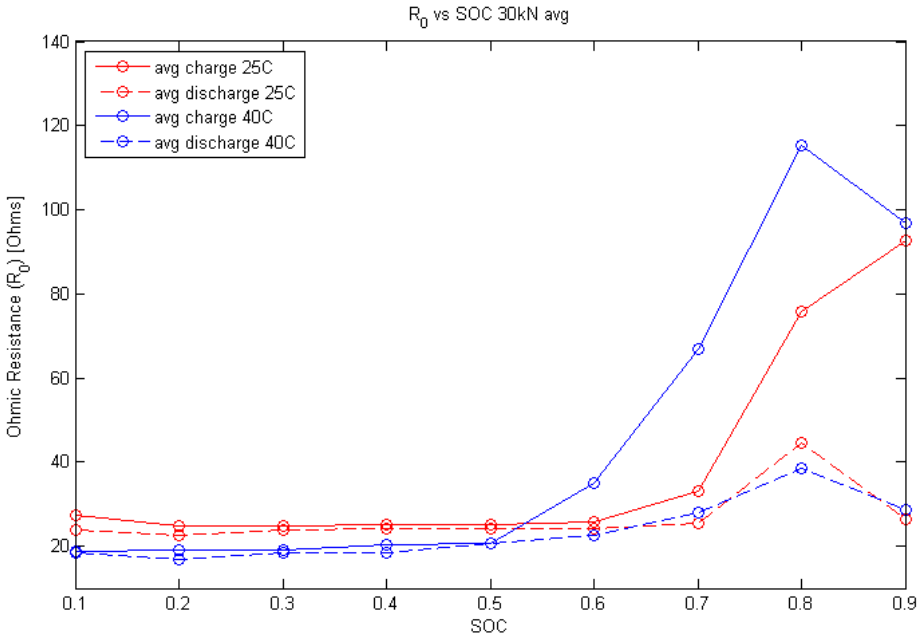

Figure 49. R0 vs SOC 30kN

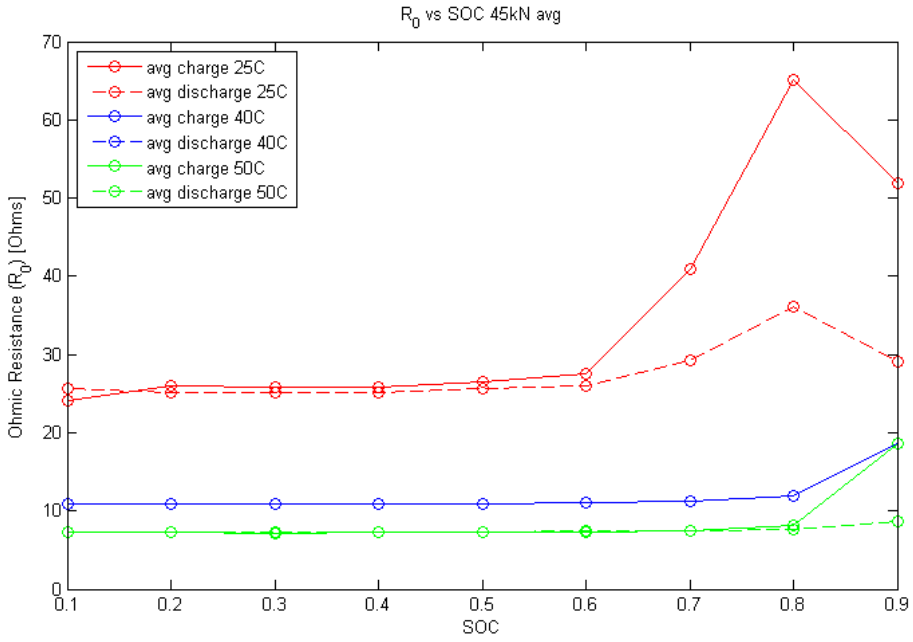

Figure 50. R0 vs SOC 45kN

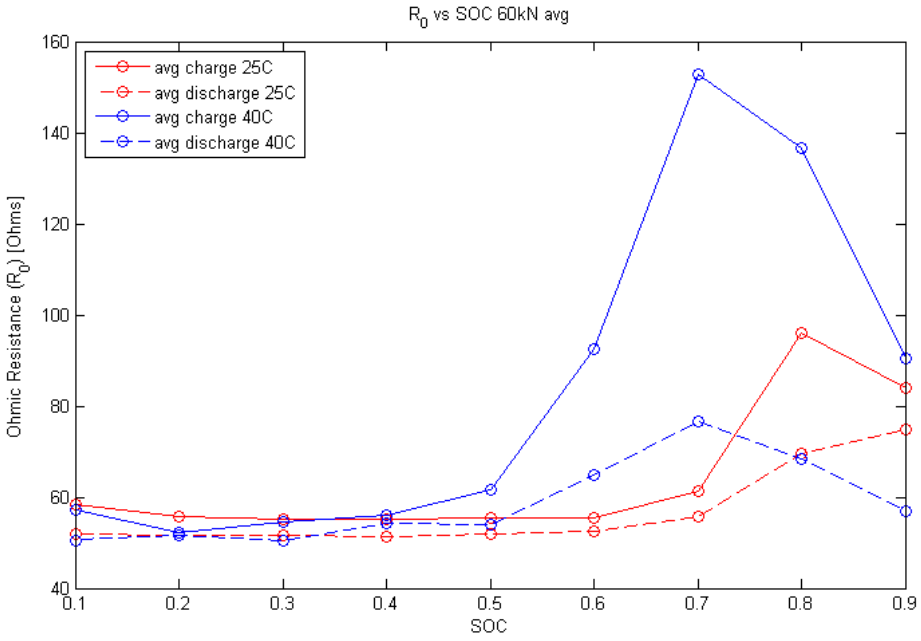

Figure 51. R0 vs SOC 60kN

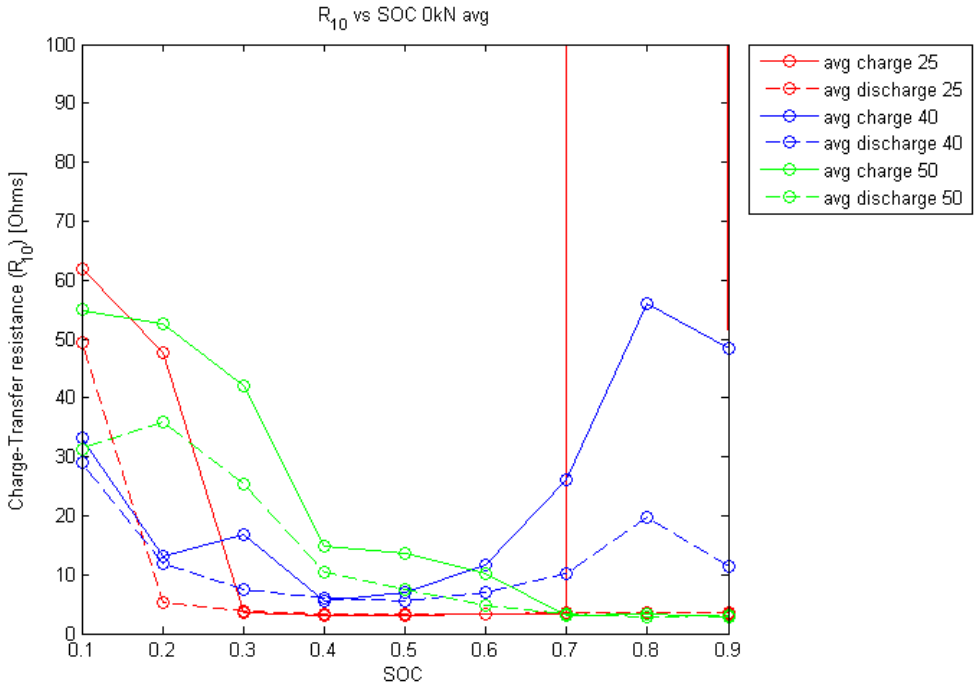

Figure 52. R10 vs SOC 0kN

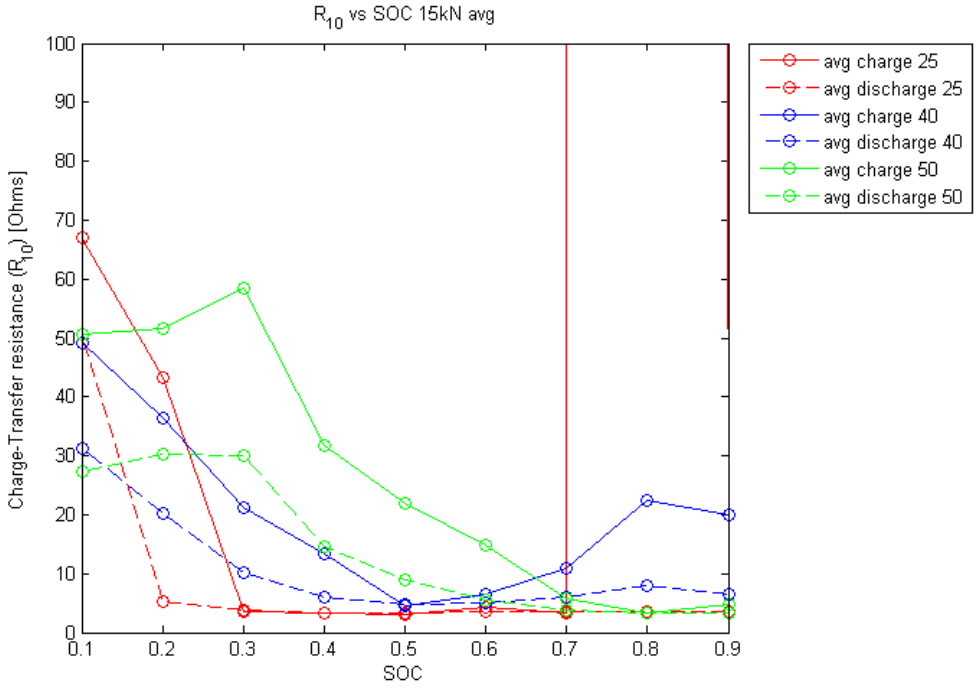

Figure 53. R10 vs SOC 15kN

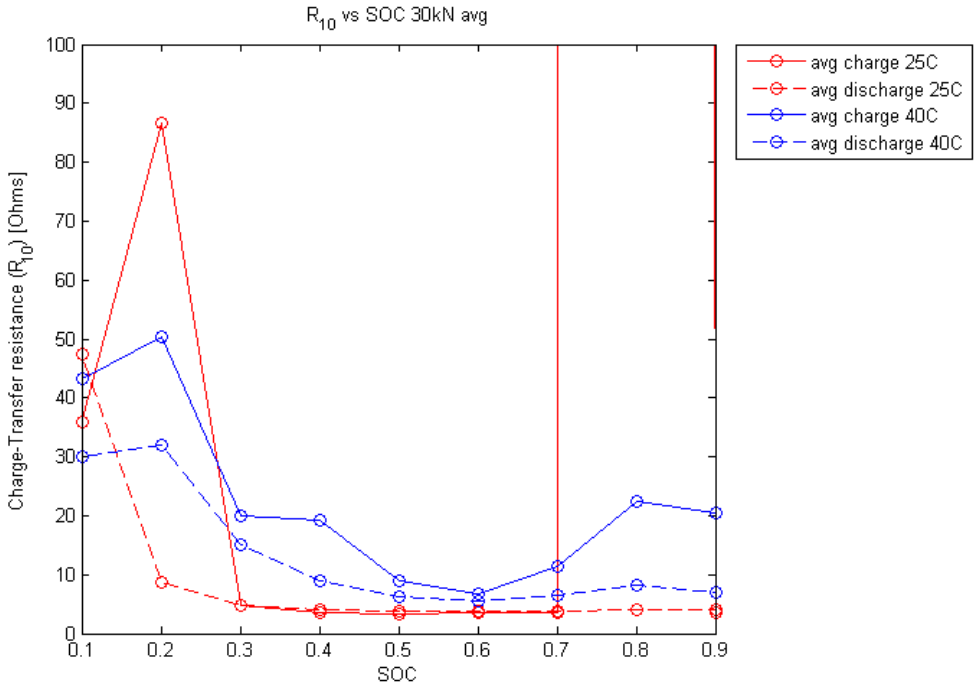

Figure 54. R10 vs SOC 30kN

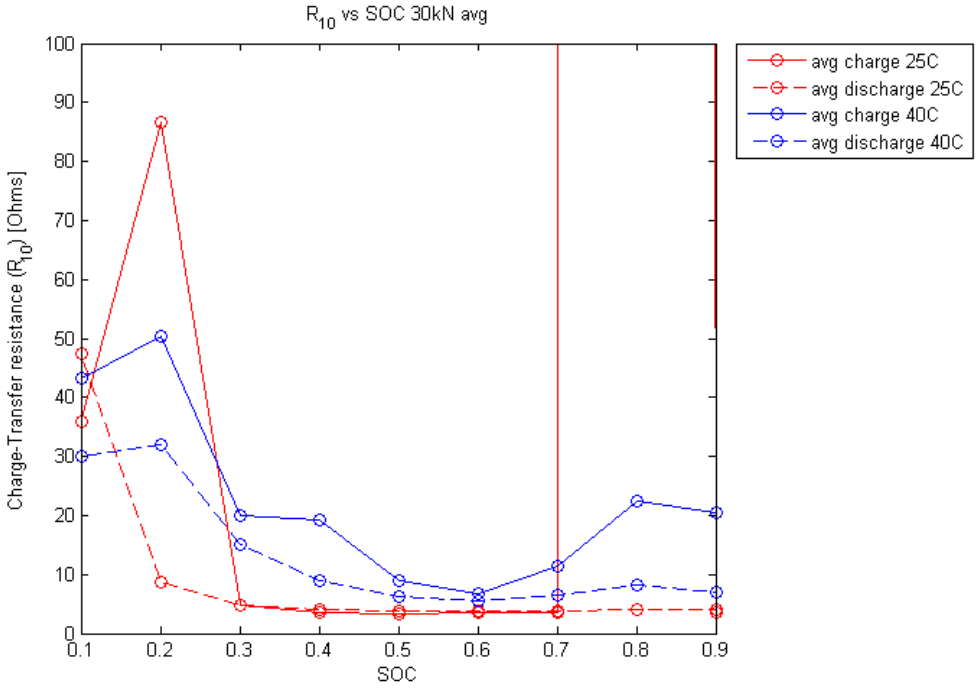

Figure 55. R10 vs SOC 45kN

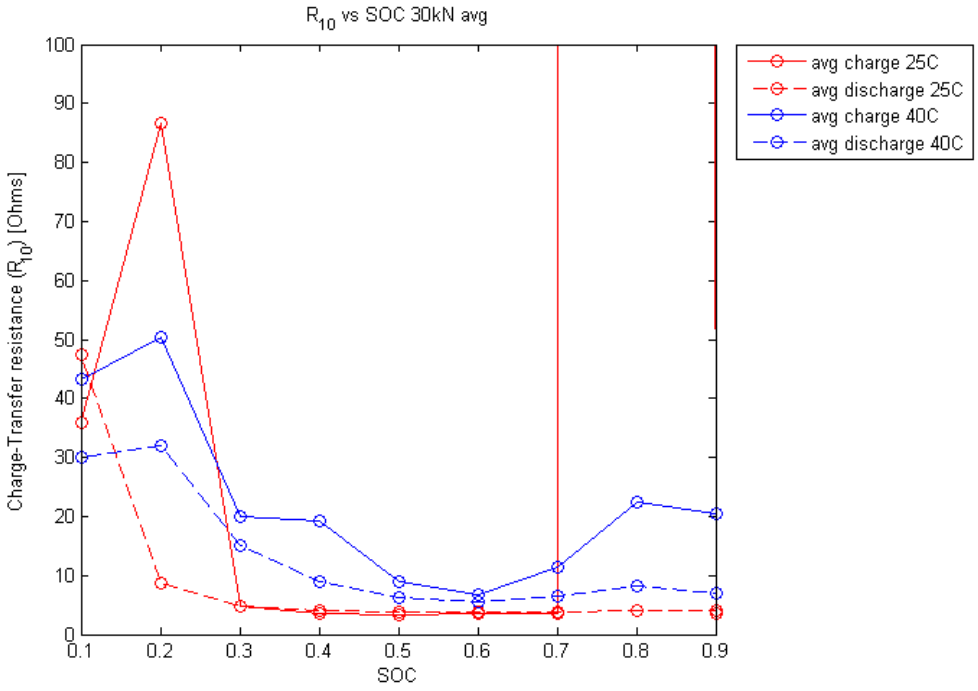

Figure 56. R10 vs SOC 60kN

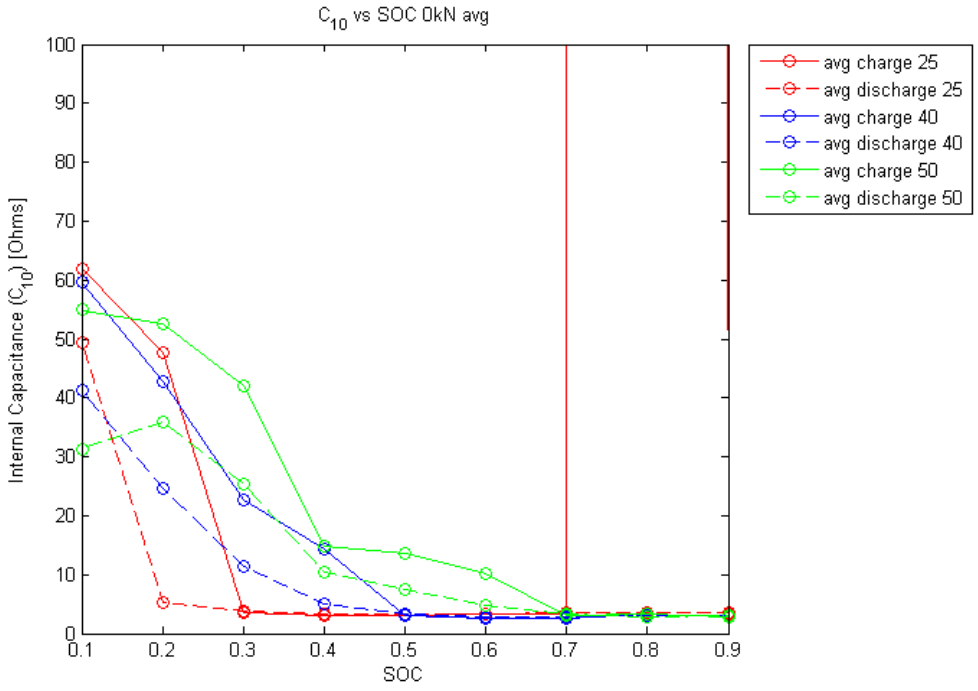

Figure 57. C10 vs SOC 0kN

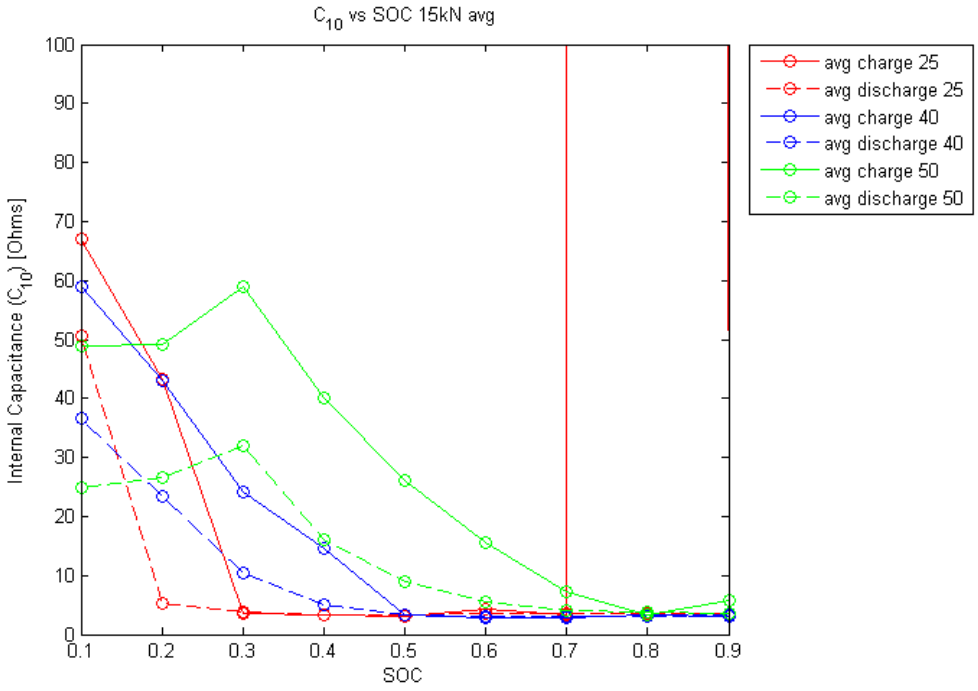

Figure 58. C10 vs SOC 15kN

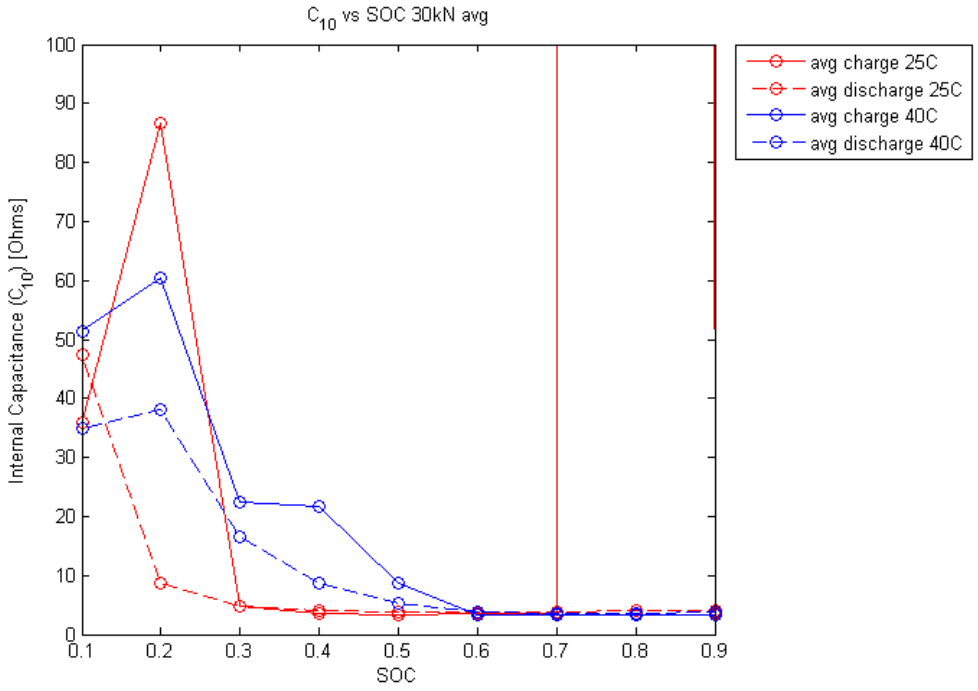

Figure 59. C10 vs SOC 30kN

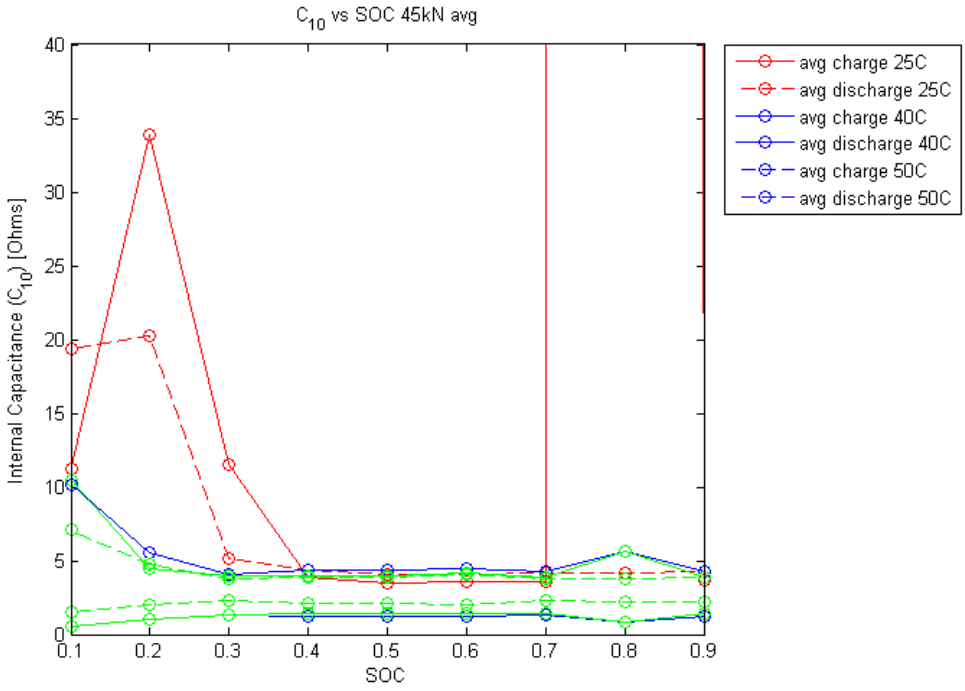

Figure 60. C10 vs SOC 45kN

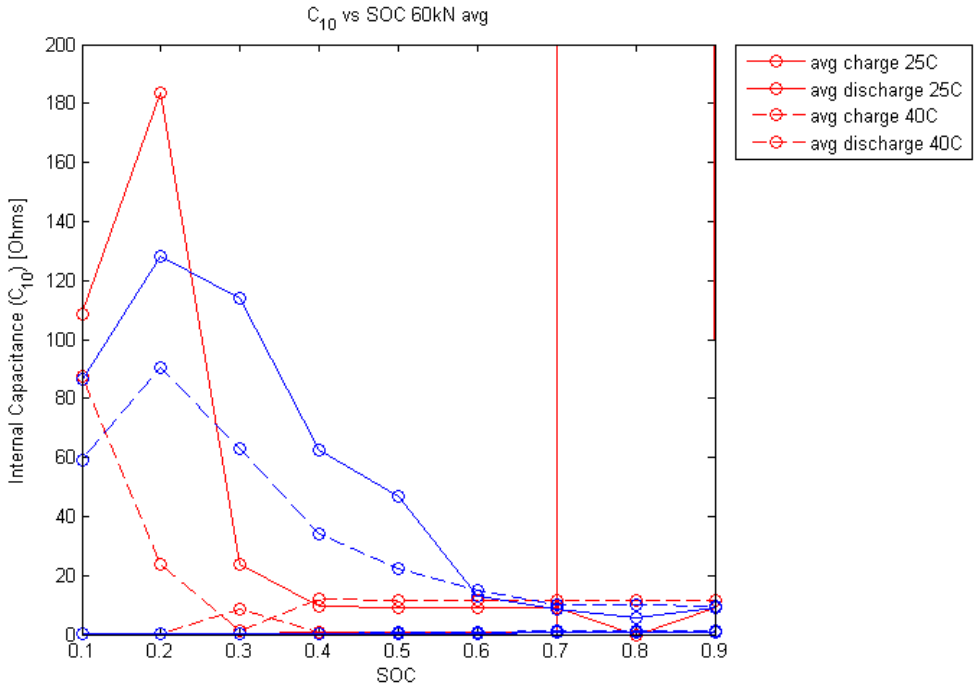

Figure 61. C10 vs SOC 60kN

CURRICULUM VITAE

ALEX B. FRANCIS

EMS Bldg Room 926
3200 N Cramer St.
Milwaukee, WI 53211
francis@uwm.edu

EDUCATION:

University of Wisconsin-Milwaukee, Milwaukee, WI
Ph.D. Candidate: Mechanical Engineering,
Minor: Mathematics
Master of Science: Mechanical Engineering, June 2014
Bachelor of Science: Mechanical Engineering, Dec, 2012

WORK EXPERIENCE:

Rexnord, Innovation Center Sep 2017 - Present

- Member of the Advanced Engineering team at the Rexnord Innovation Center solving key research questions for high impact projects.

Alphacore Solutions LLC Mar 2016 - Present

- Co-founder, helping innovators realize product ideas and bridging the gap between concept to minimum viable product or even commercial prototype. Focused on engineering and design projects, we manage the early stages of product development for clients.

www.alphacore.solutions

Isopoint Technologies LLC Feb 2014 – Feb 2016

- Founder, microfluidic technology company, providing tools for single-molecule genetic analysis.
- Commercializing the nanoparticle electrostatic trap (E-Trap): patent US 8,465,967.
- Collaborating with prominent university researchers and entities.
- Funding raised to date: > $125,000
- www.isopointtechnologies.com

UWM Advanced Manufacturing and Design Laboratory (AMDL) January 2012 - Present

- Working with a team to develop state-of-the-art Lithium Ion battery packs for use in Electric Vehicles.
    - Responsible for determining material properties of components in current Li-Ion Battery cells.

- Post-crash Li-Ion Battery cell reconstruction using CT scan data for use in structural and thermal analysis.
- Responsible for verifying computer simulation results of structural and thermal limits via physical testing.
- Design lead on multiple projects resulting in pending patents.
- **AMDL Selected Publications**:

A. Francis, I. Avdeev, J. Hamann, and S. Ananthasivan. "Accurate Characterization of Torsional Stiffness of Flexible Disk Couplings." *Journal of Engineering for Gas Turbines and Power*. Jan. 2015.

I. Avdeev, M. Martinsen, and A. Francis. "Rate- and Temperature-Dependent Material Behavior of Multilayer Polymer Battery Separator." *Journal of Materials Engineering and Performance*. Oct. 2013.

A. Francis, and I. Avdeev. "Sensitivity of Mechanical Properties to Print Parameters in FDM Fabricated Parts." *ASME IMECE Conf. Proc.* 2013. San Diego, California.

Rexnord, Gear Group (Falk) May 2016 – Aug 2016

- Responsible for critical path work bringing new technology to market through concept generation and validation activities.
- Interacted with cross-functional product development team, improving understanding of marketing, supply chain, and finance functions (other departments).
- Completed factory floor continuous improvement activities leading to 20% efficiency improvement in the shipping/receiving process (leaving the company in better condition).

UWM College of Engineering and Applied Science Sep 2015 - Present

- Instructor for the course: Product Realization
- Mentor student teams through industry sponsored design projects and maintain corporate satisfaction.

Johnson Controls Inc. March 2013 - May 2013

- Member of a team developing a showcase lab for corrosion testing.
- Duties included: CAD modeling and redesign of corrosion apparatus, source parts and work with manufacturing experts to create end product, as well as design final laboratory layout.

UWM Tribology and Energy Diagnostics Lab (TEDL) March 2011 - Dec 2011

- Assisted graduate students in the area of friction optimization (Tribology) for gears and bearings.
- Conducted tests of Graphene coatings to reduce coefficient of friction.
- **TEDL Selected Publications:**

E. Y. A. Wornyoh, D. K. Patel, Luke Schuessler, A. B. Francis, and C. S. Garnett. "Improving Rolling Element Bearing Thermal Compliance Through In Situ Cooling." *ASME Conf. Proc.* 2011, 245 (2011)

HONORS AND ACTIVITES:

Academic

- UWM College of Engineering and Applied Science Academic Excellence Award (2014)
- College of Engineering and Applied Science Dean's Scholarship (2014-2015)
- Chancellor's Graduate Student Award (2013-2014)
- SME Ch.2 scholarship recipient (2008, 2009, 2010, 2011, 2012, 2013)
- National Conference on Undergraduate Research/UWM CEAS Poster Competition (2013): Materials Testing of a Lithium Ion Battery Separator for Use in Finite Element Analysis
- UWM CEAS/MSOE IEEE Poster Competition (2012): Study of Micro Bead Behavior in the Presence of Dielectrophoretic and Electrohydrodynamic Traps
- UWM CEAS Poster Competition (2011): Investigating the Superlubricity of Graphene Oxide

Entrepreneurship

- Milwaukee Business Journal Junior Eureka Award (2014)
- UWM New Venture Business Plan Competition Grand Prize (2014): Electrostatic Trap
- UWM New Venture Business Plan Competition Third Place (2017): Alphacore Solutions
- UWM Collegiate Entrepreneurs Organization - Elevator Pitch Competition 2nd place
- UWM Student Startup Challenge Winner (2013): Electrostatic Trap
- UWM Student Startup Challenge Top 10 (2012): Industrial high-throughput 3D printer
- VentureWell (NCIIA)/Epicenter: University Innovation Fellow (2014-present)

Leadership and Involvement

- President UWM Collegiate Entrepreneurs Organization (2014-2015)
- Athlete: University of Wisconsin-Milwaukee NCAA Division 1 Cross Country and Track. (2008-2012)
- Volunteer: FIRST robotics, Panther Prowl 5K run/walk, UW-Milwaukee's Developmental Track meets

Affiliations

- American Society of Mechanical Engineers (ASME), Society of Automotive Engineers (SAE), Society of Manufacturing Engineers (SME)